101112109

Sustainable and Green Electronics for Circular Economy

Deliverable 1.6

Sustainable materials and processes, and their characteristics

Project Coordinator	Ramon Caanen, Philips Electronics Nederland B.V.		
Start date Project	June 1st 2023	**Duration**	36 months
Version	1.0		
Status	Final		
Date of issue	31-05-2025		
Dissemination level	Public		

Authors' data

Authors of the D1.6 are listed below.

Author	Beneficiary	e-mail
Sirpa Nordman, Elina Hakola, Kimmo Keränen, Kirsi Immonen	VTT: sirpa.nordman@vtt.fi , elina.hakola@vtt.fi , Kimmo Keränen@vtt.fi , kirsi.immonen@vtt.fi	
Joel Benavides Hatakeda	TNO: joel.benavideshatakeda@tno.nl	
Zareen Abbas, Miaomiao Li	UGOT: zareen.abbas@gu.se , miaomiao.li@gu.se	
Helga Szambolics	CEA: helga.szambolics@cea.fr	
Luciano Rietter, Agnieszka Rocha	PIEP: luciano.rietter@piep.pt, agnieszka.rocha@piep.pt	
Thomas Löher	FHG: thomas.löher@izm.frauhofer.de	
Matti Mäntysalo	TAU: matti.mäntysalo@tuni.fi	
Lars Herlogsson, Anurak Sawatdee, Ioannis Petsagkourakis	RISE: lars.herlogsson@ri.se , anurak.sawatdee@ri.se , ioannis.petsagkourakis@ri.se	
Stefan Bendig	WUR: Stefan.bendig@we-online.de	
Mateusz Derc	GUT: mateusz.derc@pg.edu.pl	
Krišjānis Nesenbergs	EDI: krisjanis.nesenbergs@edi.lv	
Eleonora Långström	CAN: eleonora.langstrom@canatu.com	
Pasi Lehtonen	UPM: pasi.Lehtonen@upmraflatac.com	
Julia Flaceliere	ARNP: julia.flaceliere@avantium.com	

Management Summary

In the Sustronics project, the main objective of WP1 was to develop, customise, and characterise sustainable materials and processes, ensuring that their performance aligns with the requirements of components in WP2 and pilots in WP3, and providing data to support the sustainability assessment in WP4.

WP1 comprises 4 different tasks:

• T1.1. Requirements and specifications

• T1.2. Material development

• T1.3. Manufacturing process development

• T1.4. Testing and validation of materials and processes

This deliverable presents the work conducted under T1.4, which focuses on testing of materials and processes developed in T1.2-1.3. This adheres to the testing and validation plan established in T1.4 and reported in D1.3. The material and process development work done was presented in D1.4 (Sustainable materials and their characteristics) and D1.5 (Sustainable processes and their characteristics), respectively. Main testing work was performed after the delivery of these deliverables and reported here in D1.6. Also, in this deliverable a short summary of the work already reported by partners in D1.4 and D1.5 is included.

This document provides a comprehensive overview of the testing of materials and processes. It includes detailed descriptions, tests, and results for various bio-polymers, cellulose-based materials, adhesives, inks, and other materials. Also, the developed processes are described in detail, focusing on their testing and validation and implementation in pilots.

As a summary, a wide range of sustainable materials and processes have been developed and tested, while some have been discarded based on their performance and environmental impact. Feasible materials and processes are and will be implemented in various pilots, so new reports from them will be released in later months in WP3.

List of abbreviations

ACA: Anisotropic conductive adhesive

ACF: Anisotropic conductive film

ABS: Acrylonitrile butadiene styrene

Ag: Silver

AM: Additive manufacturing

ASA: Acrylonitrile styrene acrylate

BBC: Biobased carbon content

BPA: Bisphenol A

BW: Beeswax

C: Carbon

CNF: Cellulose nano fibril

CNT: Carbon nanotube

COM: Commercial

DLP: Digital light processing

DPA: Diphenolic acid

DSC: Differential scanning calorimetry

EEG: Electroencephalography

ECA: Electrically conductive adhesive

EMIM[OAc]: 1-ethyl-3-methylimidazolium acetate

FDM: Fused deposition modelling

FDA: Food and drugs

HEC: 2-Hydroxyethyl cellulose

HIPS: High impact polystyrene

ICA: Isotropic conductive adhesive

IC: Integrated circuit

IL: Ionic liquid

IM: Injection moulding

ISCC: International sustainability & carbon certification

IV: Intrinsic viscosity

LCA: Life cycle assessment

LCIA: Life cycle impact assessment

LCP: Liquid crystal polymer

LDS: Laser direct structuring

LS: Line spacing

LW: Line width

MD: Machine direction

MDO: Machine direction orientation

MID: Mechatronic integrated devices

NCA: Non-conductive adhesive

NFC: Near-field communication

NFC-film: Nanofibririllated cellulose film

NTC: Negative temperature coefficient

OLD: Older, manufactured in previous projects

PA12: Nylon 12

PA6: Nylon 6

PCTG: Polycyclohexylene dimethylene terephthalate

PC: Polycarbonate

PEF: Polyethylene furanoate

PET: Polyethylene terephthalate

PETG: Polyethylene terephthalate glycol

PEO: Polyethylene oxide

PLA: Polylactic acid

PMMA: Poly(methyl methacrylate)

PP: Polypropylene

PPA: Polyphthalamide

PPS: Polyphenylene sulphide

PVDF: Polyvinylidene fluoride

PVA: Polyvinyl alcohol

PTH: Plated through holes

PTC: Positive temperature coefficient

QFN: Quad-flat no-leads

R2R: Roll-to-roll

SC: Supercapacitor

SH: Sheet

SDS: Sodium dodecyl sulphate

SEM: Scanning electron microscopy

SLA: Stereolithography

SMD: Surface-mount devices

SPDR: Split-post dielectric resonator

TDS: Technical data sheet

TD: Transverse direction

TGA: Thermogravimetric analysis

Tg: Glass transition temperature

TPU: Thermoplastic polyurethane

TPE: Thermoplastic elastomer

VNA: Vector network analyser

εR: Dielectric constant

tanδ: Loss tangent

ρ: Print density

σ: Electrical conductivity

Table of Contents

List of abbreviations **4**
1 Introduction **9**
1.1 Purpose of the document 9
1.2 Related documents 9
2 Description of material development and testing **11**
2.1 Bio-plastic substrates 11
2.1.1 Substrate testing at VTT 12
2.1.2 Substrate testing at TNO 22
2.1.3 Substrate testing at CEA 28
2.1.4 Substrate fabrication at ARNP 33
2.2 Cellulose based (paper, cartonboard) & wood-based substrates 35
2.2.1 Substrate testing at VTT 35
2.2.2 Substrate testing at PIEP 46
2.2.3 Substrate testing at TNO 49
2.2.4 Substrate testing at RISE 54
2.3 Adhesives 58
2.3.1 Adhesive testing at UPM 58
2.3.2 Adhesive testing at RISE 60
2.4 Inks 65
2.4.1 Ink testing at TAU 65
2.4.2 Ink testing at UGOT 67
2.4.3 Ink testing at RISE 68
2.5 Other materials 70
2.5.1 CNT film testing at CAN 70
2.6 Conclusions and next steps in material development 72
3 Description of process development **73**
3.1 Printing 73
3.1.1 Printing test results at RISE 73
3.2 3D-printing 82
3.2.1 Testing at GUT 82
3.3 Component assembly 93
3.3.1 Testing at VTT 93
3.3.2 Testing at WUR 95
3.3.3 Testing at FHG 99
3.3.4 Testing at RISE 101
3.4 Paper fluidics 104

3.4.1 Testing at VTT 104
3.5 Wearable systems 106
3.5.1 Testing at EDI 106
4 Conclusions 112
5 References 114

1 Introduction

1.1 Purpose of the document

In the Tasks 1.2-1.4 (Material development, Process development, Validation and Testing plan) a vast variety of sustainable substrates, inks, adhesives, and other materials as well as processes were introduced, developed and tested. The main material and process development work has been done by M18, and results of the development work were reported in D1.4 and in D1.5 with focus on material and process properties and performance. Main material characterisation results can thus be found in D1.4, This document reports only the testing results that were not available when D1.4 was submitted. The results focusing on more extensive testing done in T1.4, such as printability and component assembly testing, are also reported in this document. Therefore, deliverables D1.4, D1.5 and D1.6 report all the development and testing results from WP1 and together ensure that all the planned tests described in D1.3 are performed and justify the possible deviations from the plan.

D1.4, D1.5 and D1.6 are also used as a tool to ensure that the results are aligned with component and device requirements from WP2 (described in D2.1), and with pilot requirements from WP3 (described in D3.1 and D3.2). Consistency with material and process specifications as described in D1.1, and D1.2 is reviewed in WP3 (D3.2-3.4).

The focus of this document is mainly on the testing results. The material processing and testing methodologies are described in more detail in D1.3, D1.4 and D1.5.

1.2 Related documents

D1.2 ‘Processes Specifications and initial testing plan’ (M6) that describes the process requirements and target specifications per pilot needs

D1.3 ‘Validation and testing plan’ (M15) that describes the various materials developed in WP1, and a plan for characterizing the materials, as well as validating/testing their suitability to meet pilot requirements through e.g. printability trials

D1.4 ‘Sustainable materials and their characteristics’ (M18)

D1.5 ‘Sustainable processes and their characteristics’ (M18)

D2.1 ‘Requirements specification for component and devices’ (M6) that describes the process requirements for components and devices

D2.2 ‘Report on sensors and transducers’ (M24), D2.3 ‘Report on energy storage and energy management’ (M24); D2.3 ‘Report on communication and energy harvesting hardware and protocols’ (M27); D2.4 ‘Report on ASIC development’ (M24); D2.5 ‘Report on hybrid and integrated components’ (M30); and D2.6 ‘Report on software functionalities’ that will describe the use of selected processes in components and devices

D3.1 ‘Initial system specification and design for pilots, including circularity aspects’ (M3) that describes the material requirements per pilot

D3.2 ‘Gen 1 prototypes, including characterisation and updates to system specification and design for Gen 2’ (M15) that describes the use of selected processes in pilot Gen 1

D3.3 ‘Gen 2 prototypes, including characterisation and updates to system specification and design for Gen 3’ (M27) and D3.4 ‘Final prototypes for Gen 3, including validation data and end user engagement’ (M36) that will report the use of selected processes in pilot Gen 2 and 3, respectively.

D4.2 ‘Analysis of life cycle-based environmental impacts and end-of-life processes of sustainable materials in electronics’ (M18) that describes the environmental impact and end-of-life potential of sustainable materials

D4.4 ‘End-of-life concepts and new processes for sustainable electronics’ (M30) that will describe the end-of-life for selected materials

2 Description of material development and testing

The sustainable materials developed in Sustronics include bio-polymers, cellulose-based and other substrates, inks, adhesives and some other materials that could not be classified as one of the mentioned. In this section, only testing results gained after the delivery of D1.4 are reported. The development process nor validation and testing methods are not described here. The detailed description of planned testing and validation methods can be found in D1.3.

2.1 Bio-plastic substrates

A list of bio-polymers developed by different partners in Sustronics is presented in Table 1. Description of the material properties of bio-polymer substrates whose development has been finalized since D1.4 are presented in the following sub-sections per material, when applicable. Bio-polymer substrates that are not reported here can be found fully reported in D1.4.

Table 1. Bio-polymer substrates developed in the Sustronics project.

Technology	Owners	Sustainability claims						Pilots targeted									
		Bio-based	Renewable	Recycled	Sustainable sourcing[1]	EoL: Recyclable	EoL: Compostable	Pilot#1.1	Pilot#1.2	Pilot#1.3	Pilot#2.1	Pilot#2.2	Pilot#2.3	Pilot#3.1a	Pilot#3.1b	Pilot#3.2	Pilot#3.3
Bio-plastics	• VTT: commercial pellets/granules processed into films • ARNP: own commercial & experimental • UPM: own commercial & experimental	X		X	X	X	X[2]		X	X	X	X	X				X

[1] e.g. side streams
[2] some grades

The bio-polymer substrates, besides PEF, were fabricated at VTT's pilot film processing facility located in Tampere. Granulate form materials were processed to films using laboratory or pilot-scale cast film equipment depending on the availability of materials. Four of the materials (Danna, Franplast, Hexpol, UPM Formi) were provided only on few kilograms scale and processed with laboratory scale equipment. The rest of tested materials were provided on larger scale (25 kg bags) and therefore processing was enabled in pilot-scale cast film extrusion PLASCO-line. The fabrication procedures are fully described in D1.4.

2.1.1 Substrate testing at VTT

Many new materials were fabricated and tested by VTT. In Table 2 the summary of bio-polymers and their testing reported in D1.4 is presented. Some materials could not be included into D1.4, due to timing issues relating to the deadline. This is understandable since the bio-polymer material section comprises of so many materials with various testing methods by several partners.

Table 2. Summary table of the materials and their testing reported by VTT in D1.4.

Substrate	Tests carried out	Linkage to pilots
PLA Luminy L175 (Total Corbion)	Plasco-pilot scale film, Tensile strength, DSC, TGA, Surface roughness, Transmission, Surface energy, Contact angle with water	Pilots #1.3, #2.2 and #2.3
Bio-PET Eastlon CB602AB	Plasco-pilot scale film, Tensile strength, DSC, TGA, Surface roughness, Transmission, Surface energy, Contact angle with water	Pilots #1.2 and #2.3
Cuma-PET L04-100 (chemically recycled PET)	Plasco-pilot scale processing test was not successful	Pilots #1.2 and #2.3
Cuma-PET 1704R (chemically recycled PET, Dufor Polyester Specialities)	Plasco-pilot scale film, Tensile strength, DSC, TGA, Surface roughness, Transmission, Surface energy, Contact angle with water	Pilot #2.3 thermoforming
Brightplus Loimu Tough heat	Plasco-pilot scale film, Tensile strength, DSC, TGA, Surface roughness, Transmission, Surface energy, Contact angle with water	Pilots #1.3, #2.2 and #2.3
Durabio D5380R	Plasco-pilot scale film, Tensile strength, DSC, TGA, Surface roughness, Transmission, Surface energy, Contact angle with water	Pilot #2.3
Ecozen T95G	Plasco-pilot scale film, Tensile strength, DSC, TGA, Surface roughness, Transmission, Surface energy, Contact angle with water	Pilot #2.3
Bio-TPU Estane Eco 12T80E (Lubrizol)	Plasco-pilot scale film, Tensile strength, DSC, TGA	Pilot #3.3
Bio-TPE Chemiton® LSA_NA70 (Franplast)**	Brabender laboratory-scale film processing, Tensile strength, DSC, TGA	Pilot #3.3
Hexpol TPZ**	Brabender laboratory-scale film processing, Tensile strength, DSC, TGA	Pilot #3.3
DANNA PLH*	Brabender laborator-scale film processing, Tensile strength, DSC, TGA	Pilot #3.1
UPM Formi 3D20**	Brabender laboratory-scale film processing, Tensile strength, DSC, TGA	Pilot #1.3 Luminaire
Natureflex NP42 (Commercial film with thickness of 42 µm, Futamura)**	Tensile strength, DSC, TGA	Pilots #1.3 Luminaire, #2.2 or #3.1

*Too little sample amount for R2R testing received

**These have not been tested in R2R printing

Film samples with thicknesses of 125 and 250 µm were sent to VTT in Oulu, TAU, TNO and CEA for further testing. PLA and Natureflex samples were sent also for SCR.

2.1.1.1 Bioplastic substrate printability trials

Several different bioplastic substrates were selected for the printability trials in roll-to-roll (R2R) environment, as presented in Table 3Table 3. Both commercial films and films manufactured at VTT in pilot-scale from granulates (see D1.4) were printed, and the achieved print qualities were compared with each other and with reference substrates. Reference substrates were polyethylene terephthalate (PET) film from DuPont Teijin Films and thermoplastic polyurethane (TPU) film from Covestro. Commercial bioplastic films included two Forest Film™ label substrates from UPM Raflatac made of wood-based bio-naphtha raw materials, Natureflex regenerated cellulose film from Futamura, and partly bio-based TPU (thermoplastic polyurethane) film from Covestro. Pilot-scale manufactured films were partly bio-based PET (Bio-PET), chemically recycled PET (CumaPET), mechanically recycled PET (r-PET), polylactic acid (PLA) bio-polymer, glycol-modified PET with plant-derived biomass components (Ecozen®), bio-based polycarbonate derived mainly from plant-based isosorbide (Durabio™), bioplastic from Brightplus (BrightBio® Loimu), and partly bio-based TPU (Estane®).

Table 3. Summary table of material testing made at VTT.

Substrate	Tests carried out	Linkage to pilots
PET Melinex ST506 (Ref., Commercial)	<u>Substrate characterization</u> R_a roughness - white-light interferometer	Ref. for Pilots #1.2, #2.1, #2.2 and #2.3
Bio-PET Eastlon CB-602AB		Pilot #1.2 and #2.3
CumaPET RE 1704R (Chemically recycled)	Surface energy and contact angle with water - contact angle meter	Pilot #1.2 and #2.3
r-PET (Mechanically recycled)	Transmission - UV-Vis	Pilot #1.2 and #2.3
PLA Luminy L175	Thermal stability in the convection oven – visual inspection	Pilot #1.3, #2.2 and #2.3
Ecozen T95G		Pilot #2.3
Durabio D5380R	<u>Printability</u>	Pilot #2.3
Loimu ToughHeat	Printability and print quality – visual inspection, microscope	Pilot #1.3, #2.2 and #2.3
Forest PE CLEAR FTC85 (Commercial)	Ink spreading, minimum gap width - microscope	-
Forest PP CLEAR FTC50 (Commercial)	Minimum conductive line width – digital multimeter	-
Natureflex 45NK (Commercial)	Sheet resistance and volume resistivity - digital multimeter and calculation	Pilot #1.3 Luminaire, #2.2 or #3.1
TPU Platilon U073 (Ref., commercial)	Tape adhesion - digital multimeter	Pilot #3.3
Bio-TPU Platilon LPT4201 AUV (Commercial)	Layer thickness - surface profilometer	Pilot #3.3
Bio-TPU Estane Eco 12T80E		Pilot #3.3

The substrate properties were measured prior to the printing trials, as shown in Table 4. More detailed description of the measurement methods can be found in deliverable *D1.4 Sustainable materials and their characteristics*. Average roughness (R_a) was measured with Bruker ContourX-500 optical profilometer based on white-light interferometry. Transmission of the substrates from 200 to 800 nm was analysed with Varian UV-Vis spectrophotometer. Krüss DSA25S drop shape analyser was used to measure surface energy and contact angle with water. Film thickness was measured using Mitutoyo digital thickness gauge by placing substrate sheets between two-disc contact points and reading the thickness in micrometres

from the gauge. Thermal stability was tested by placing small sheets of the bioplastic films into a convection oven for 30 minutes at temperatures of 80 °C, 100 °C, 120 °C, and 140 °C, and then evaluating the dimensional, optical, and other visual changes of the sheets. Every substrate was tested at all the selected temperatures and the maximum temperature that the substrate withstood was considered as the thermal stability temperature.

The orientation process in machine-direction (MDO) of the pilot-scale manufactured bioplastic films affected greatly their thermal stability. Bio-PET, CumaPET, Ecozen®, and Durabio™ films without the MDO process did not withstand temperatures above 80-100 °C without large dimensional, optical (haziness, whitening), and visual (blistering) changes, thus making them unsuitable for R2R printing/processing with conductive inks. Commercial Forest PE film was also discarded from the printing trials because of the poor thermal stability of its label adhesive. In the case of the Natureflex substrate, the thermal stability was slightly poorer which could affect the printability and registration of multilayer structures.

Both bio-based TPU substrates had very low surface energy (<30 mN/m) and high contact angle with water (>90 °C), thus causing easily ink transfer, wetting, levelling, and spreading issues. Other bioplastics had lower contact angle and higher surface energy values due to which proper ink transfer and behaviour on the substrate was expected. Substrate transmission does not affect the printability but can limit the suitability of the substrate for certain applications where substrate transparency is important. Loimu had lower transmission of <70% because of its whitish colour but other bioplastics were highly transparent with transmission values above 86%. Highest transmission values above 90° were seen with PLA, Ecozen®, Durabio™, and Bio-TPU Estane substrates. The reference PET film was the smoothest substrate followed by Ecozen® and Durabio™ substrates. Commercial TPU substrates and Loimu substrate had the highest surface roughness.

Table 4. Properties of the bioplastic and reference substrates. Both commercial (COM) and pilot-scale manufactured films were used. Some pilot-scale manufactured films were oriented in machine-direction (MDO) during the manufacturing, some were manufactured in previous projects (OLD), and some were only available as sheets (SH). Substrates that were finally printed in R2R environment are marked with bold font. Green accent colour means that the substrate has some excellent characteristic, yellow colour means that some property of the substrate can have a bad effect on printability or the final application, and red colour means that this substrate characteristic adversely affects the printability, runnability, or print quality.

Substrate	Thickness (µm)	Ra roughness (nm)	Transmission 400-800 nm (%)	Surface energy (mN/m)	Contact angle with water (°)	Thermal stability
PET Melinex ST506 (Ref., COM)	125	7.6	89.5	46.3	68.1	140 °C
Bio-PET Eastlon CB-602AB, No MDO	125	33.7	89.9	46.1	79.3	<80 °C
Bio-PET Eastlon CB-602AB, 3.0xMDO (OLD)	50-70	48.0	89.7	51.0	70.1	120 °C
Bio-PET Eastlon CB-602AB, 3.0xMDO (SH)	125	33.7	87.8	53.0	64.1	140 °C
Cuma-PET RE 1704R, No MDO (SH)	125	34.0	88.3	46.0	71.8	<100 °C
Cuma-PET RE 1704R, 3.2xMDO (OLD)	100	58.3	89.4	55.8	59.1	120-140 °C
r-PET, 3.2xMDO (OLD)	100	48.6	89.2	53.3	66.4	120-140 °C
PLA Luminy L175, 3.5xMDO (SH)	125	87.9	93.4	45.0	71.6	120-140 °C
PLA Luminy L175, 3.0-3.3xMDO	125	41.9	93.3	47.5	66.3	120-140 °C
Ecozen T95G	125	11.2	91.0	48.5	74.9	80 °C
Durabio D5380R	125	23.2	92.5	51.3	69.1	<80 °C
Loimu ToughHeat, 3.0xMDO	125	874.3	65.1	49.2	63.9	120 °C
Forest PE CLEAR FTC85 (COM)	85	83.8	86.4	40.3	77.6	<100 °C
Forest PP CLEAR FTC50 (COM)	50	100.5	89.2	37.8	82.6	120 °C
Natureflex 45NK (COM)	45	85.5	89.4	42.3	74.2	100-120 °C
TPU Platilon U073 (Reference, COM)	100	420.4	89.0	43.4	72.1	140 °C
Bio-TPU Platilon LPT4201 AUV (COM)	50	456.7	89.1	27.3	90.1	120 °C
Bio-TPU Estane Eco 12T80E (SH)	125	104.4	91.9	29.0	106.4	120 °C

Suitable bioplastic substrates were rotary screen printed with VTT's ROKO R2R printing line using Asahi LS-411AW silver (Ag) ink and Loctite PF-407A carbon (C) ink (Figure 1). Prior to the printing, the substrates were thermally pre-treated with the ROKO line at 120 °C using the speed of 2 m/min. The printing layout contained horizontal, vertical, and inclined line and gap

patterns having widths between 50 µm and 1000 µm, antenna patterns with different line (100, 200, 500, 1000, and 1500 µm) and gap (100, 200, 500, and 1000 µm) widths, and solid tone patches. The mesh count of the screen was either 305 lines/inch (Ag ink) or 215 lines/inch (Ag ink with TPU substrates, C ink). The printing speed was 2 m/min with the Ag ink and 3 m/min with the C ink. The printed layers were dried inline in the hot air ovens of ROKO directly after the printing unit at 120 °C. The dwell time in the drying was approximately 2.4-3.0 min depending on the printing speed.

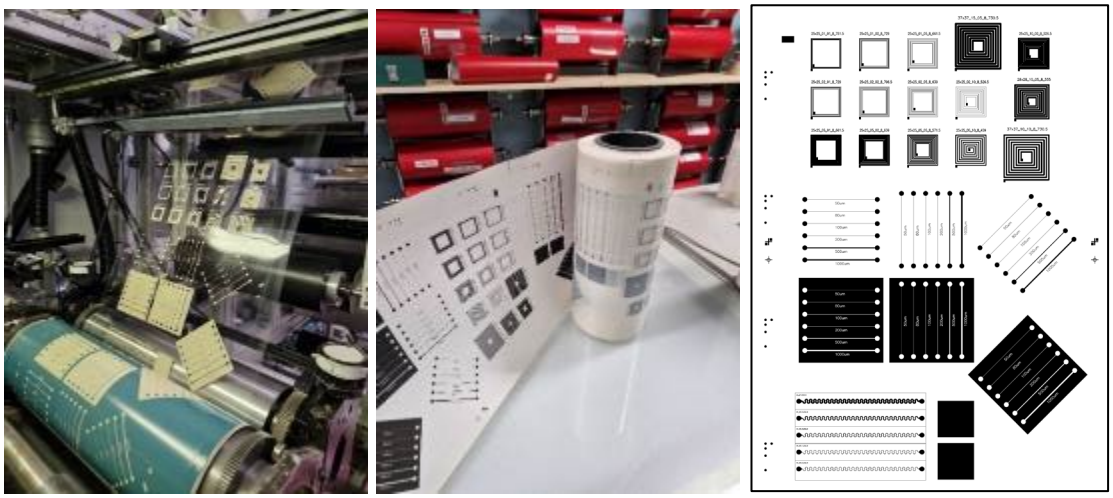

Figure 1. Rotary screen printing onto PLA substrate (left), R2R printed carbon test patterns on Loimu substrate (middle), and printing layout (right).

The printability, visual print quality, and minimum reproducible gap was assessed with OGP's SmartScope 250 ZIP microscope. This same microscope with the image-analysis software was used to measure the printed horizontal and vertical line widths, i.e., the ink spreading. The minimum conductive line width was evaluated by measuring the resistance of vertical, horizontal, and inclined lines with Fluke 289 digital multimeter. The layer thickness was measured using Veeco's Dektak 150 surface profilometer from printed 1000 µm wide vertical and horizontal lines. The resistance (*R*) across all line and antenna patterns was measured with the digital multimeter after which sheet resistance (*SR*) and volume resistivity (*VR*) values were calculated by means of measured line width (*w*), layer thickness (*h*), and line length (*l*): $VR=SR*h=R*w*h/l$. Digital multimeter was also used to assess the ink adhesion/cohesion by measuring the resistance of a meander line before and after tape peeling and calculating the resistance change in percentages.

The printability of bioplastics was good and high print quality was achieved, as shown in Figure 2, Figure 3, and Figure 4. In addition, their print quality was comparable to that obtained on the reference PET foil, thus making the tested bioplastics a good alternative substrate for R2R printing with increased sustainability. Pilot-scale manufactured bioplastic films had process-*related* machine-directional/stripes on their surface that occasionally caused the ink to spread along them, as seen with Loimu and CumaPET substrates (Figure 3). This phenomenon was discarded from the print quality analysis since the groove formation was only related to the manufacturing equipment. Commercial Natureflex substrate stretched at 120 °C to some extent and the low relative humidity (<25 %) during printing made the substrate more brittle, thus creating some pinholes (poor ink transfer) and increased the probability to web breaks (unpredictable substrate runnability). The main difference in ink spreading between the substrates was seen with horizontal lines that tended to spread more than vertical lines. For example, Ag ink spread more on Loimu and PLA than on other substrates, thus decreasing their detail rendering. With C ink, the ink spreading was smaller on Forest PP film than on other substrates.

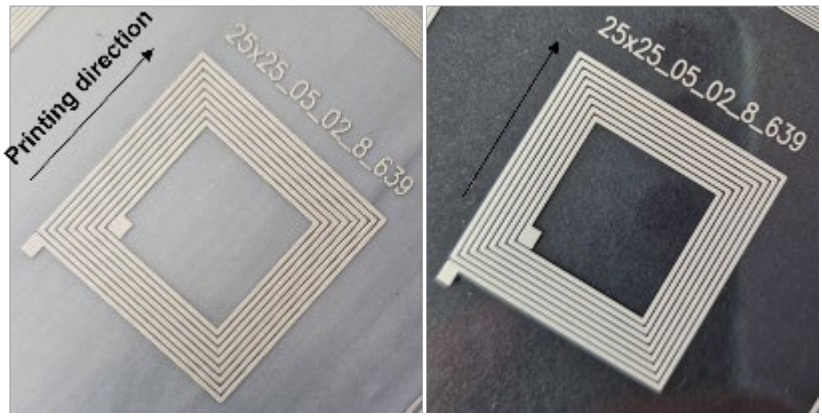

Figure 2. Printed antenna patterns on Loimu (left) and PLA (right) substrates. Black arrow shows the printing direction.

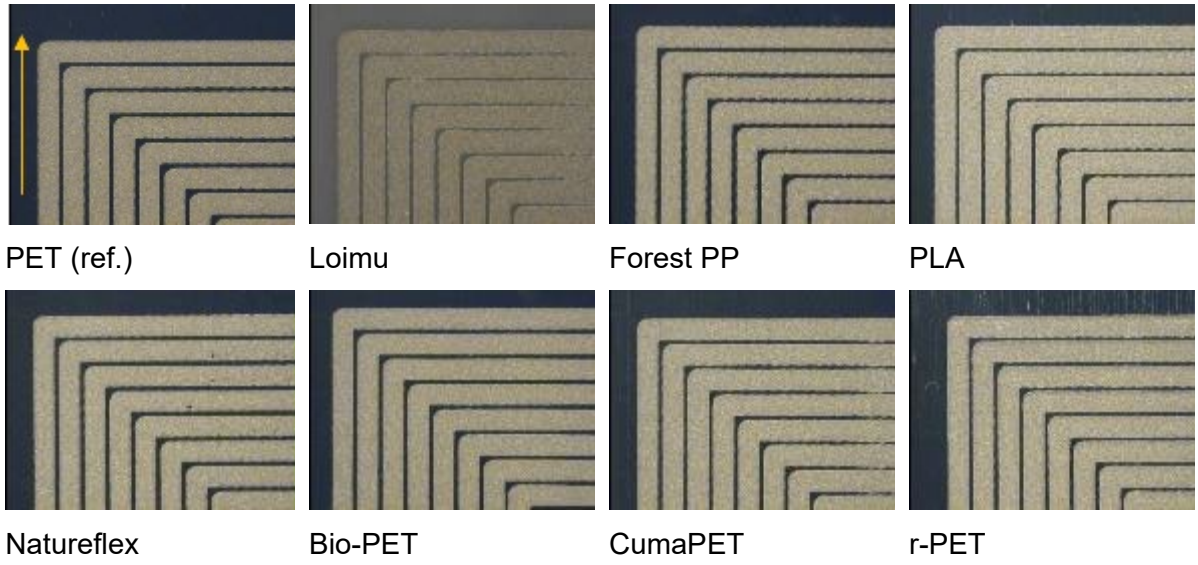

Figure 3. Quality of the printed antenna pattern (line-gap: 500-100 µm) on different bioplastic substrates using LS-411AW Ag ink. The mesh count of the screen was 305 lines/inch. The magnification is x37.7. Yellow arrow shows the printing direction.

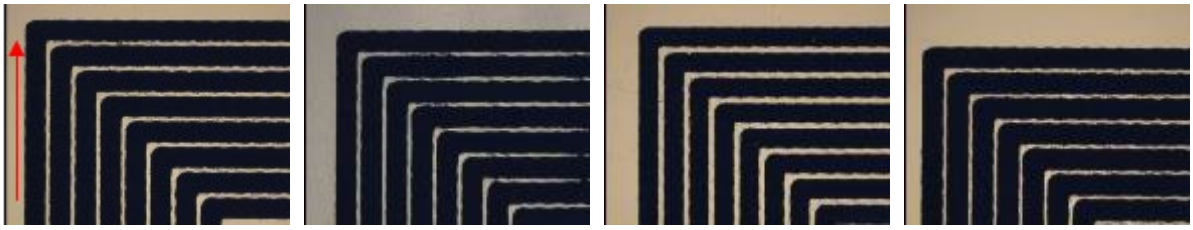

Figure 4. Quality of the printed antenna pattern (line-gap: 500-100 µm) on different bioplastic substrates using EDAG PF-407A C ink. The mesh count of the screen was 215 lines/inch. The magnification is x37.7. Red arrow shows the printing direction.

The detail rendering was good with bioplastics and only minor differences to PET were observed, as shown in Figure 5 and Figure 6. Inks spread more on PLA substrate than on PET, thus increasing both the minimum gap width and measured line width. With Loimu and r-PET substrates, the ink flow along the process-related surface grooves increased the minimum gap width but had no effect on the measured line width, i.e. ink spreading. The inks spread less on Forest PP substrate because of its slightly higher contact angle with water and lower surface energy. The minimum conductive line widths were 125-175 µm or 100-150 µm with Ag and C inks, respectively. However, the difference in the minimum conductive line widths as compared to the width on PET was only 25 µm.

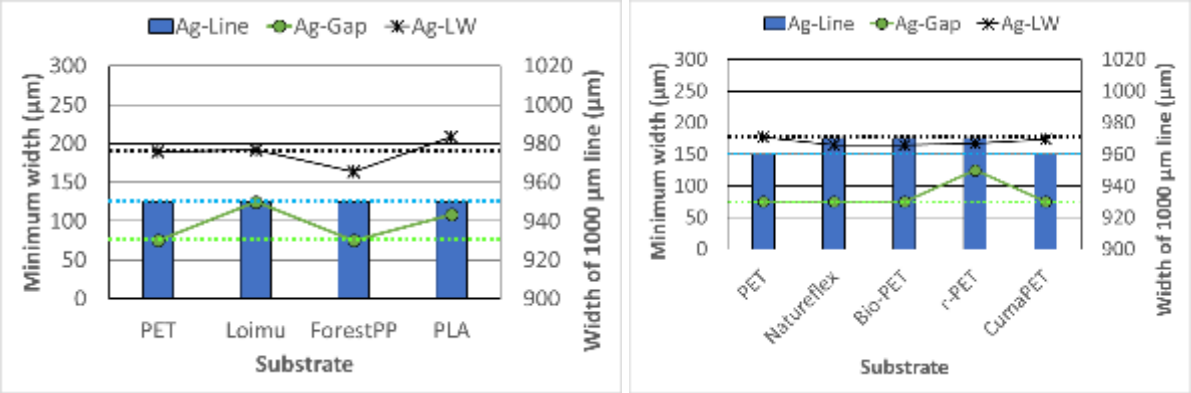

Figure 5. Detail rendering of silver ink on bioplastics. Minimum conductive line width, minimum gap width, and measured line width (LW) are presented. Dotted lines mark the quality level of the reference PET.

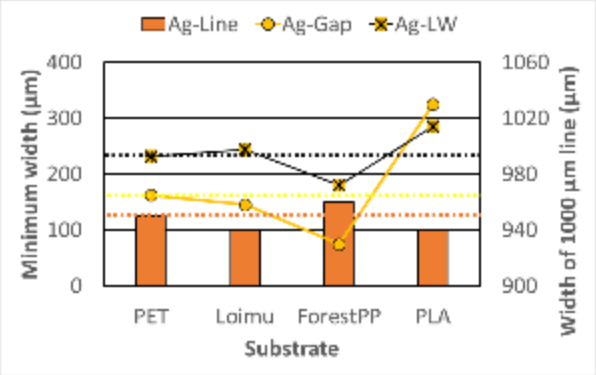

Figure 6. Detail rendering of carbon ink on bioplastics. Minimum conductive line width, minimum gap width, and measured line width (LW) are presented. Dotted lines mark the quality level of the reference PET.

Figure 7 shows the sheet resistance and volume resistivity values of Ag and C ink layers on bioplastics. As expected, C ink layers had significantly lower conductivity than Ag ink layers. With the Ag ink, both sheet resistance and volume resistivity values were lower (better conductivity) on bioplastics than on PET. This resulted most likely from the better solvent removal during drying with the thinner bioplastic substrates and better particle alignment on rougher surfaces, thus increasing the particle-to-particle contact points. Highest conductivities were achieved on Loimu and Natureflex substrates whereas PET-based substrates had lowest conductivities. As a conclusion, bioplastics offer a good alternative to fossil-based reference substrate with the Ag ink. In the case of the C ink, the sheet resistance was the lowest on Loimu. In addition, higher volume resistivity values were obtained on bioplastics than on PET meaning that carbon flakes require smoother surfaces for the flakes to come into better contact with each other.

Both silver and carbon inks had mainly good ink layer adhesion (Figure 8) to all substrates. Poor adhesion with severe ink layer delamination was only seen with PLA substrate when printing with the carbon ink.

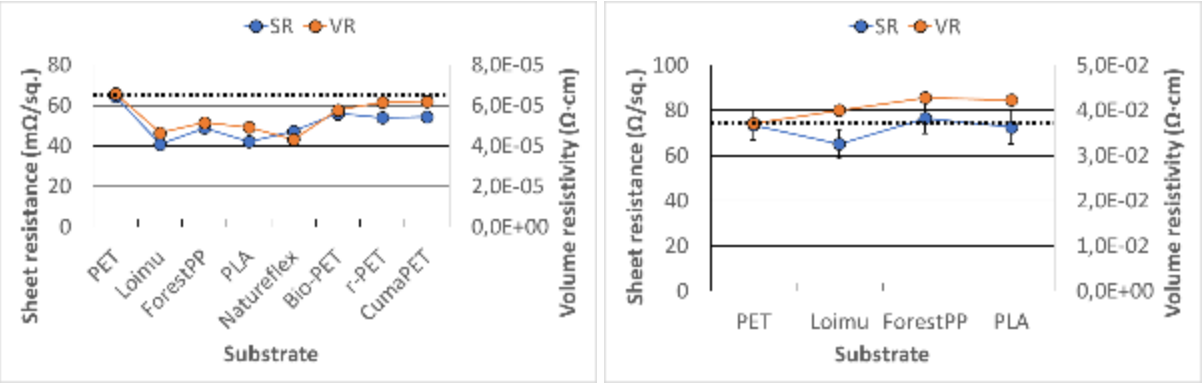

Figure 7. Sheet resistance (SR) and volume resistivity (VR) on bioplastics using either silver (left) or carbon (right) ink. Dotted line marks the quality level of the reference PET.

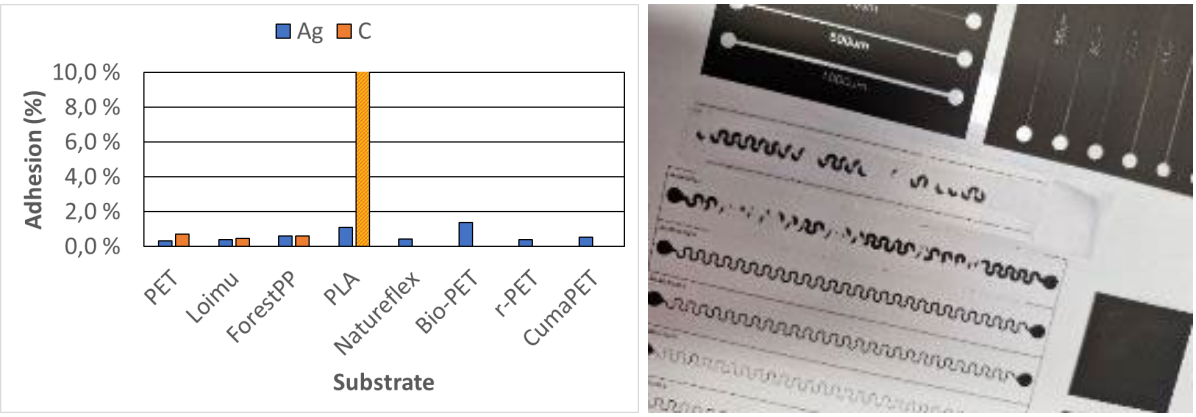

Figure 8. Ink adhesion of printed ink layers on bioplastics (left) and poor carbon ink adhesion to PLA substrate (right).

When considering multilayer printing (two or more layer are deposited in register onto each other), the repetition length (printed pattern that is printed when the printing roller/screen rotates once, layout presented in Figure 1 represents the patterns printed in a single repetition) of the printed layout should remain stable and not differ too much from the repetition length of the printing line. Larger repetition length difference than 1 mm indicates the formation of registration errors and difficulties in adjusting the speeds of the printing process rollers for multilayer printing (adjustment tolerance reached). As seen in Figure 9, the repetition length deviations were small thus, the layer-to-layer registration process should be stable. However, the repetition lengths with Loimu and Natureflex substrates were over 1 mm shorter than the original repetition length. This indicates that multilayer printing can face difficulties in layer-to-layer registration because of the too large adjustment requirement.

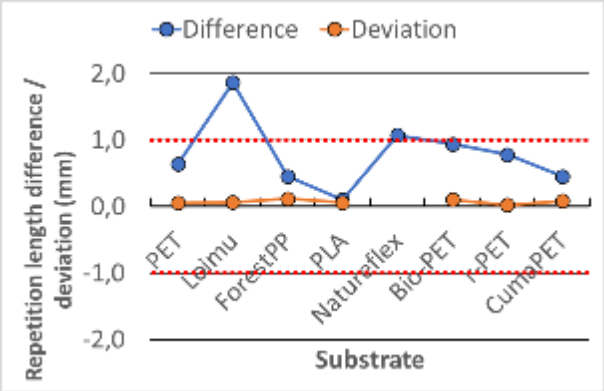

Figure 9. Difference in repetition length achieved on bioplastics as compared to the ideal repetition length of the printing line.

Ag ink spread less on TPU than on PET substrate, as seen in Figure 10. This resulted from the rougher surface of TPU that prevented ink from flowing along the surface of the substrate. In the case of Bio-TPU substrate, the very low surface energy (<30 mN/m) and high contact angle with water (90.1°) created ink wetting and levelling issues, thus resulting in ragged and splashed printed lines with ink layer necking, i.e., decreased line width.

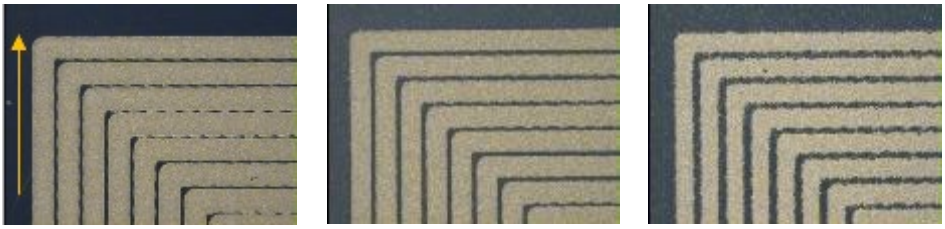

PET (ref.) TPU (ref.) Bio-TPU

Figure 10. Quality of the printed antenna pattern (line-gap: 500-100 µm) on TPU substrates using LS-411AW Ag ink. The mesh count of the screen was 215 lines/inch. The magnification is x37.7. Yellow arrow shows the printing direction.

Figure 11 shows the detail rendering and layer conductivity data with TPU substrates in comparison with PET. The higher surface roughness of the reference TPU substrate increased the minimum conductive line width but decreased ink spreading (narrower lines and smaller minimum gap). The wetting, levelling, splashing issues with the Bio-TPU substrate decreased the measured line width but increased the minimum gap width. These together with the rougher surface than PET increased also the minimum conductive line width. However, the layer conductivity was better on both TPU substrates than on PET because of the better particle-to-particle contact formation on rougher surfaces. No difference in conductivity was seen between TPU substrates. Although Bio-TPU suffered from ink wetting and levelling issues, the ink adhesion was good (Figure 12).

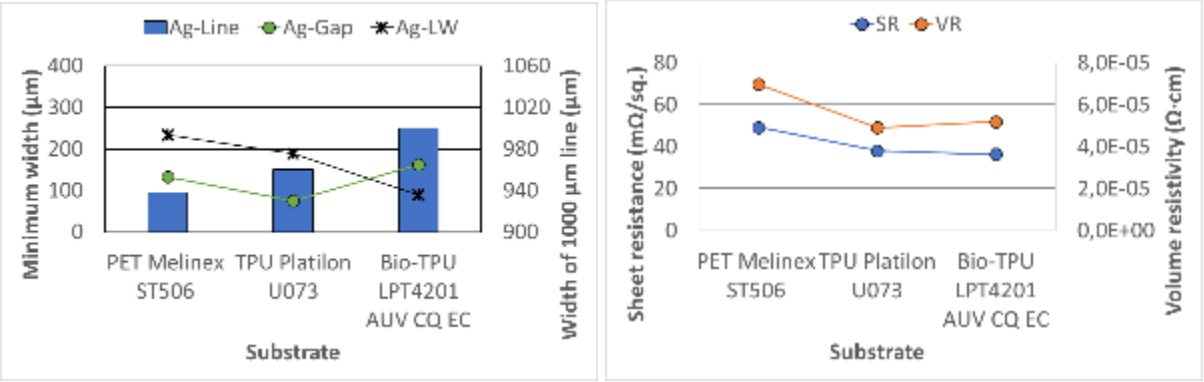

Figure 11. Minimum conductive line width (Line), reproducible gap width (Gap), and measured line width (LW) (left) and sheet resistance as well as volume resistivity values (right) on TPU substrates.

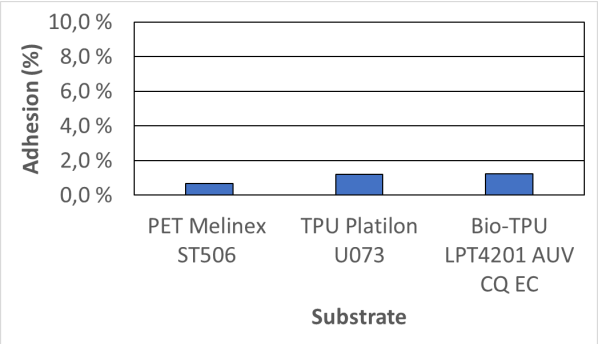

Figure 12. Silver ink adhesion to TPU substrates.

As shown in Figure 13, the multilayer printing most likely could face difficulties with Bio-TPU substrate because the repetition length was over 2 mm longer than designed.

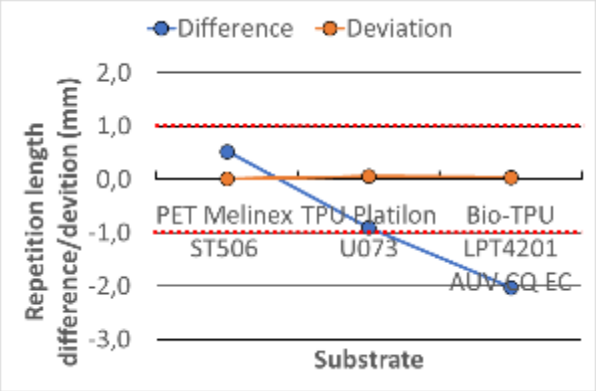

Figure 13. Deviation from the original repetition length and deviation of the repetition length in the case of stretchable TPU substrates.

Conclusions:

Bioplastics can be used to replace fossil-based PET substrate in R2R printing. The printability, print quality, and detail rendering on bioplastics are similar to that achieved on PET. With silver ink, the conductivity is even higher on bioplastics than on PET because of their higher substrate roughness that increases the number of particle-to-particle contacts.

However, bioplastics do have also some limitations. Typically, their thermal stability is not as good as with PET and process-related surface grooves causes ink to flow along them, thus creating print defects. In addition, Bio-TPU suffered from poor ink wetting and levelling as well as ink splashing, thus decreasing the print quality and detail rendering. Carbon ink, for its part, had poor adhesion to PLA substrate with high ink spreading, i.e. poorer detail rendering. In addition, with Loimu, Natureflex, and Bio-TPU substrates, the repetition lengths differed over 1 mm from the original repetition length, thus making the printing of multilayer structures in register difficult. This comes from the fact that the adjustment tolerances of the printing process are reached, and the dimensions of the overprinted ink layer cannot match the dimensions of the underlying layer.

2.1.2 Substrate testing at TNO

Printability tests for Sheet to Sheet process at A4 size on CumaPET 1704R (CumaPET), Brightplus Loimu (Loimu) and Hexpol TPZ (Hexpol) were not ready for reporting in D1.4, as pointed out in

Table 5.

Table 5. Summary of the work reported by TNO in D1.4. Printability assessment was not performed by TNO since the PET version received was not thermally stable enough to meet the ink's curing temperature requirements (120 °C for 10 minutes). The CumaPET substrate changes in colour during the curing step. Shrinkage needed to be verified before continuing to printability testing.

Table 5. Summary of the work reported by TNO in D1.4.

Substrate	Tests carried out	Linkage to pilots
PLA Luminy L175 (Total Corbion)	Heat shrinkage, printability	Pilots #1.3 and #2.3
Bio-PET Eastlon CB602AB	Heat shrinkage, printability	Pilots #1.2 and #3.3
Cuma-PET 1704R (chemically recycled PET, Dufor Polyester Specialities)	Heat shrinkage,	Pilot #2.3 thermoforming
Brightplus Loimu Tough heat	Heat shrinkage, *printability?*	Pilots #1.3 and #2.3
Durabio D5380R	Heat shrinkage, printability	Pilot #2.3
Ecozen T95G	Heat shrinkage, printability	Pilot #2.3
Bio-TPU Estane Eco 12T80E (Lubrizol)	Printability	Pilot #3.3
Bio-TPE Chemiton® LSA_NA70 (Franplast)	Printability	Pilot #3.3
Hexpol TPZ	*printability?*	Pilot #3.3
Natureflex NP42 (Commercial film with thickness of 42 µm, Futamura)	Heat shrinkage	Pilots #1.3 Luminaire or #3.1
PEF film from Avantium/ARNP	Thermal stability, printability	Pilot #1.3

For the CumaPet there was no printability testing as the thermal stability results were not good; therefore, it did not make sense to continue with printing.

New results from TNO after the delivery of D1.4 are presented below.

2.1.2.1 Loimu

For the Loimu material there was no printability testing as the thermal stability results were not good. Nevertheless, thermal stability of Loimu substrate was tested with the procedure described in Appendix 1 in D1.4. The result of the shrinkage test is presented in *Table 6*. Current version of material was not thermally stable enough to meet the ink's curing temperature requirements (120 °C for 10 minutes). Therefore, printability was not assessed.

Table 6. Thermal stability of Loimu in shrinkage test.

Shrinkage test	80 °C for 30 min	100 °C for 30 min	120 °C for 30 min
Warpage present already at 80 °C (specifically in "semi-transparent" region where there is less material)	 MD:<3.0% TD:<1.0%	 MD:<5.5% TD:<1.0%	 MD:<9.0% TD:<1.0%

2.1.2.2 Hexpol

TNO carried out the printability tests for Hexpol substrate, and the procedure is described in Appendix 1 of D1.4. Summary of the results of optical characterization is presented in Table 7. Summary of the results of mechanical characterisation of Hexpol in presented in Table 8.

Table 7. The results optical characterisation of Hexpol substrate.

Optical characterisation		
Feature 1	Feature 2	Full square areas
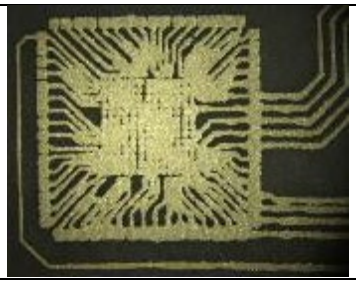	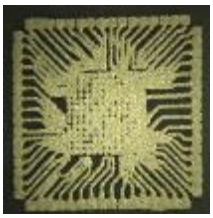	

Table 8. The results of mechanical characterisation of Hexpol.

Mechanical characterisation	
Cyclic loading results after 1000 cycles	Resistance vs. cycle
Residual strain: 5.95% Initial resistance: 15.69 Ω Resistance after cycle 1: 25.10 Ω Resistance after cycle 1000 with 30 seconds of relaxation: 102.39 Ω	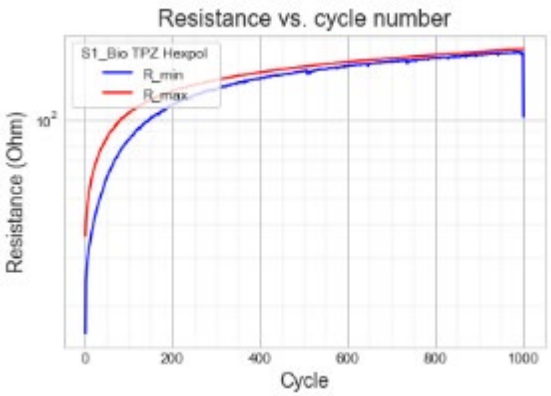

Reference TPU

For comparison, the reference TPU is TE-11C from Celanese (substrate comes with liner). Summary of the results of optical characterization is presented in Table 9. Summary of the results of mechanical characterisation is presented in

Table 10.

Table 9. The results optical characterisation of reference TPU substrate.

Optical characterisation		
Feature 1	Feature 2	Full square areas
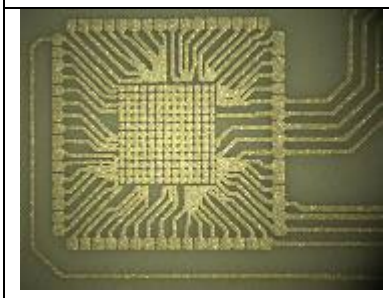	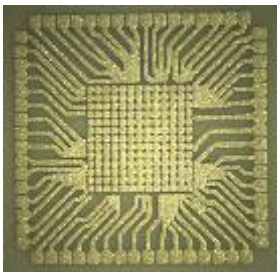	

Table 10. The results of mechanical characterisation of reference TPU substrate.

Mechanical characterisation	
Cyclic loading results after 1000 cycles	Resistance vs. cycle
Residual strain: 4.04% Initial resistance: 8.23 Ω Resistance after cycle 1: 12.11 Ω Resistance after cycle 1000 with 30 seconds of relaxation: 95.33 Ω	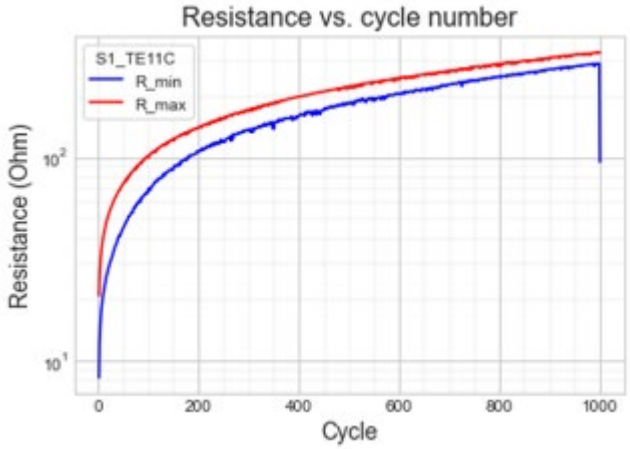

Conclusions:

- Liner could not be provided with the material foils. Consequently, swelling from wet ink interaction is to be expected and printability can't be fully assessed. For the material to be used in an application, liner must be provided as well.
- Ink spreading is seen, which leads to shape deformation and Ag tracks merging; however, this outcome is expected considering the standard printing settings used.
- Pinholes were not observed in full area features.
- Further printing optimisation is needed but, without a liner, a stable process will not be achieved.
- Residual strain after cyclic loading test is low (comparable to reference TPU substrates) but test was only performed on one sample. A definitive conclusion can only be given with more samples.
- Substrates show steady increasing resistance until 1000 cycles (similarly to reference TPUs). However, test was only performed on one sample. A definitive conclusion can only be given with more samples.

2.1.3 Substrate testing at CEA

Pilot #2.3 consists of two functional foils: one decorative and one technical/electronics that are assembled by injection moulding. One of the objectives within the project was to find alternatives to the standard material used as substrate for the foils, which is polycarbonate (PC). VTT was able to provide several such materials, and they were all tested by CEA for compatibility with the fabrication process of pilot #2.3. In D1.4 CEA reported the material testing results described in Table 11.

Table 11. Summary of the tests at CEA performed on VTT materials. Results are reported in D1.4.

Substrate	Tests carried out	Linkage to pilots
PLA Luminy L175 (Total Corbion)	Printability, thermoforming	Pilot #2.3
Bio-PET Eastlon CB602AB	Printability	Pilot #2.3
Cuma-PET 1704R (chemically recycled PET, Dufor Polyester Specialities)	Printability, thermoforming	Pilot #2.3
Durabio D5380R	Printability, thermoforming	Pilot #2.3
Ecozen T95G	Printability	Pilot #2.3

CEA received from VTT five different substrates (around 50 sheets of each):

- PLA (thickness 200 µm)
- Eastlon bio-PET (thickness 250 µm)
- CumaPET (recycled, thickness 250 µm)
- Durabio bio-based PC (thickness 250 µm)
- Ecozen (thickness 250 µm)

VTT provided glass transition information and input on thermal behaviour of the substrates during curing. The fabrication process of the foils is described by VTT in D1.4. Results reported by CEA in D1.4 are summarised in Table 11.

The fabrication steps of these two foils comprises a screen printing and a thermoforming step. The material validation process is described in D1.5. Other processing steps like pick-and-place and injection are studied in WP2 and WP3.

Preliminary results on the screen printing and thermoforming tests are reported in D1.4 and D1.5. The main results were the following:

- Foils have a wavy aspect due most certainly to the extrusion process. The foils can be used for the technical film, but they might need improvement for the decorative layer. However, for feasibility tests the quality of the foils should be acceptable. VTT to try to improve this aspect.
- Ecozen material is not selected for Pilot #2.3 because of large variations in thickness, which is problematic for thermoforming. The material also deteriorates during curing.
- Eastlon is not selected for Pilot #2.3 because it does not withstand the curing of the Ag ink.
- Characterisation and further tests continue on Durabio, PLA and CumaPET materials, with a focus on resolution and electrical properties. These are the materials that are reported in this document.

The following section describes the tests done after the release of D1.4.

2.1.3.1 Durabio, PLA and CumaPET

This section describes the tests carried out on Durabio, PLA and CumaPET that were performed after the release of D1.4.

Samples were fabricated using CEA's layout that was designed for testing material compatibility with thermoforming. For all the samples, the same commercial thermoformable Ag ink was used. This ink is already implemented in GEN1 of the pilot; therefore, its compatibility is already proven.

The layout consists of several patterns that are used for electrical and mechanical characterisation of the screen-printed materials, before and after thermoforming (Figure

14Figure 14). The patterns called “centre”, “arc” “souris” and “cone” allow measuring electrical resistance, track width and height, on 200 and 400 µm wide tracks. They allow to verify dispersion on the foil. They are placed in regions where the foil is not thermoformed. A printed pattern is shown on the left side of the layout. The other larger patterns correspond to various deformation geometries and percentages of elongation. A picture of a standard PC foil is shown on the right in Figure 14.

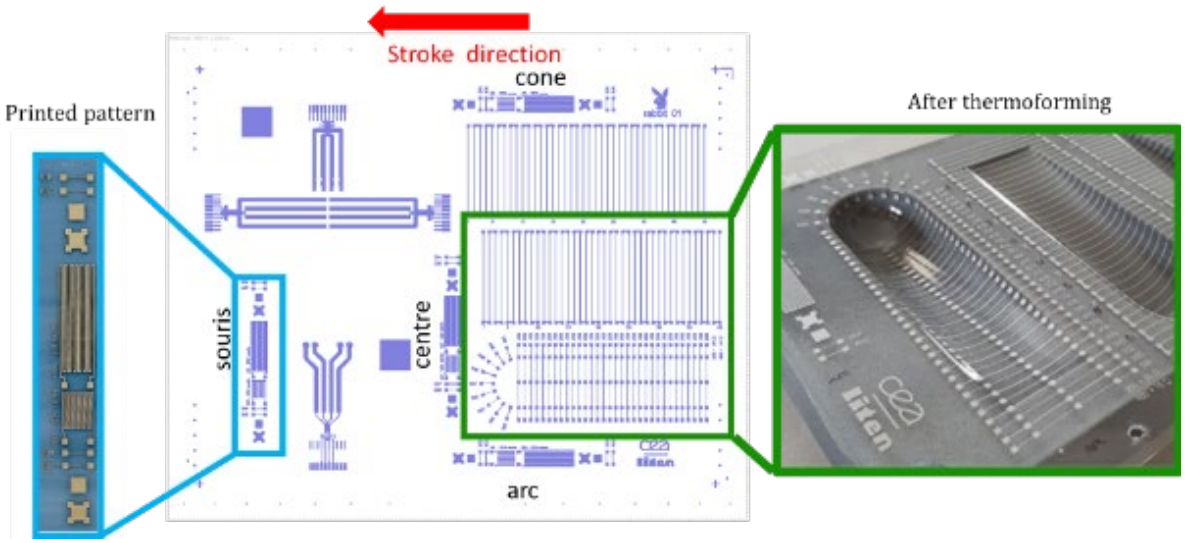

Figure 14: Printed and thermoformed patterns and the layout that is used for thermoforming validation.

A first screen printing run was carried out with the aim of checking ink compatibility with the substrates and film behaviour during printing and curing of the ink. In this first run an old screen and ink were used, and standard curing conditions (optimised for the reference PC material) were applied. The experiment is repeated on 5 sheets of each material and results were compared with standard PC foils processed in the same conditions. As an example of the collected results, Figure 15 Figure 15: Resistance values of 200 µm wide tracks on different substrates compared to the reference substrate, named stdPC.shows the resistance measured on the four patterns placed across the sheet, for track width of 200 µm. The values correspond to an average over the 5 sheets. The figure shows that there is little dispersion across the sheet. The average values are higher than expected, we suppose this is due to the screen and ink quality. It was also noted that PC and Durabio show very similar behaviour. The observations on the 400 µm tracks are similar.

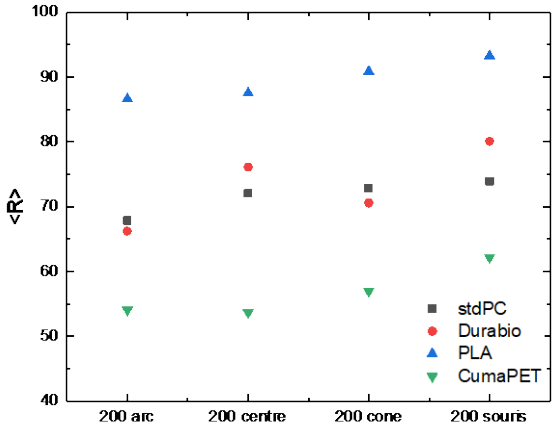

Figure 15: Resistance values of 200 µm wide tracks on different substrates compared to the reference substrate, named stdPC.

The geometry of the tracks is analysed as well (Figure 16). By measuring the track width, it was noted an average around 250 µm for a theoretical value of 200 µm. The print quality with this ink is quite acceptable; the patterns are well defined and equally spaced on all the three substrates.

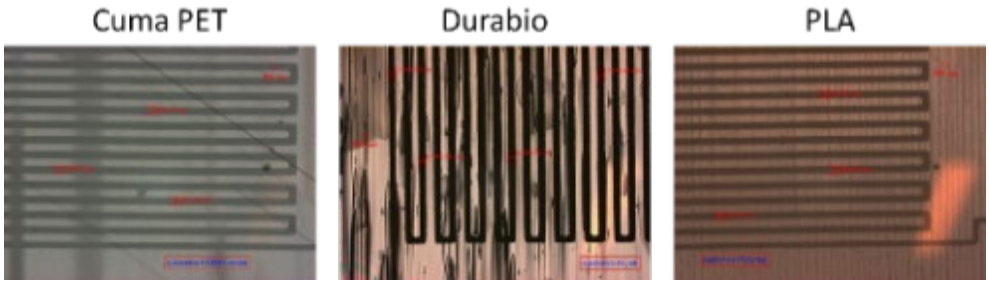

Figure 16: Microscope images of 200 µm wide tracks on Cuma PET Durabio and PLA. These images are used to determine track width and print quality.

The main conclusion of this first run of screen printing is that all the materials seem to be compatible with the process. PLA seems unaffected by the curing conditions; however Durabio and Cuma PET show some deformation. Durabio is an encouraging alternative to PC, as resistance and track geometry values are quite similar on the two substrates.

A second run of screen printing of Ag ink was carried out on the Durabio substrate with the aim of optimising the curing conditions of the ink and preserve the substrate.

A new screen and ink were used for these experiments. Screen printing was done on two substrates: the reference PC with standard curing conditions and Durabio. The curing conditions for Durabio were the following:

120 °C for 20 minutes for Durabio
100 °C for 30, 60 or 90 minutes on Durabio

The experiments were repeated on three sheets for each curing condition.

Again, the four patterns are exploited. Figure 17 shows the resistance values versus curing conditions of Durabio foils, for sake of simplicity on a single pattern, highlighted on the layout. The analysis of the other patterns gave similar conclusions. The upper part was plotted for track width of 400 µm, while the lower part is for the 200 µm track width. The coloured plain lines represent the resistance values, averaged on 3 PC foils and 3 Durabio foils processed using standard curing conditions. In the case of 400 tracks on the “arc” pattern, the average R is slightly different: 35 Ω for standard PC and 38 Ω for Durabio. For the 200 µm wide tracks, the average R is of 40 Ω in the same curing conditions. A small variation of the resistance is

observed of 2-3 Ω from one sheet to another, an acceptable value for the present application. The curing times of 60 and 90 minutes give the results closest to the reference, and with little or no gain when increasing curing time, therefore we concluded that curing at 100 °C for 60 minutes are optimal conditions for the Durabio substrate.

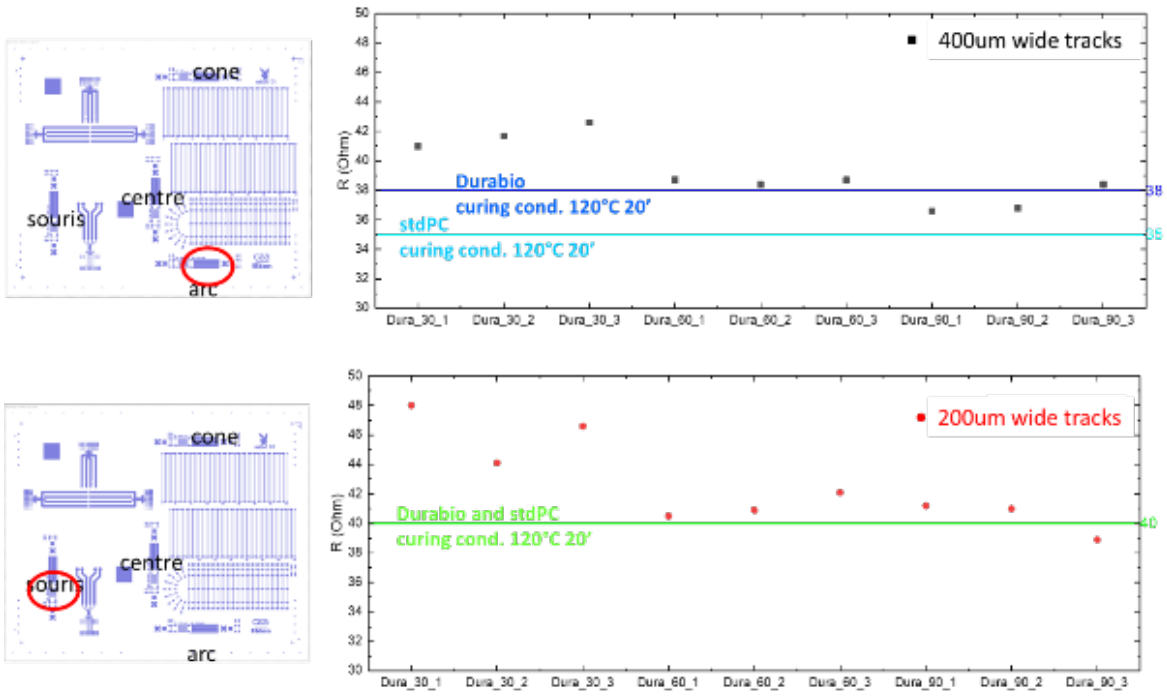

Figure 17: Resistance values measured on two patterns: 400 µm wide "arc" pattern and 200 µm wide "souris" pattern versus curing conditions.

Some geometrical features of the tracks were looked to as well. The Figure 18 shows profilometer plots of 200 µm and 400 µm wide tracks for the various processing conditions. It is obvious that the track geometry is not dependent on the curing of the ink.

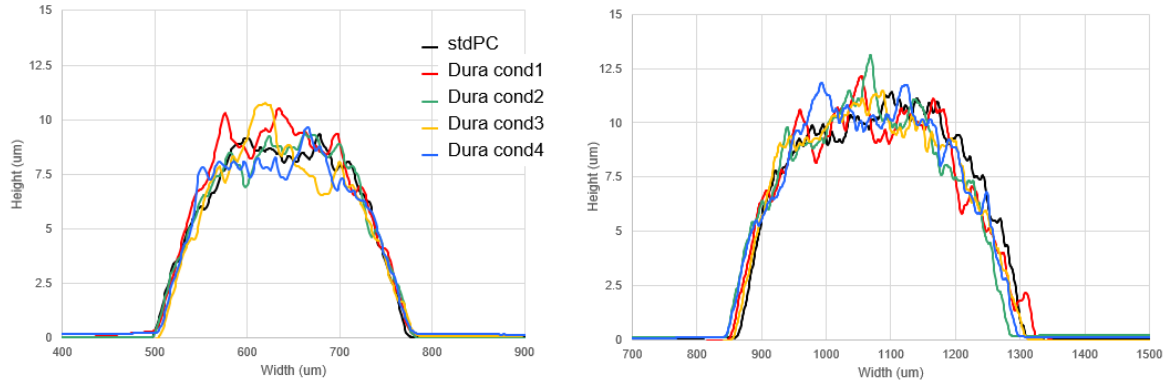

Figure 18: Track height of 200 µm and 400 µm wide patterns. The various colours correspond to different curing conditions.

Thermoforming tests were carried out in parallel. Based on the Tg values provided by VTT, various conditions were selected and tested on each material. The main conclusions are the following:

PLA

Tests on virgin films at various thermoforming conditions (90 and 96 °C) show that it is not thermoformable. The foils do not withstand the applied pressure and break.

Cuma PET

Thermoforming temperatures were 85 and 88 °C.

Tests on virgin films: thermoforming conditions tuned and process validated.

Tests on films that have screen printed Ag (cured at 120 °C): films are brittle and cannot withstand the forming process.

Durabio

Thermoforming temperatures were 100 and 106 °C.

Tests on virgin films: thermoforming conditions tuned and process validated.

Tests on films that have screen printed Ag (cured at 120 °C): process validated. Elongation values are equivalent to those on standard PC being up to 31.5 %.

Conclusions:

Five substrates were provided by VTT. In preliminary tests several issues emerged on Eastlon and Ecozen -> substrates were eliminated.

Screen-printing and thermoforming tests of Ag tracks were made only on CumaPET, PLA and Durabio. CumaPET turns white (not compatible with decorative film) and would require a very low curing temperature. PLA is not thermoformable. For Durabio, printing was OK, but curing conditions had to be optimized. Thermoforming worked OK.

Perspectives:

Check the printing of dielectric on top of Ag to validate stacking of printed layers on this substrate

Integrate in GEN2 device of Pilot #2.3.

2.1.4 Substrate fabrication at ARNP

2.1.4.1 Fabrication method for PEF film

The PEF substrate was fabricated by ARNP using the film processing facility of one of ARNP's partner. PEF was used in granulate form and processed into films using a cast film line.

It was not clear which IV[1] of PEF would be most suitable to make printable PEF cast film with suitable thermal properties with a shrinkage target <1% (at 120 °C). Therefore, the PEF film was produced in 3 different IV's: low, medium and high (15 kg for each IV) and the best film was selected based on its aspects and thermal stability performances.

All PEF materials were pre-dried before cast film extrusion at 140 °C for 16 h under dry air with a dryer. The equipment used included three extruders in ABC setup with A and C both

[1] IV is an abbreviation of Intrinsic Viscosity, referring to a measure of polymer's molecular weight and its ability to flow, which in turn indicates the material's strength. A higher IV means the polymer has a greater molecular weight and is more resistant to cracking and tearing.

25 mm single screw extruders and B the middle layer with 30 mm single screw extruder. The same PEF material was running in the three extruders at once to produce PEF monolayer films. The screw geometry used for the trials is designed for melt processing of polyesters. The three extruders were connected to a manifold and equipped with a 300 mm wide sheet die with adjustable die gap.

Furthermore, three temperature-controlled, glossy chill rolls with adjustable line speed were used after the sheet die. The main parameters and notes are presented in Table 12. Edge trimming equipment was used to cut the thicker edges of the PEF rolls to provide the film with the most even thickness distribution.

Table 12. Parameters used for small scale cast film extrusion trials.

Material	Melt T extruders, °C	Manifold and Die T, °C	Chill rolls T, °C	Film thickness, µm	Shrinkage at 120°C, %	Film suitable for further printability tests
PEF low IV	250–260	250	60, 73, 75	300	< 1	Yes
PEF medium IV	250–260	250	60, 73, 75	300	> 1	No
PEF high IV	250–260	250	60, 73, 75	300	> 1	No

The selected PEF cast film was the film made with the low IV PEF because it displayed the best thickness distribution and the lowest shrinkage at 120 °C.

- Width: 235 mm (after slitting of the thicker edges)
- Thickness: 297 µm (± 4 µm)
- Thermal stability test done at 120 ºC for 30 min (10x10 cm square placed in a convection oven): MD 0.65 %, TD 0.75 % (average of 2 measurements).

The films were shared with both TNO and CEA. At the time of finishing this delivery, their evaluation is ongoing, so testing results are not available for reporting in D1.6. The substrates will be used in selected pilots and further reporting of their performance will be done within WP3 deliverables.

2.2 Cellulose based (paper, cartonboard) & wood-based substrates

A list of cellulose-based and other substrates developed by different partners in Sustronics is presented in Table 13. Development of two of the initially specified materials, namely UPMFormiEcoAce SPB40 (Bio-PP base) and UPMFormiEcoAce HPB40 (Bio-PP base), was discontinued, since they were found unsuitable for any of the project pilots (explained in D1.4). A detailed description of the cellulose-based and other substrates testing is presented in the following sub-sections per material.

Table 13. Cellulose and other substrates developed in the Sustronics project.

Technology	Owners	Sustainability claims						Pilots targeted									
		Bio-based	Renewable	Recycled	Sustainable sourcing[1]	EoL: Recyclable	EoL: Compostable	Pilot#1.1	Pilot#1.2	Pilot#1.3	Pilot#2.1	Pilot#2.2	Pilot#2.3	Pilot#3.1a	Pilot#3.1b	Pilot#3.2	Pilot#3.3
Cellulose based (paper, cartonboard) & wood based	• TER: own commercial & experimental • TNO: commercial	X	X			X	X		X	X	X	X		X	X	X	
Nanocellulose film or foam	• VTT: own experimental	X	X			X	X			X		X		X	X		
Plastics	• UPM: own commercial & experimental • CAN: commercial • PIEP: LDS		X			X				X	X			X			

2.2.1 Substrate testing at VTT

In this project different types of cellulose-based substrates were to be tested. In Table 14 the summary of the substrate testing is presented.

Table 14. Summary of the work reported by VTT in D1.4.

Substrate	Tests carried out	Linkage to pilots
Semi-transparent mechanically nanofibrillated cellulose film (NFC-film)	Spotlight scattering	Pilots #1.3, #2.2, #3.1a and #3.1b
Blotting board		
Partially dissolved blotting board		
Foam formed fibre mat		

Summary of the work after the release of D1.4 made at VTT in Table 15 shows the manufactured CNF-based materials for optical diffuser testing. Developed materials were based on materials reported in D1.4. Aim was to create a CNF-based material with suitable transmission and scattering properties.

2.2.1.1 NFC-film

Semi-transparent mechanically nanofibrillated cellulose films (NFC-film) were obtained by processing bleached Finnish hardwood (birch) pulp. The CNF films were prepared from the CNF-suspension using VTT's nanocellulose film manufactured at VTT with VTT's pilot scale concept in Espoo, Finland. Summary of the work is presented in Table 15 below.

Table 15. Summary of the work made at VTT Espoo after the release of D1.4.

Substrate	Tests carried out	Linkage to pilots
CNF (pure)	Optical properties: • Light transmission • Light scattering	Pilot #1.3
CNF + TiO_2		
CNF + support substrate		
CNF+TiO_2 +support substrate		

Figure 19 shows the measurement device for optical transmission testing and Figure 20 shows results for transmission spectra. CNF has good transmission properties. Addition of TiO_2 and increasing the film thickness result in decrease in transmission. The results for scattering spectra are shown Figure 21.

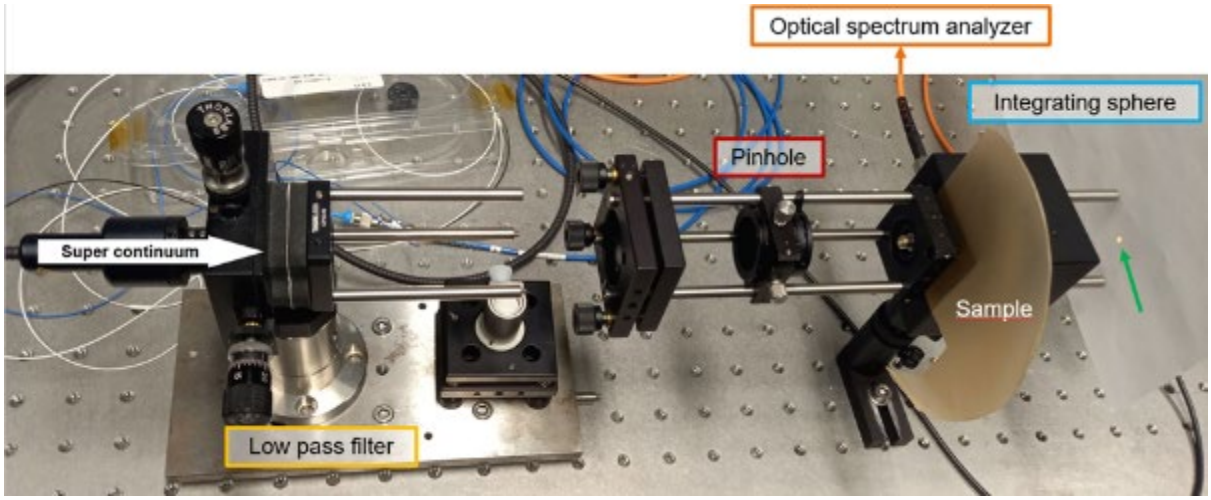

Figure 19. Measurement device for optical transmission testing.

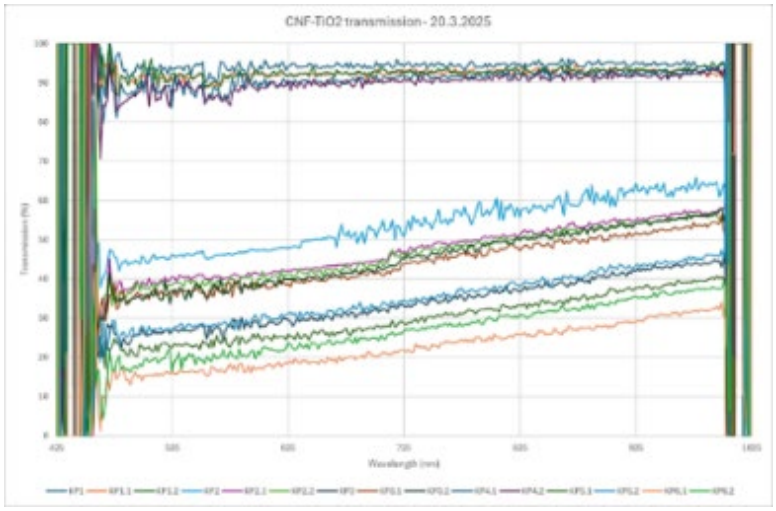

Figure 20. Results for transmission spectra measurement.

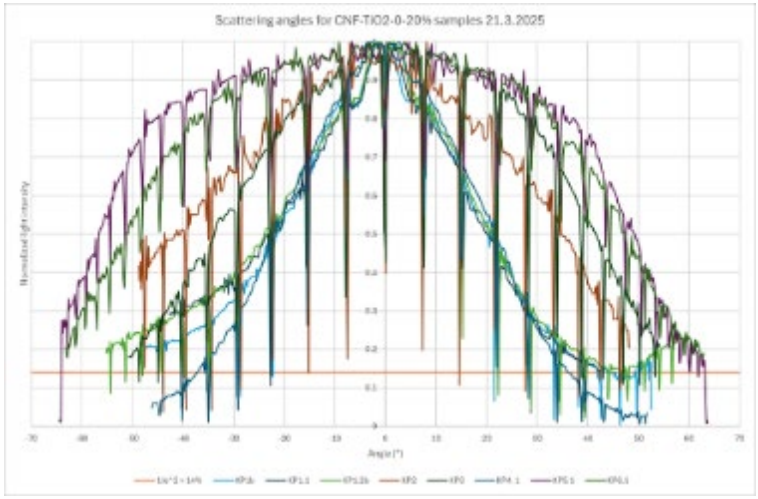

Figure 21. Results for scattering spectra measurement.

Measurements demonstrate that with suitable combination of CNF and TiO_2 it is possible to find a good balance between transmission and light scattering. Aim is to have approximately at least 60 % transmission with 80° diffusion angle. Next step is to optimise the TiO_2 content for functional prototype.

Table 16

Table 16 (Printability testing at VTT) shows the properties of the selected paper-based substrates for rotary screen-printing trials at VTT Oulu. The substrate properties were measured before the R2R printing trials using the same methods as the ones described in Chapter 3.1.1.

Table 16. Printability testing at VTT after the release of D1.4.

Substrate	Tests carried out	Linkage to pilots
PET Melinex ST506 (Ref.)	Substrate characterisation R_a roughness - white-light interferometer Surface energy and contact angle with water - contact angle meter Transmission - UV-Vis Thermal stability in the convection oven – visual inspection Printability Printability and print quality – visual inspection, microscope Ink spreading, minimum gap width - microscope Minimum conductive line width – digital multimeter Sheet resistance and volume resistivity - digital multimeter and calculation Tape adhesion - digital multimeter Layer thickness - surface profilometer	Reference material corresponding to state-of-the-art printed electronics
Translucent SYLVICTA paper from Fedrigoni Special Papers		-
Coated paper (Ref.)		-
Tervakoski 021528 paper		Pilot #3.1a

Table 17 Table 17shows the properties of the selected paper-based substrates for rotary screen printing trials at VTT Oulu. The substrate properties were measured before the R2R printing trials using the same methods as in Chapter 3.1.1. All the substrates showed excellent thermal stability with good surface energy and contact angles. Paper-based substrates were much rougher than the reference PET foil. Translucent paper had the highest roughness, and the smoothest paper-based substrate was Tervakoski paper. As expected, the transmission of the papers was low, but the translucent paper had much higher transmission.

Table 17. Properties of the paper-based and reference substrates. Both commercial (COM) and pilot-scale manufactured substrates were used. Substrates that were printed in R2R environment are marked with bold font. Yellow accent colour means that some property of the substrate can have a bad effect on printability or the final application.

Substrate	Thickness (µm)	Ra roughness (nm)	Transmission 400-800 nm (%)	Surface energy (mN/m)		Contact angle with water (°)	Thermal stability
PET Melinex ST506 (Ref., COM)	125	8	89.5	46.3		68.1	140 °C
Translucent paper - SYLVICTA, 145 gsm (COM)	112	3837	70.0	42.4		73.1	140 °C
Coated paper, 90gms (Ref., COM)	68	2090	13.2	47.5		84.8	140 °C
Tervakoski 021528 paper	50	595	17.5	47.5		74.9	140 °C

Paper-based substrates were printed with VTT's ROKO printing line using rotary screen printing. Both Ag (Asahi LS-411AW) and C (Loctite EDAG PF-407A) inks were printed using the same layout as with the bioplastics (see Chapter 2.1.1. and Figure 1). These substrates were thermally pre-treated at 120 °C before the printing at the speed of 2 m/min. The mesh count of the screens were 305 lines/inch and 215 lines/inch with Ag and C inks, respectively. Silver ink was printed at the speed of 2 m/min and carbon ink was printed at the speed of 3 m/min. The printed layers were dried at 120 °C, thus making the dwell time in the ovens to be 2.4-3.0 min. Similar printability and print quality analysis was performed as in the case of bioplastics (see Chapter 2.1.1.)

Translucent paper and Tervakoski paper showed both some printability and print quality issues although both substrates could be properly printed in the R2R process (Figure 22 and Figure 23). The Ag ink did not transfer properly onto the translucent paper, thus creating holes in the printed layer, and the printing unit required heavy adjustments to start the ink transfer. In addition, the C ink tended to splash and spread on the translucent paper, thus decreasing the print quality and detail rendering. With Tervakoski paper, the printing process went smoothly with both inks, but the microscopic analysis showed that the silver ink had some ink transfer issues resulting in pinholes and thinner parts. It seemed that the high porosity of the Tervakoski paper caused the smaller ink flakes to be absorbed into the paper matrix, thus leaving larger flakes onto the surface (Figure 24).

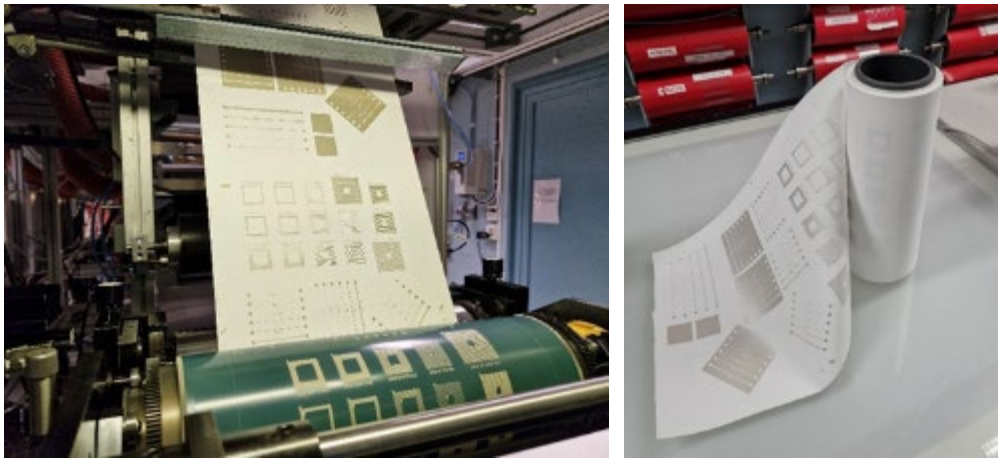

Figure 22. Rotary screen printing of Asahi LS-411AW silver ink onto Tervakoski paper (left) and printed test patterns on Tervakoski paper (right).

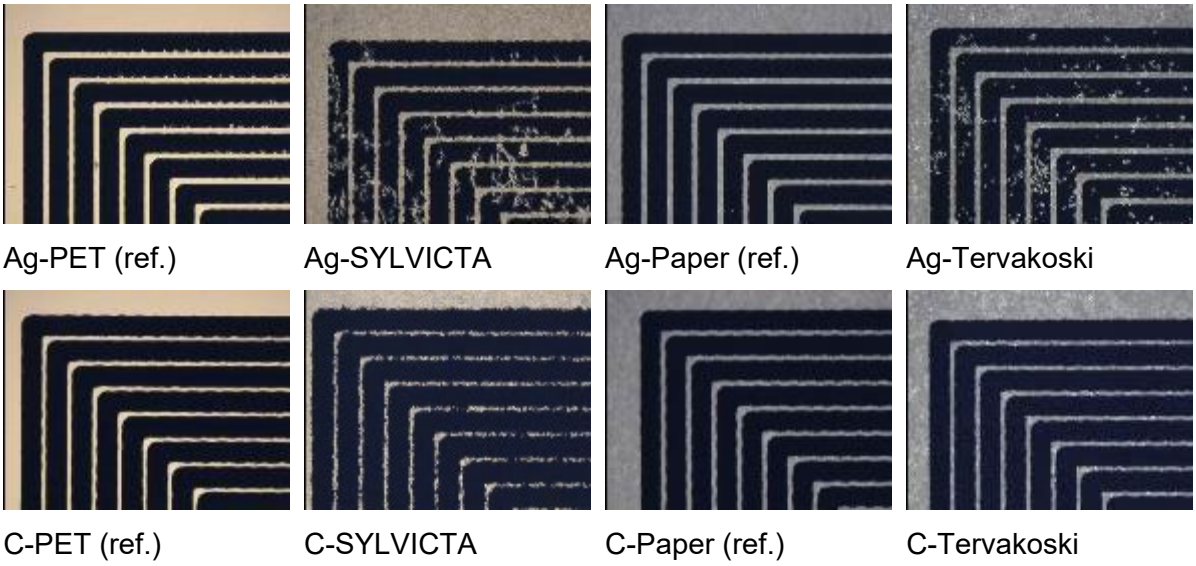

Figure 23. Quality of the printed antenna pattern (line-gap: 500-100 µm) on paper-based substrates using LS-411AW Ag ink (top) and EDAG PF-407A C ink (bottom). The mesh count of the screen was either 305 lines/inch (Ag) or 215 lines/inch (C). The magnification is x37.7.

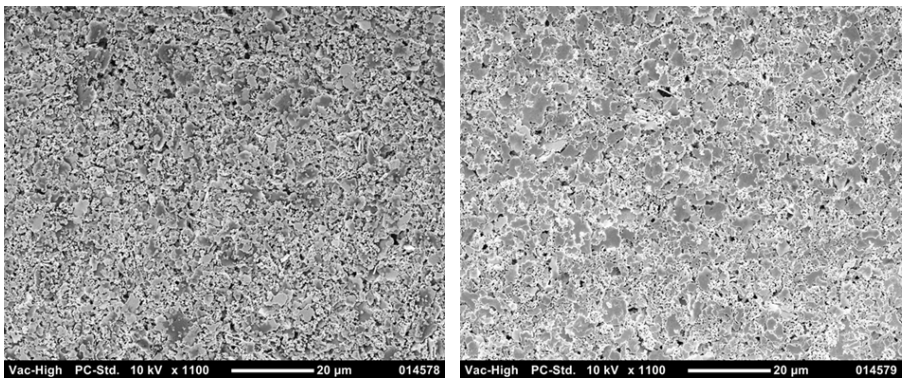

Figure 24. SEM images of the surface of the silver layer printed onto reference paper (left) and onto Tervakoski paper (right). More larger flakes are seen on Tervakoski paper. The magnification is x1100 and the scale bar is 20 µm.

Figure 25 shows the detail rendering of Ag and C inks on paper-based substrates. Due to the poor Ag ink transfer and holes in the printed layer, the minimum conductive line widths with the translucent and Tervakoski papers were significantly higher than with the reference substrates. The C ink, for its part, had ink splashing and ink spreading issues only with the translucent paper, thus increasing heavily its minimum gap width and measured line width. Less ink spreading was seen on the reference paper and Tervakoski paper with both inks, thus decreasing the minimum gap widths and measured line widths as compared to that with PET.

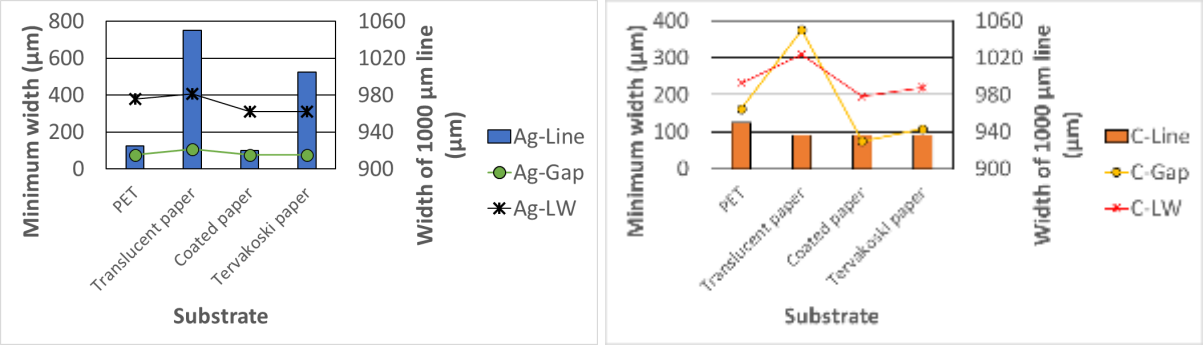

Figure 25. Detail rendering of the paper-based substrates using Ag (left) and C (right) inks.

Silver ink layers had high conductivity as seen in

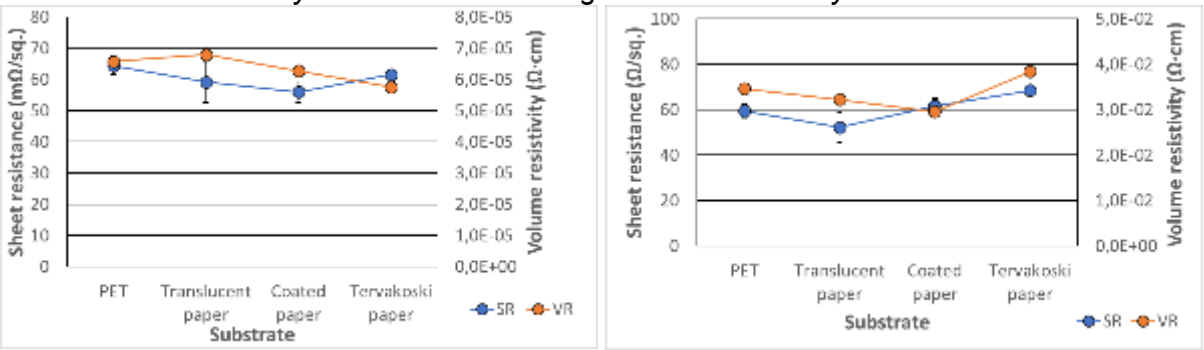

Figure 26. Higher conductivities were obtained on reference paper and on Tervakoski paper than on PET. This indicated that higher surface roughness was beneficial for the particle-to-particle contact formation. The lowest volume resistivity values were seen with Tervakoski paper despite of its ink transfer issues but the small particle penetration can aid in the particle-

to-particle contact formation. The ink transfer issues with the translucent paper increased the volume resistivity and the deviations in the sheet resistance. Figure 21 also shows the conductivity of the printed carbon layers. On translucent paper, the conductivity was better than on PET but the ink splashing increased the conductivity deviations. On Tervakoski paper, for its part, the conductivity was the poorest. Reference paper gave similar sheet resistance value than PET but much lower volume resistivity value meaning that carbon flakes could get into better contact with each other on porous substrate.

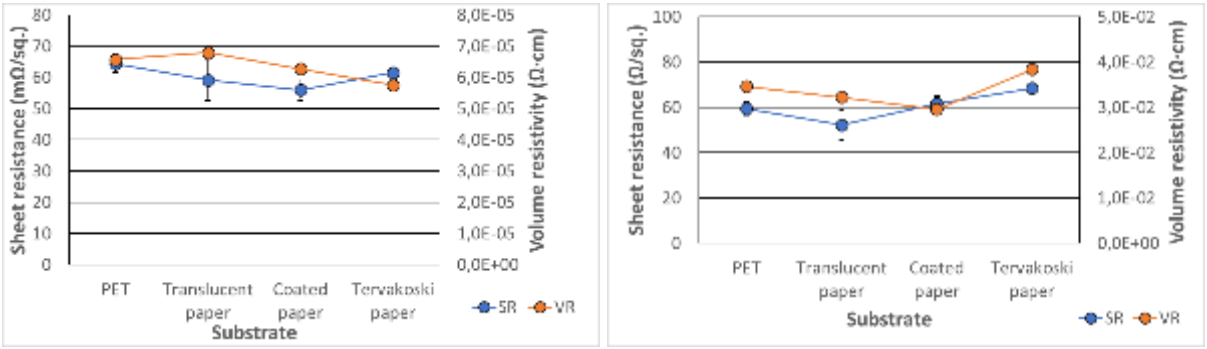

Figure 26. Sheet resistance and volume resistivity of printed layers on paper-based substrates using Ag (left) and C (right) inks.

Tape adhesion test could not be performed with the reference paper and Tervakoski paper since the tape peeled off the surface of the paper completely, as seen in Figure 27. The ink adhesion to the translucent paper was excellent and similar to that of the PET foil. Repetition length deviations were small, and the repetition lengths were less than 1 mm smaller than designed, thus making paper-based substrates suitable for multilayer printing (Figure 28).

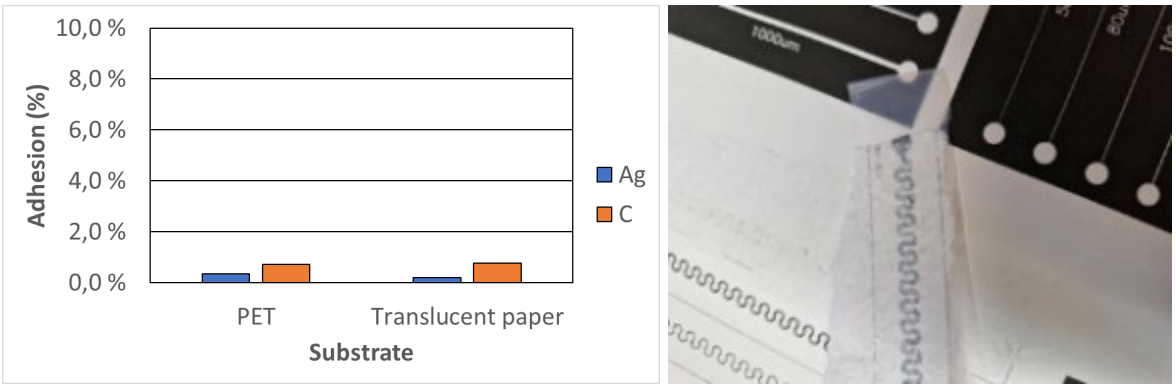

Figure 27. Ink adhesion to PET and translucent SYLVICTA paper (left) and total delamination of the paper surface during the tape test (right).

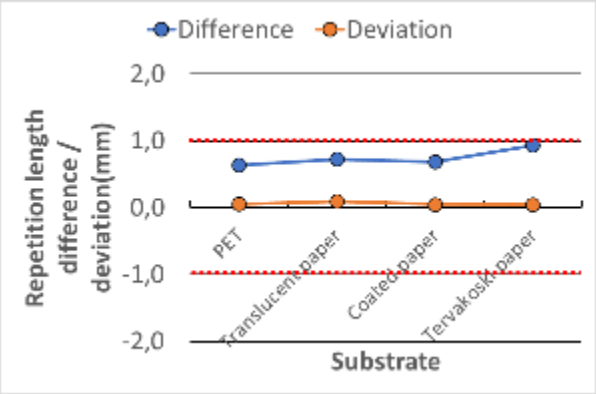

Figure 28. Deviation from the original repetition length and deviation of the repetition length in the case of paper-based substrates.

Conclusions:

Paper-based substrates show some limitations for the R2R printing. The Ag ink shows high conductivity on Tervakoski paper with good detail rendering, but the absorption/penetration of small ink particles or ink transfer issue increases the minimum conductive line width and impairs the visual quality. With the C ink, good detail rendering and printability is achieved on Tervakoski paper, but the conductivity is slightly poorer than with other paper-based substrates. Translucent paper suffers from poor ink transfer with the Ag ink and high ink spreading (poor detail rendering) with the C ink. However, these do not affect the conductivity much.

2.2.2 Substrate testing at PIEP

2.2.2.1 LDS materials in sensor module-Discard PCB board in favour of 3DMID

Initial tests were performed to adapt the best laser parameters to the materials. It was possible to see that all of them metallised. However, the PPA presented greater humidity absorption, common for this material. This created visual problems and oxidation of the circuit built. The same problem didn't occur in the PCs, so PPA will be dropped. The summary for the work reported by PIEP in D1.4 is presented in Table 18 below.

Table 18. Summary of the work reported by PIEP in D1.4.

Substrate	Tests carried out	Linkage to pilots
TECACOMP PPA LDS black 1014979 from Ensinger	Conductive test; visual inspection. 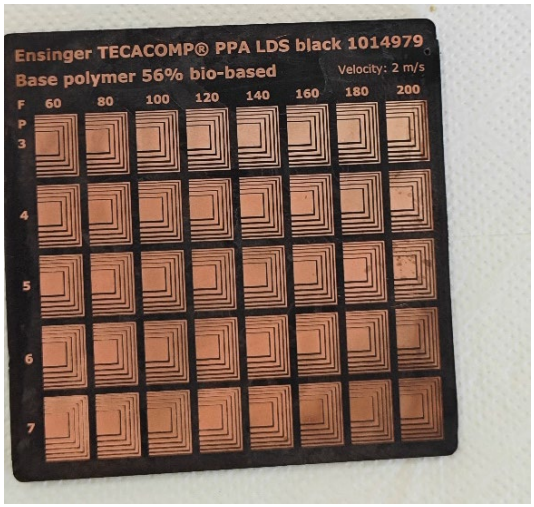 Bad quality of metallisation, oxidation.	Pilot # 2.1
PC LNP ELCRIN DX11355RC	Conductive test; visual inspection. 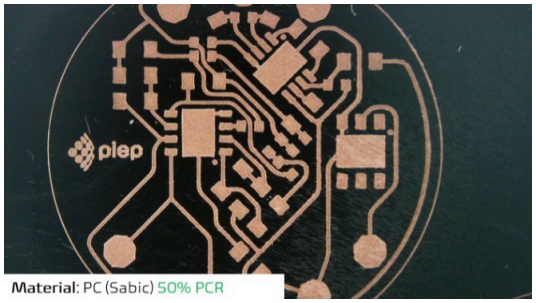 Good performance. Few short circuits.	Pilot # 2.1

PC XANTAR LDS 3760E from Mitsubishi	Conductive test; visual inspection. 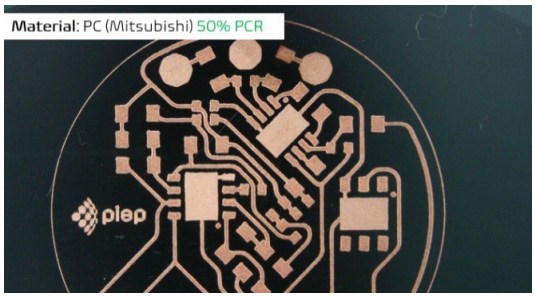 Good performance. Few short circuits.	Pilot # 2.1

New results from PIEP since the delivery of D1.4 are presented below.

Due to the existence of short circuits, the design of the circuit was improved by reducing the thickness of the traces, which helped to prevent the short circuits in specific areas (see Figure 29).

Before:

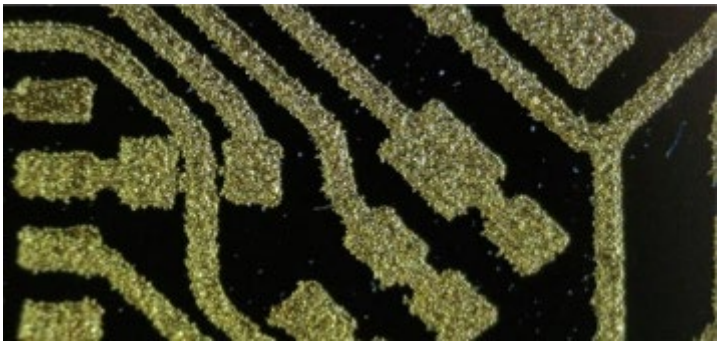

After:

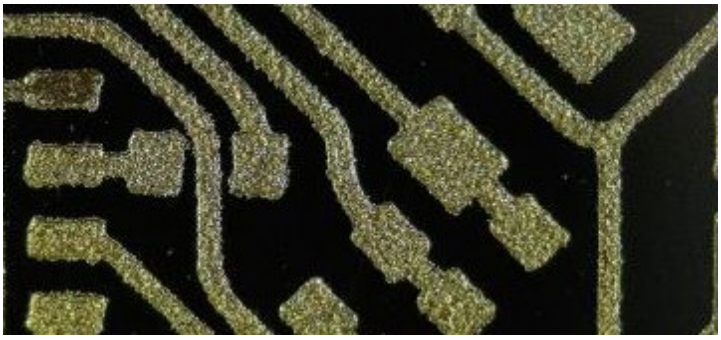

Figure 29. The design of the circuit improved by reducing the thickness of the traces. The top figure is before, and the bottom figure is after the improved design.

In addition, a new material was acquired to be used in the final prototypes as it has a light colour, which is preferred by Pilot # 2.1. The material is from the same family as the already tested Mitsubishi PC XANTAR LDS 3764E (the 3760 is black). However, due to delays in the delivery of this material, it was not tested yet, although the quality is expected to be the same as the black version already validated. As the laser interacts differently for white coloured materials, tests with white materials produced by additive manufacturing were performed. This way the quality of LDS could be evaluated in advance. The material tested was PC XANTAR LDS 3764 (the non-eco version), produced by Additive Manufacturing. Microscope image of the LDS circuit of Pilot # 2.1 in a disc produced by additive manufacturing is shown in Figure 30.

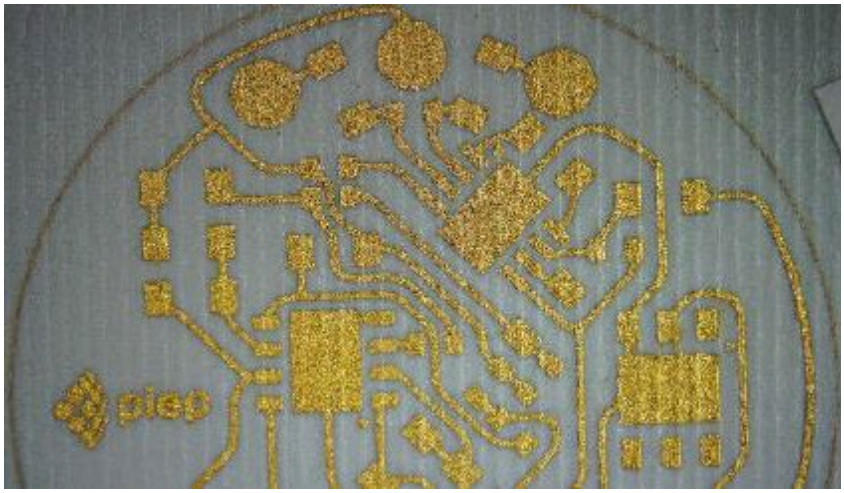

Figure 30. Microscope image of the LDS circuit of Pilot # 2.1 in a disc produced by additive manufacturing.

The existence of the wave form in the surface, common in additive manufactured pieces, was not a limitation. No short circuits or breaks were observed. Perspective of the size of the 0402 component to be assembled in the circuit produced by LDS is shown in Figure 31.

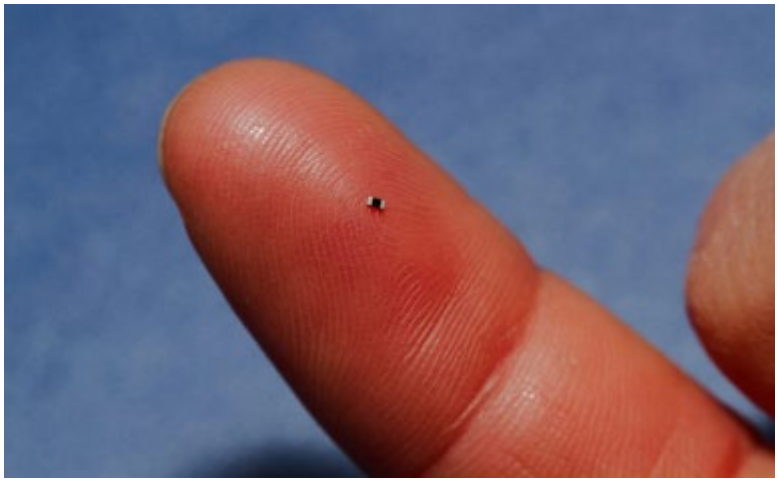

Figure 31. Perspective of the 0402 component to be assembled in the circuit produced by LDS.

Microscope image (size 2 x 2 mm) shows the circuit track with thickness of 0,16 mm passing through a 0402 component (1 x 0,5 mm) with no short circuits and well-defined dimensions (see Figure 32).

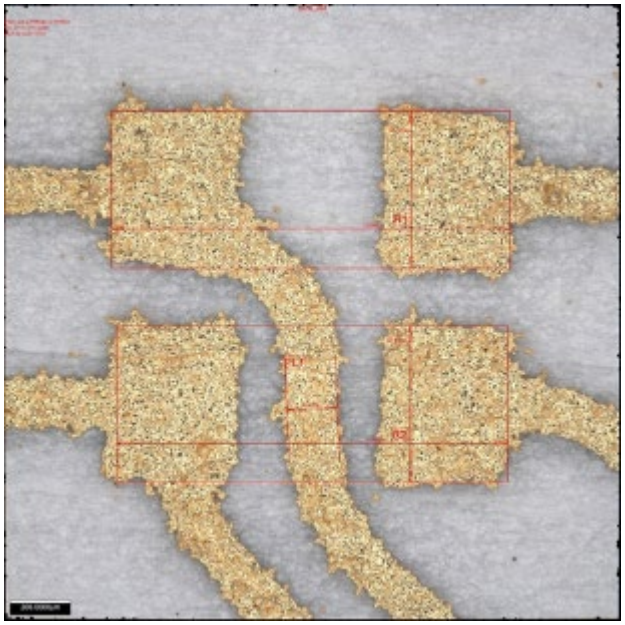

Figure 32. Microscope image (2 x 2 mm) showing the circuit track with thickness of 0,16 mm passing through a 0402 component (1 x 0,5 mm).

Conclusion:

The absence of short circuits, as well the existence of well-defined circuits supports the good expectations for the Mitsubishi Xantar LDS 3764E (white colour, eco version of the Polycarbonate grade acquired).

2.2.3 Substrate testing at TNO

2.2.3.1 PCR PET

Electromechanical tests

The material was a white polyester film with 40% post-consumer waste embedded (used in water bottles). Technical performance equals to fossil-based polyester. Replacing virgin raw materials with post-consumer raw materials enables to reduce sustainability targets (LCA calculations pending). TNO has carried out printability tests and the procedure is described in Appendix 1 of D1.4, and the testing results reported in D1.4. The results of optical and mechanical characterisation are presented in

Table 19

Table 19

Table 19 and in Figure 33 respectively.

Electromechanical tests related are profoundly reported in Juuso Puutio's MSc thesis, Electrochemical characterisation for wearable electronics.[2]

[2] https://urn.fi/URN:NBN:fi:tuni-202501061100

Table 19. Optical characterisation of printed circuits.

Optical characterisation				
Width (300 µm) / Pitch (600 µm) / Space (300 µm)	Square size (250 µm) - Space (200 µm)	Horizontal line width (500 µm)	Vertical line width (500 µm)	Diagonal line width (500 µm)
				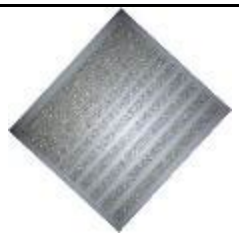
Width (200 µm) / Pitch (400 µm) / Space (200 µm)	Square size (250 µm) - Space (100 µm)	Horizontal line width (250 µm)	Vertical line width (250 µm)	Diagonal line width (250 µm)
				
Width (100 µm) / Pitch (200 µm) / Space (100 µm)	Square size (250 µm) - Space (50 µm)	Horizontal line width (150 µm)	Vertical line width (150 µm)	Diagonal line width (150 µm)
				

Mechanical characterisation	
Cross hatch	Dektak profile (Horizontal lines of 5 cm in length and widths of 100 µm, 500 µm and 1000 µm)
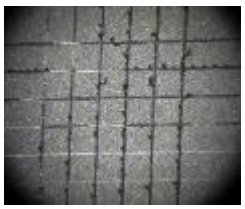 ISO/JIS classification:1	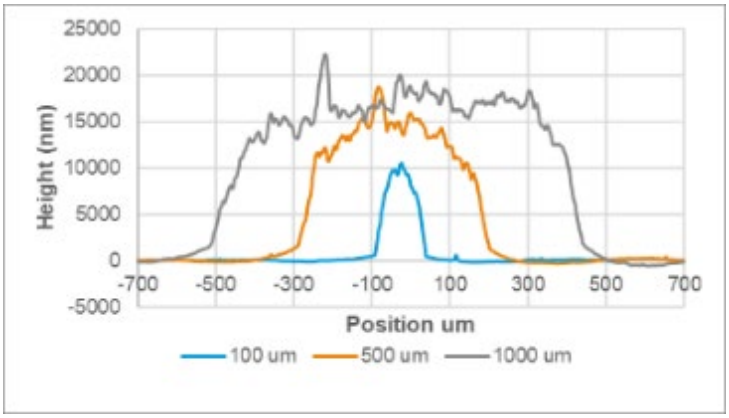

Figure 33. Mechanical characterization of printed circuits.

Conclusions:

- Ink adhesion is comparable to what is expected from industry standard flexible substrates like PET (polyethylene terephthalate).
- Ink spreading leads to shape deformation (circular shape instead of square-like) and to bad resolution in small features (100 µm in width and pitch); however, this outcome is expected considering the standard printing settings used and similar results seen in industry standard flexible substrates like PET.
- Overall printability is good.

This material is a possible candidate for a next generation of Pilot #3.3 on smart wound dressing or the Pilot #1.2 on personal care product. Pilot #2.2 is evaluating the technical performance in the application among other selected raw materials.

2.2.4 Substrate testing at RISE

Summary table for the work reported by RISE in D1.4 is presented in Table 20 below.

Table 20. Summary of the work reported by RISE in D1.4.

Substrate	Tests carried out	Linkage to pilots
Paper - 10005059 thinbarrier eco H-WS 45 gsm	Initial printability tests	Pilot #3.2
Paper - 10003899 thinbarrier eco M-2S-WS 30 gsm	Initial printability tests	Pilot #3.2

New results from RISE after the release of D1.4 are presented below.

2.2.4.1 Paper substrates from TER

Three paper substrates from TER have been tested and evaluated at RISE, primarily for use as a substrate material in the sensor labels in Pilot #3.2. The materials are:

- Thinbarrier eco H-WS 45 gsm
- Thinbarrier eco M-2S-WS 30 gsm
- Thinstar plus 45 gsm

Printability tests have been performed on paper substrates in sheet format by screen printing test patterns using a commercial silver ink, a DEK Horizon 03iX semi-automated flatbed screen printing machine and a Natgraph conveyer belt oven for thermal drying and UV curing. The specially developed test pattern includes various test structures including:

- Line test structures with varying line width (LW), line spacing (LS) and directions
- Vertical lines printed in the machine direction (MD), equivalent to the printing direction
- Horizonal lines printed in the transverse direction (TD), perpendicular to MD
- Test structures for sheet resistance and resistivity measurements
- Large rectangular features for cross-cut adhesion tests

Besides printing the ink directly on the substrate, the conductive ink was also printed on paper substrates with a global screen-printed dielectric layer since this is a relevant material stack for Pilot#3.2. One of the substrates, thinstar plus 45 gsm, has also been used in printability tests of inks for the sensing layers in temperature and humidity sensors, in the testing of screen-printed copper conductors as well as substrate for bonding of bare die microchips. Results from these tests are reported in other sections in this deliverable.

The printed test structures were inspected by optical microscopy and optical profilometry (Sensofar PLu neox 3D) to assess the dimensions and the quality of the printed features.

Cross-cut tests (ISO 2409) were done to investigate the adhesion of the printed layers to the substrate.

The sheet resistance of printed silver lines was investigated by performing 4-wire I-V measurements using a parameter analyser (Keithley 4200A-SCS) on special test structures. The actual dimensions of the printed test structures were measured to get accurate values of the sheet resistances.

Optical microscopy images of different printed line test structures with varying LW and LS are shown in Figure 34. Lines with 100 µm LW are of special interest as such features are needed for assembly of microchips in Pilot #3.2. Such lines can be printed with acceptable quality on all three substrates. However, the best results are clearly obtained with thinstar plus. The lines printed on the thinbarrier eco substrates have noticeable edge roughness while the lines on thinstar plus have very well-defined edges.

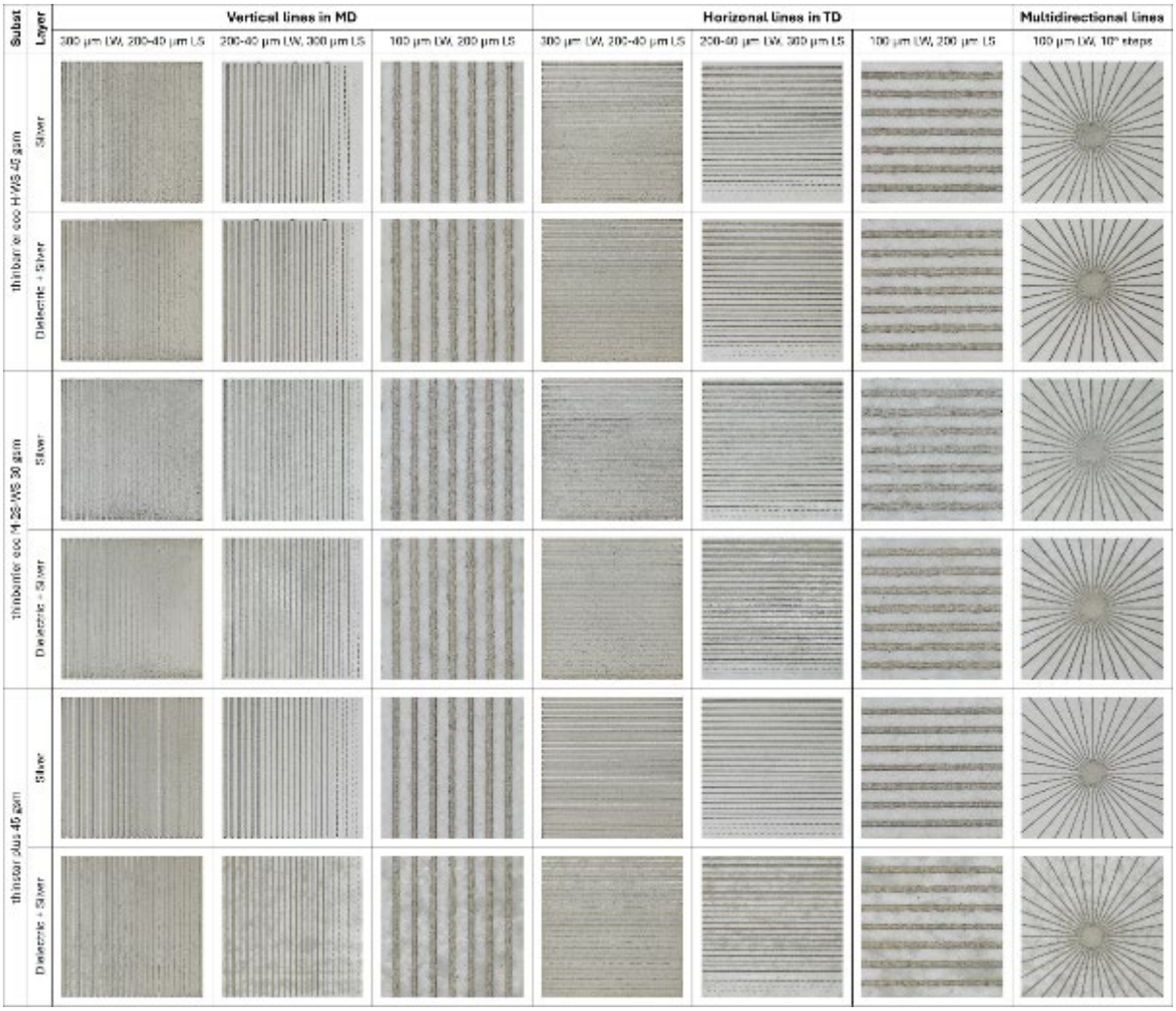

Figure 34: Optical microscopy images of different test patterns screen printed on the three tested substrates using a commercial silver ink. Silver ink was printed both directly on the paper substrates as well as on screen printed dielectric layer. The nominal LW and LS are indicated for each pattern.

Surface topography and profiles, measured by optical profilometry, of silver lines with 100 µm LW printed on dielectric coated substrates are shown in Figure 35. The unevenness and roughness of the dielectric coated paper substrates makes it challenging to acquire good quality images. However, it can be observed that the thinbarrier plus substrate is smoother and gives more uniform conductor profiles.

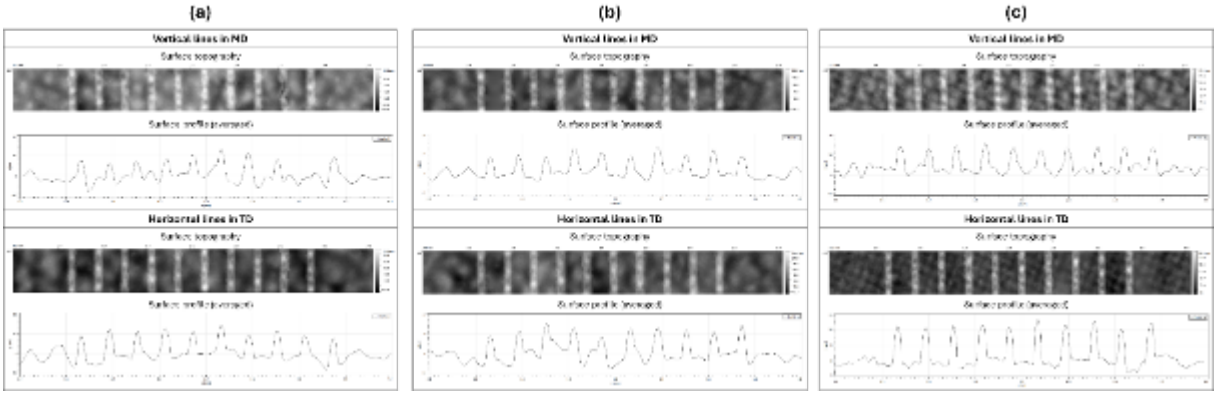

Figure 35. Results from optical profilometry of silver lines with 100 µm LW and 200 µm LW printed on substrates with dielectric coatings. (a) thinbarrier eco H-WS 45 gsm, (b) thinbarrier eco M-2S-WS 30 gsm, and (c) thinstar plus 45 gsm.

The widths of nominally (in design) 100 µm wide printed lines were measured by optical microscopy and the resulting average values are shown in Figure 36. The lines printed on the thinbarrier eco substrates are clearly wider than the lines printed on thinstar plus. Interestingly, the lines printed on dielectric coated substrates become somewhat wider. The orientation of the printed lines has minor influence of the line width.

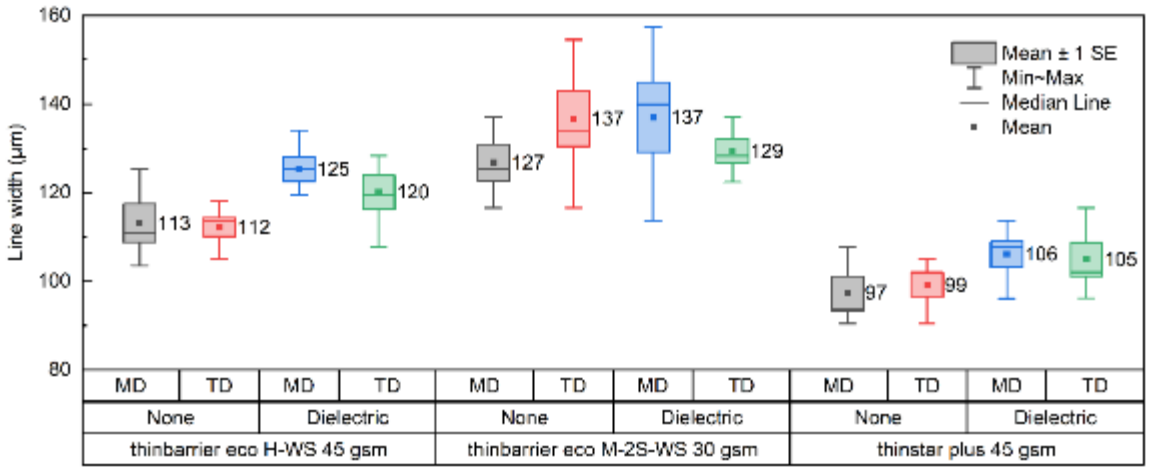

Figure 36: Results from measurements on printed silver lines with a nominal width of 100 µm.

The results from sheet resistance measurements on the printed lines are shown in Figure 37. There are minor differences between the substrates and typical sheet resistance values are obtained. Interestingly, the horizontal lines printed in TD generally display lower sheet resistance values. This is mostly due to the fact that these lines are somewhat thicker.

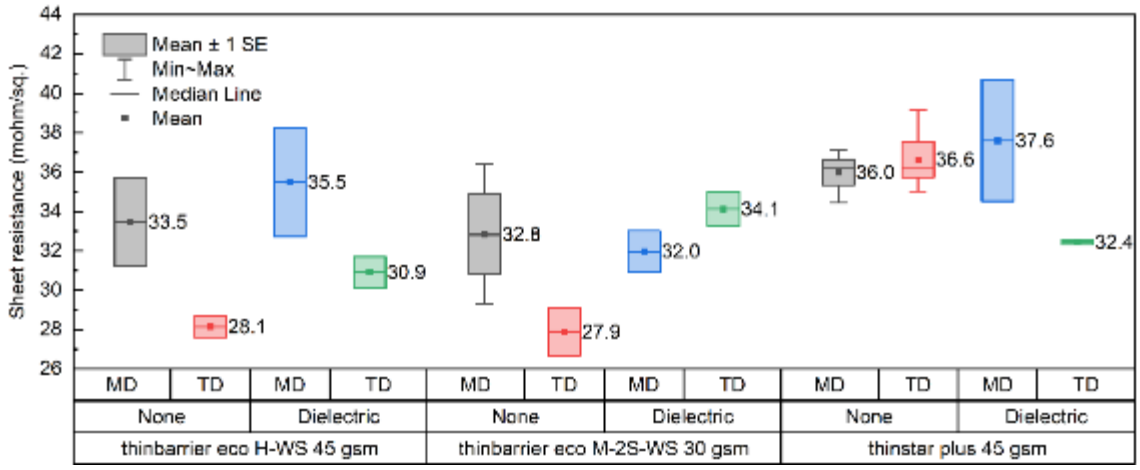

Figure 37: Results from sheet resistance measurements.

The results from cross-cut adhesion tests are shown in Table 21Table 21 (classification: 0 = excellent adhesion, 5 = poor adhesion). The silver ink has good adhesion when printed directly on the paper substrate. However, the dielectric layers printed on the thin barrier eco substrates have very poor adhesion. As a result, the results for silver printed on dielectric are also poor for these substrates. However, the thinstar plus substrate shows very good adhesion to both screen printed dielectric and silver.

Table 21. Results from cross-cut adhesion tests.

Cross-cut adhesion test results (classification 0-5)				*
Substrate	**Printed layers**			
	Dielectric	Silver	Dielectric + Silver	
thinbarrier eco H-WS 45 gsm	5	0	5	
thinbarrier eco M-2S-WS 30 gsm	5	1	5	
thinstar plus 45 gsm	0	0	0*	

Conclusions:

Functional layers can be screen printed on all three tested substrates from TER and the results are mostly acceptable. However, the best results are clearly obtained with thinstar plus 45 gsm paper. The printed silver features display better definition and less variation. Narrow lines with narrow spacing can be printed with good results, which is of special importance in Pilot#3.2, where contact pads for bare die microchip assembly with 100 µm line width and 200 µm pitch are needed. The thinstar plus 45 gsm paper clearly allows for this. Moreover, great adhesion with both printed dielectric and silver is also a significant advantage.

A challenge with all three substrates, and paper substrates overall, is dimensional changes due to uptake or release of water. This can make alignment of subsequently printed layers challenging. It can also make the substrates nonplanar and difficult to handle during manufacturing, especially in sheet-to-sheet processing. However, methods to handle these challenges have already been developed.

The substrate thinbarrier eco H-WS 45 gsm was used for the Gen 1 prototype of Pilot#3.2. However, thinstar plus 45 gsm will be used for Gen 2, and likely also for Gen 3.

2.3 Adhesives

List of adhesives developed by different partners in Sustronics is presented in Table 22Table 22. A detailed description of the adhesives per material is presented in the following sub-sections.

Table 22. Adhesives developed in the Sustronics project.

Technology	Owners	Sustainability claims								Pilots targeted									
		Bio-based	Renewable	Recycled	Abundant	Energy efficient processing	Safe solvents	EoL: Recyclable	EoL: Compostable	Pilot#1.1	Pilot#1.2	Pilot#1.3	Pilot#2.1	Pilot#2.2	Pilot#2.3	Pilot#3.1a	Pilot#3.1b	Pilot#3.2	Pilot#3.3
Pressure sensitive adhesives	• UPM: own commercial & experimental	X						X				X		X				X	
Non-conductive & conductive adhesives	• RISE: own development • VTT: commercial					X		X				X		X		X		X	

2.3.1 Adhesive testing at UPM

The summary table of the work reported by UPM in D1.4 is presented in Table 23Table 23 below.

Table 23. Summary of the work reported by UPM in D1.4.

Adhesive material	Tests carried out	Linkage to pilots
RPMD	General characterisation	Pilot #3.2
RPMD	Basic adhesion measurements based on the FINAT Standard	Pilot #3.2

New results of adhesive testing from UPM after the release of D1.4 are presented in the section below.

2.3.1.1 Skin irritation tests

Skin irritation test for products adhesives RPMD and RC3P, and substrates Pharmatight FSC (Thinstar+ 45) and Forest Film were performed. Testing method description is as follows:

Skin sensitisation: ISO 10993-10

- In vitro alternative for skin sensitisation testing as a part of the Biological Evaluation of Medical Devices according to ISO 10993-10:2021 Annex C.

Skin Irritation: ISO 10993-23

- The skin model is based on a 3D reconstituted human epidermis which consists of human-derived keratinocytes that mimic the properties of in vivo skin, including a multi-layered stratum corneum.

The test item extracts, prepared according to ISO 10993-12, are directly applied to the skin tissue surface at the air-liquid interface, and skin irritancy is determined by measuring the cell viability with the MTT assay. The results of skin irritation test are presented in Table 24Table 24 below.

Table 24. Results of the skin irritation test.

Substrate tested	ISO 10993-10 (Sensitisation)	ISO 10993-23 (Irritation)
RC3P (Non skin irritant adhesive)	Non-Sensitiser	Non-irritant
RPMD	Sensitiser	Non-irritant
Forest PP White FTC 60	Not tested	Non-irritant

Irritants are classified as such if the polar and/or non-polar extract of the test item decreases the cell viability below a defined threshold level (50% for UN GHS category 2) and as non-irritant if the viability is greater than 50%. Polar and non-polar extracts of the test item are prepared according to ISO 10993-12

RC3P non-skin-irritant adhesive

RC3P is a clear permanent radiation-cured UV-acrylic adhesive. RC3P conforms to FDA 21 CFR 175.125 (indirect food contact). An accredited laboratory has given the adhesive an approval for direct contact with dry, moist and fatty foods.

In Sensory Analysis for Indirect Transition of Taste according to EN 1230-2 (Robinson test) RC3P gets score less than 2 (moderate off-flavor). RC3P also meets the requirements of ISO10993-5 and is considered to have no cytotoxic potential. Typical technical values of RC3P are:

- Tack 17 N/25mm FTM 9
- Labelling temperature min 10 °C
- Service temperature min -20 °C
- Service temperature max 140 °C

ISO tests performed are listed below. Term PASS means that the material passed all the product safety tests:

- ISO 10993-5 Cytotoxicity done. Adhesive considered as non-cytotoxic (Pass)
- ISO 10993-10 Skin sensitization. Adhesive considered as non-sensitiser (Pass)
- ISO 10993-23 Skin irritation. Adhesive considered as non-irritant (Pass)

As an addition to above face materials, Forest PP White FTC60 & Pharmatight FSC were tested according to ISO 10993-5 for cytotoxicity. Both can be considered as non-cytotoxic.

Conclusions:

Based on the new tests results RPMD suitability for direct skin contact needs to be evaluated due to sensitisation potential. RC3P has passed all the product safety tests performed and is therefore primary option for skin contact applications. As an additional product safety test, Forest PP White FTC60 and Pharmatight FSC were tested in cytotoxicity, and both are considered safe in the planned applications.

2.3.2 Adhesive testing at RISE

The aim was to develop adhesives that are one-component compositions with a high content of bio-based materials, having short thermal curing time and latent curing kinetics. Both non-conductive and conductive adhesives were developed. Anisotropic conductive adhesives (ACAs) were developed for being used in flip-chip bonding of microchips. The summary of the work reported by RISE in D1.4 is presented in Table 25 below.

Table 25. Summary of the work reported by RISE in D1.4.

Adhesive material	Tests carried out	Linkage to pilots
RISE conductive adhesive	Not tested	Pilots #2.3 and #3.2

New results from RISE after the release of D1.4 are presented below.

2.3.2.1 Epoxy-based conductive adhesives

The materials developed needed to undergo further development and optimisation. Next steps include synthesis of hydrolysable diphenols, and preparation of ACAs based on the developed binder system with fillers of conductive particles, e.g. spherical copper particles or metallised polymer sphere particles.

Epoxy-based conductive adhesives have been developed by RISE in WP1. The electromechanical performance of the electrically conductive adhesive along with its curing behaviour can vary heavily based on the components of the adhesive; the main epoxy molecule, several chemical additives (i.e. initiators) and the conductive filler. As a first step of our work, we selected between two different epoxy binder configurations with the basis of ARALDITE CY221 as the epoxy resin. The first configuration was a 3-component mixture of the epoxy resin with two curing agents: Amicure CG-1440F and 2-ethyl-4-methylimidazole and the second configuration comprising a mixture of the epoxy resin only with 2-ethyl-4-methylimidazole. Imidazoles such as the one above, are conventional curing agent for epoxy systems and thus are chosen as a trial material. Furthermore, the concentration of the various curing agents in the epoxy matrix can act as a tuning tool for the curing temperature and the mechanical resistance of the adhesive itself. [Ham et al, 2010]

To identify the curing behaviour of the adhesives, we conducted differential scanning calorimetry (DSC) on these two configurations with a rate of 40 °C/min. The results from the DSC are presented in Figure 38 below.

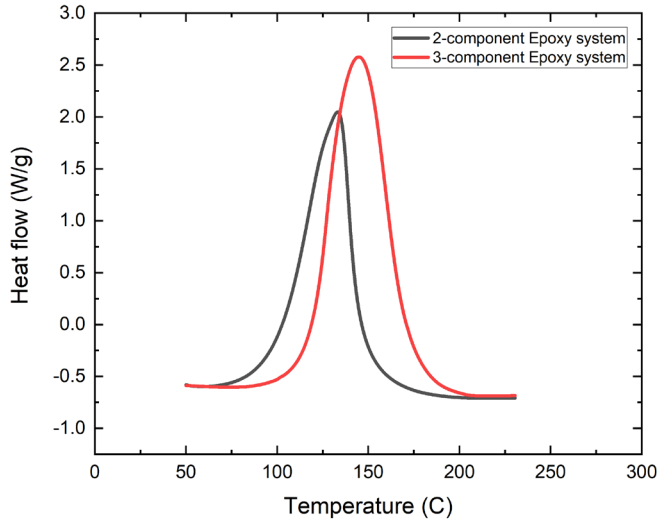

Figure 38: DSC plot for the epoxy systems.

Both configurations exhibited an exothermic reaction, which is in good agreement with the curing of epoxy binder, while the 2-component configuration exhibited a lower onset (~60 °C) and lower peak temperature (~125 °C) than the 3-component configuration (onset temperature ~80 °C, peak temperature ~150 °C). Given that we require a fast-curing electrically conductive adhesive for the assembly needs of the project, the 2-component configuration of the epoxy Araldite CY221 and 2-ethyl-4-methylimidazole is chosen as a matrix configuration of the development of electrically conductive adhesive (ECA).

The target application for our ECA is component assembly of electronic components such as surface mounted devices (SMD) and bare die microchips, thus the curing process for the deposition of the adhesive needs to be engineered towards this direction. For that reason, we utilised a thermode (MIYACHI, see Figure 39) as the bonding equipment, which emulates the conditions used in large scale assembly of electronics. With the thermode, we can apply a controlled temperature, for a controlled force, at a controlled timeframe, using a contact 'head' that matches the dimensions of the components, thus we can engineer the bonding conditions for our developed adhesive (force, temperature, time).

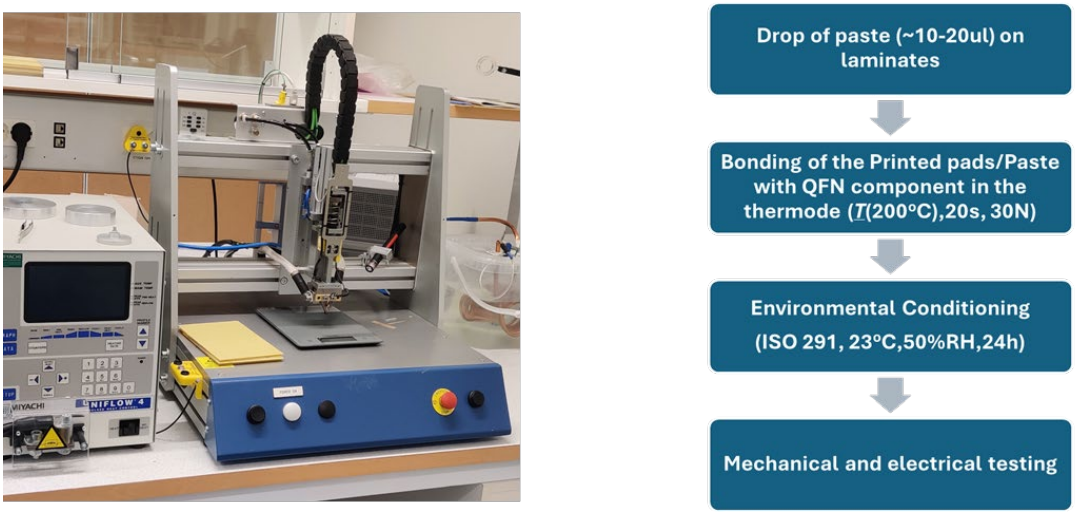

Figure 39: The thermode used in the presented work (on the left), and the flow diagram for the engineered ECA deposition and curing process (on the right).

As part of this engineering process and the further electromechanical evaluation of the adhesive, we bonded two copper laminates with our adhesive, using the thermode. Even though the copper laminates might not be the optimal substrate for mechanical tests, we opted to use them because the developed ECA will be used to bond two conducting (and metallic) surfaces, between the substrate and the component.

For the engineering of the curing conditions with the thermode, we used a bonding overlap area of 5x5 mm and had a PASS/FAIL test of bonding for a variety of temperature/time packages. The result of this investigation is presented in Table 26. The adhesive binder that we used for this engineering study was initially a mixture of 15% in the imidazole in the adhesive binder. It should be noted that our adhesive is solvent-free which means that we don't need a step to remove the solvent from the adhesive. As seen in Table 26, temperature of 200 °C for 20 s in the thermode provided a good combination of the curing conditions for the adhesive. In Figure 39 the flow diagram of our deposition and curing process used for our adhesives is presented.

Table 26. Various conditions that were explored for the ECA deposition and curing engineering.

% w/w imidazole	Temperature (°C)	Time (s)	PASS/FAIL
15	140	10	FAIL
15	140	20	FAIL
15	180	10	FAIL
15	180	20	FAIL
15	200	10	FAIL
15	200	20	PASS
25	140	10	FAIL
25	140	20	FAIL
25	180	10	FAIL
25	180	20	FAIL
25	200	10	FAIL
25	200	20	PASS
25	140	90	PASS

Consequently, we chose these conditions and proceeded in blending a conductive filler to the binder/curing agent matrix. In conventional ECAs, noble metals or nickel are used as the conductive fillers, which results in either a high price for the ECA or higher toxicity for the adhesive. Copper is a cheaper and more sustainable metal alternative while for ECA for component mounting, a spherical size of the filler is more ideal. As a result, for our developed ECA, we choose to use conductive copper spheres (diameter ~10 μm) as the conductive filler and varied the conductive filler concentration at 5.35 %-w/w and 50 %-w/w.

For testing the electromechanical performance of the adhesive, we manufactured Cu-laminate/ECA/Cu-laminate test samples and performed the mechanical tests adapted from the DIN EN 1465:2009-07 standard for shear testing (bond overlap 5x5 mm, shear speed 10 mm/s). Meanwhile, we exposed our bonded samples to environmental conditioning based on the ISO 291 (23 °C, 50% RH, 24 h) before testing them. The shear testing was also conducted using the Tensile Tester Z3 by Thumbler GmbH. For the electrical performance of the adhesive, a 4-probe measurement was used between the bonded samples, and the I-V curves were recorded with a Keithley 4200A-SCS.

The mechanical performance of the adhesive did not change significantly with the addition of the conductive filler, as seen from the representative Stress/Displacement plots (

Figure *40*a). From these plots we extracted the Stress at Break, meaning the value of the stress that the bonded sample broke during the shear stress. The average Stress at Break and standard deviations between three samples are presented in

Figure *40*b.

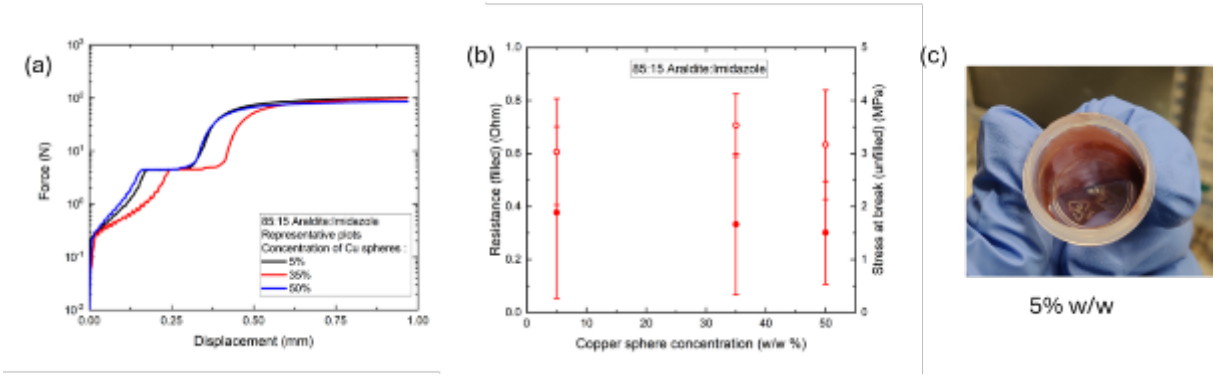

Figure 40: (a) The representative Stress/Displacement plots for the ECA (b) the Electrical Resistance and Stress at Break vs the Copper Sphere concentration for this ECA configuration. (c) a photographic depiction of the 5%w/w ECA.

We observed that the Stress at Break did not change significantly with the conductive filler concentration. Similarly, the electrical performance of the ECA did not seem to be significantly affected by the increasing filler concentration. However, we observed that both the Stress at Break and the electrical resistance had high statistical standard deviations. Potentially this originates from a low dispersibility of the conductive filler in the binder matrix. Indeed, as seen in

Figure *40*c, the conductive filler does not appear to disperse well in the binder matrix.

In order to address this issue, we modified the binder matrix; we increased the imidazole concentration up to 25%-w/w as a means to increase the viscosity of the binder system. Indeed, as seen in Figure 41, the adhesive was more homogenous. Consequently, we had to engineer the deposition conditions in the thermode for this new configuration. As seen in Table 26, the necessary time and temperature in the thermode were the same, thus we did not change our flowchart (see Figure 39).

Positively, we noticed that with this new configuration we can cure the adhesive at lower temperatures, for a larger timeframe; an observation that might open the door in future investigations for low temperature ECAs. Subsequently, we proceeded in investigating the effect of the conductive filler concentration for the 25%-w/w in imidazole configuration. As seen in Figure 41, the mechanical behaviour of the adhesives in the Stress/Displacement plots are quite similar to the ones presented in
Figure *40*.

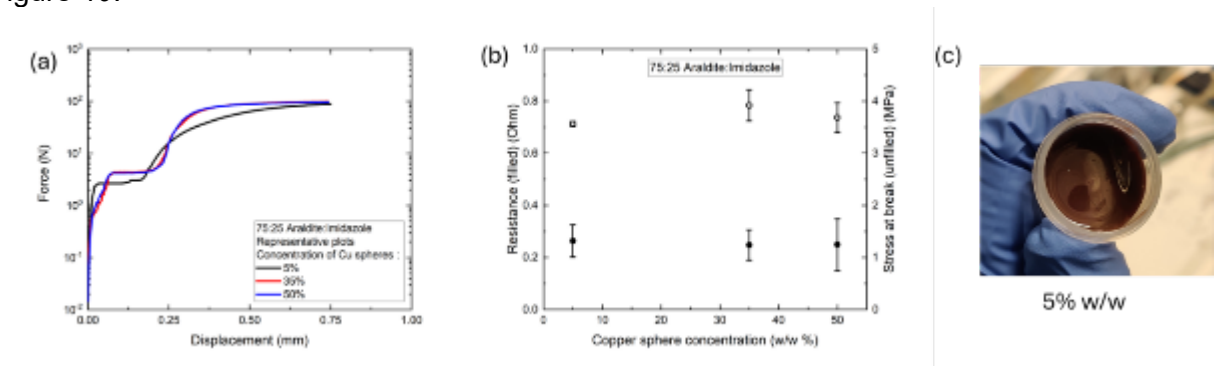

Figure 41: (a) The representative Stress/Displacement plots for the ECA with 25%w/w in imidazole (b) the Electrical Resistance and Stress at Break vs the Copper Sphere concentration for this ECA configuration. (c) a photographic depiction of the 5%w/w ECA

Furthermore, while plotting the Stress at Break and Electrical resistances over the concentration of the conductive filler, we observed that a concentration of 35%-w/w in the

conductive filler gave an optimal electromechanical behaviour, even though there were small variations between the other concentrations. It is noteworthy, that the statistical standard deviations of Figure 41 (over three samples) were much lower in comparison to

Figure *40*, which is inherent to the higher dispersibility of the conductive filler in the matrix.

An ECA can behave either as an anisotropic conductive adhesive (ACA) or/and as an Isotropic Conductive Adhesive (ICA). The major difference between ACA and ICA is that the electrical conduction in the ACA occurs only in the z-axis (i.e. along the bond direction) while for the ICA there is a 3-dimensional electrical conduction, meaning that there are electrical conductions in z-axis but also in the xy-axis. Based on our current tests that are presented above, our developed ECA exhibits electrical conduction along the z-axis (Cu-laminate/bond/Cu-laminate). Thus, in order to classify whether the ECA is an ICA or only an ACA, we need to investigate the electrical conduction in the xy-axis. For that reason, we printed Ag pads (250 μm width and 250 μm spacing) on Kapton foil (a relatively robust substrate from a temperature or humidity perspective). Subsequently, we followed the process presented in Figure 39 in order to laminate a piece of Kapton foil on the pads (Figure 42); if the ECA is an ICA, there should be electrical conduction between the different electrical pads.

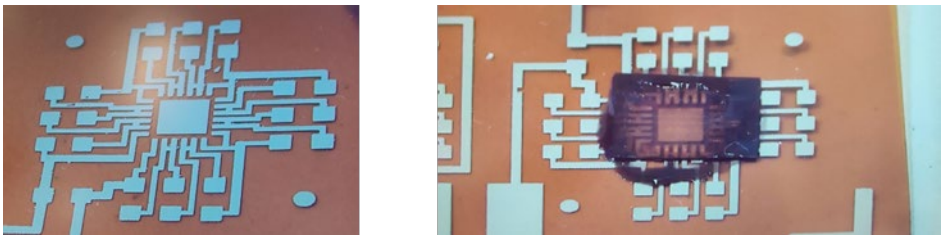

Figure 42: Photographic depiction of the printed pads on Kapton foil (on the left) and the printed pads with the bonded ECA and top Kapton foil (on the right).

However, upon bonding, we did not observe any electrical conduction between the Ag pads, even for a conductive filler concentration as high as 50%-w/w. As a result, we classify our ECA as an ACA. For microchip mounting, an ACA is essentially a necessity since an isotropic electrical conduction might create short circuits that would thwart the functionality of the electronic device.

Conclusions:
Various tests including DSC, thermal curing and shear bond strength tests have been performed on ECAs developed at RISE to identify and verify appropriate adhesive compositions and curing conditions. The shear bond strength measurements also indicate that the developed ECA is sufficiently strong for assembly of components. Moreover, electrical characterisation of the ECA show that the electrical conductivity is acceptable, and that the adhesive indeed can be classified as an ACA. Based on these results, RISE will proceed in using the developed ACA (25% imidazole, 35% Cu) for mounting of components (e.g. microchips) on relevant substrates in the project. The ACA has already been used for bonding of bare die microchips from IFAT on paper substrates with printed silver conductors (see section 3.3.4).

2.4 Inks

List of inks developed by different partners in Sustronics is presented in Table 27Table 27. A detailed description of the inks is presented in the following sub-sections per material.

Table 27. Inks developed in the Sustronics project.

Technology	Owners	Sustainability claims								Pilots targeted									
		Bio-based	Renewable	Recycled	Abundant	Energy efficient processing	Safe solvents	EoL: Recyclable	EoL: Compostable	Pilot#1.1	Pilot#1.2	Pilot#1.3	Pilot#2.1	Pilot#2.2	Pilot#2.3	Pilot#3.1a	Pilot#3.1b	Pilot#3.2	Pilot#3.3
Inks for sensor functional layers	• RISE: experimental for temperature and humidity • UGOT/ESS: experimental for enzymes						X											X	
Electrode ink	• TAU: experimental						X									X		X	
Conductive ink	• CAN: experimental				X			X								X			

2.4.1 Ink testing at TAU

Survey on environmentally friendly DES electrolytes. The supercapacitor electrode was prepared at TAU. The structure is based on previous research work. Electrode ink contains activated carbon (Kuraray YP-80F), chitosan binder solution, and deionised water. The ink is suitable for blade coating. The results presented in D1.4 show that it is compatible with screen printing as well. The summary of the work reported by TAU in D1.4 is presented in Table 28Table 28 below.

Table 28. Summary of the work reported by TAU in D1.4.

Item	Tests carried out	Linkage to pilots
Electrode ink development	• Electrode ink testing with different electrolytes (D1.4); blade coating	Pilot #P3.1a Pilots #P3.2 and #P3.3 under evaluation
Supercapacitor fabrication method	• Monolithic supercapacitor fabrication process vs. F2F lamination • Blade coating • Performance tests: • Electrochemical tests (i.e. capacitance, leakage current, equivalent series resistance)	Pilot #P3.1a Initial performance tests to meet the #P3.1 specifications #P3.2 and #P3.3 under evaluation

New testing results from TAU after the delivery of D1.4 are described below.

2.4.1.1 Electrode ink development

Next step was to find an alternative for Texilac to improve the specific capacitance. TAU continued the electrode ink development to find alternative approach to remove the retardant agent from electrode ink. As shown in D1.5, presence of retardant agent hinders the specific capacitance of the electrode. As a solution, TAU developed thermal modification process for the electrode to eliminate the retardant agent. The thermal modification process has shown

the improvement in printability i.e., the ink is not drying to the screen making the screen-printing process more reliable. This increased the capacitance 2-2.5 times compared to electrode with Texilac.

Related to electrolytes, TAU performed a literature survey and selected potential environmentally friendly DES electrolytes to increase the cell voltage and energy density. Increase of maximum cell voltage (V_{max}) from 1.2 V (aqueous NaCl) to 1.8 V (DESx) increases the energy density by factor of 1.4. Furthermore, the improved capacitance can increase the energy density even further. The results of the selected DES electrolytes are shown in Table 29Table 29 below.

Table 29. Environmentally friendly DES electrolytes selected from literature and their electrochemical performance.

Electrolyte	C (mF)	ESR_{GCD} (Ω)	$I_{leakage}$ (μA) [max]	V_{max} (V)	ED (Wh/kg)	PD (kW/kg)
NaCl (aq)	191.7	13.7	11.0	1.2	5.8	4.3
DES1	213.5	16.0	26.3	1.8	13.5	7.5
DES2	193.5	18.8	19.6	1.8	12.3	6.4
DES3	199.7	17.8	22.8	1.8	13.5	7.2
DES4	271.3	17.5	46.5	1.8	17.3	6.9

The results show performance increase in capacitance (C), energy density (ED), and power density (PD). Unfortunately, equivalent series resistance (ESR_{GCD}) and leakage current ($I_{leakage}$) increase as well. Related material and fabrication details as well as comprehensive electrochemical characterization will be discussed in the D2.3.

Summary of the results:

- The selected DES electrolytes improve the energy density 2-3 times depending on the combination. Power density improves by a factor of 1.5-1.7.
- ESR increases as well, but the absolute value is still acceptable for selected use-cases.
- The main disadvantage of the selected electrolyte is the increase of leakage current. It should be noted that the leakage current decreases exponentially as a function of voltage. The impact of the leakage current to the pilots should be further investigated.

The results shows that selected materials and processes are potential for selected pilots. The detailed electrochemical analysis will be reported in T2.3. *Energy storage and management.*

Electrode material is used in supercapacitors. First supercapacitors are tested for Pilot #3.1a Gen 1. Use of supercapacitors in Pilot #3.2 and Pilot #3.3 is under evaluation.

2.4.2 Ink testing at UGOT

2.4.2.1 Metal oxide-based gel for enzyme sensor

The gel is based on porous silicon dioxide particles along with conducting polymer and electrolyte. The enzyme to be detected is Trypsin present in feces. The gel was deposited on the three electrodes system consisting of working gold electrode, silver/silver chloride reference electrode and counter electrode. The gel has also been tested on carbon-based electrodes where working and counter electrodes are of carbon and reference electrode is of silver/silver chloride. Summary of the work reported in D1.4 can be found in Table 30Table 30.

In near future UGOT shall perform more tests on different electrodes, curation time, effect of humidity, temperature and pH on the electrochemical response. UGOT shall also evaluate if two electrodes system based on carbon is workable or not.

Table 30. Summary of the work reported by UGOT in D1.4.

Substrate	Tests carried out	Linkage to pilots
Metal oxide (SiO_2) based gel for sensing enzyme (Trypsin) in the Hygiene products	Effect of parameters relevant for the hygiene product environment (pH, temperature, enzyme concentration) has been validated.	Pilot #3.2

New testing results from UGOT after the delivery of D1.4 are described below.

UGOT has tested the response of sensor and evaluated the effect of parameters which are relevant for the hygiene product environment (see Table 31Table 31). UGOT has validated some parameters which are relevant for hygiene products.

Table 31. Results of sensor response parameter validation.

Material	Tests carried out	Linkage to pilots
Metal oxide (SiO_2) based gels for enzyme (Trypsin) sensing in hygiene products	• Working of enzyme regarding the parameters relevant for the environment in the hygiene product have been tested. • Effect of temperature up to 40 ºC, pH and the relevant concentrations of enzyme has been tested. • Response of gel cured for two months at room temperature has been evaluated.	Pilot #3.2

Conclusions:

The response of sensing gel in temperature ranges from 20 °C to 40 °C, enzyme concentration ranging from 0.01 to 2.5 w-% and curing at room temperature up to two months have been tested. In this period carbon-based electrodes have been used, and the gold electrodes have been abandoned. This makes the gel more environmentally friendly.

Integration of enzyme sensor into sensor strip having pH, temperature and humidity sensors developed by RISE will be the next step, and testing in hygiene product environment. This will be done when sensor strip from RISE will be available. This material is mainly intended to be used in Pilot #3.2 smart hygiene product.

2.4.3 Ink testing at RISE

RISE has developed ink formulations for screen printing of the functional sensing layer in temperature sensors. The development of the printed temperature sensors is done in T2.2 and are reported in D2.2. Screen printing and curing processes were developed for the inks as a part of T1.3. The developed inks display good printability and adhesion on different substrates. A summary of the work reported by RISE in D1.4 is presented in Table 32 below.

Table 32. Summary of the work reported by RISE in D1.4.

Ink material	Tests carried out	Linkage to pilots
Ink for functional layer in temperature sensors	• Initial printability tests • Electrical characterisation (temperature coefficient)	Pilot #3.2
Ink for functional layer in humidity sensors	• Initial printability tests • Adhesion	Pilot #3.2

The inks needed to undergo further development and optimisation. It was to be investigated to see if the silver-carbon ink can be made even more sustainable by further reducing the silver content. The inks will be tested and evaluated in accordance with plan, and the results will be reported in this document.

New results from RISE after the release of D1.4 are presented below.

2.4.3.1 Screen-printable ink for Humidity sensors

Some additional tests have been performed on the inks developed by RISE This includes rheological measurements of the Lignin-based humidity sensor ink. A viscosity flow curve for the ink is shown in Figure 43. The ink displays a viscosity of about 70 Pa·s at low shear rate, but the viscosity decreases monotonically as the shear rate is increased. Thus, the ink displays a shear thinning behaviour. The obtained viscosity results are typical for screen printing inks. It can be mentioned that the ink can be diluted with a suitable solvent mixture (ideally the same solvent composition as in the ink) if the printing equipment used would require a lower viscosity.

The stability of the humidity sensor ink has also been investigated by performing printing tests on the same ink formulation batch at different occasions, up to 3 months after the ink manufacturing. No noticeable difference in the printing characteristics was observed in these tests, thus indicating that the humidity sensor ink can be regarded as quite stable overtime.

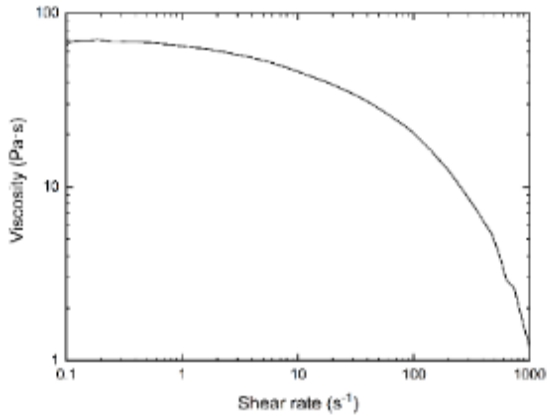

Figure 43: Viscosity flow curve for the humidity sensor screen printing ink.

Conclusions:

The temperature and humidity sensor inks developed by RISE are well adapted for screen printing and the materials have been used extensively in the development of fully printed temperature and humidity sensors (WP2, T2.2) as well as in the development of sensor labels in Pilot#3.2, with good results.

2.5 Other materials

List of other materials developed by different partners in Sustronics is presented in Table 33Table 33. A detailed description of the other materials is presented in the following sub-sections per material.

Table 33. Other materials developed in the Sustronics project.

Technology	Owners	Sustainability claims								Pilots targeted									
		Bio-based	Renewable	Recycled	Abundant	Energy efficient processing	Safe solvents	EoL: Recyclable	EoL: Compostable	Pilot#1.1	Pilot#1.2	Pilot#1.3	Pilot#2.1	Pilot#2.2	Pilot#2.3	Pilot#3.1a	Pilot#3.1b	Pilot#3.2	Pilot#3.3
LDS metallization	• PIEP: experimental				X	X		X					X						
Carbon nanotubes	• CAN: own commercial & experimental		X		X		X	X								X	X		

2.5.1 CNT film testing at CAN

2.5.1.1 CNT film

Multiwalled carbon nanotube film (CNT) as electrode material. These high-performance CNT's were produced using CAN's proprietary reactor and patented manufacturing technology. The summary of the work reported by CAN in D1.4 is presented in Table 34 below.

Table 34. Summary of the work reported by CAN in D1.4.

Substrate	Tests carried out	Linkage to pilots
Polyethylene Terephthalate (medical grade)	• Adhesion of carbon nanotube film • Electrochemical Biosensor evaluation	Pilot #3.1a

The prepared CNT film was subsequently used to fabricate electrodes for applications in biosensor development, specifically for a C-peptide and creatinine electrochemical biosensor. The material served as a platform to immobilise the sensing biomolecule of interest. The biosensor stack was tested and demonstrated excellent results, successfully achieving the relevant clinical working range for detecting C-peptide concentrations in buffer solutions.

New testing results from CAN after the delivery of D1.4 are presented below.

In Figure 44, a carbon nanotube film adhesion on paper substrate is shown.

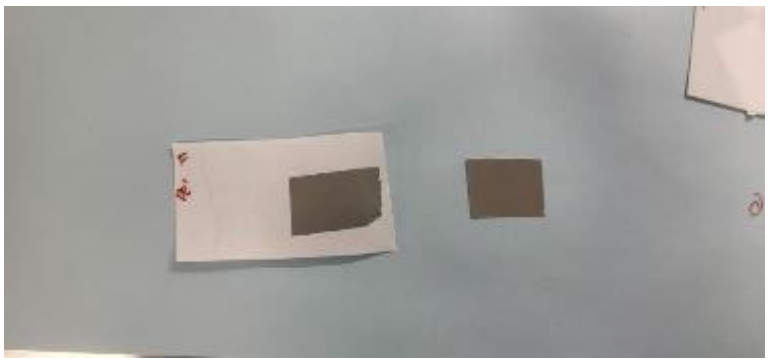

Figure 44. Carbon nanotube film adhesion on paper substrate.

Conclusions:

- Successful immobilization of C-Peptide and Ab against C-Peptide on CANATU's CNT film
- Competitive and Sandwich Assay format has been developed
- Wide measurement range obtained
- CNT-film transferred to paper substrate (see Figure 1.) -> Paper has been chemically modified (CANATU's proprietary surface chemistry) -> R value (ohms): 109 Ω/sq.m.

2.6 Conclusions and next steps in material development

A broad spectrum of sustainable bio-polymers, cellulose-based materials, adhesives, inks, and various other materials have been developed, thoroughly investigated, rigorously tested, and successfully utilised within the Sustronics project.

These materials have undergone extensive characterisation to assess their suitability and performance for the intended applications. Some other materials initially included in the plan, have been discarded. This process involved assessing the materials' effectiveness, environmental impact, and compatibility with other components, ensuring that only the most promising and sustainable options are carried forward in the project.

As outlined in the document and summarised in the materials tables, several of these materials are employed across multiple pilots, which not only highlights the extensive interaction and collaboration among the project partners but also underscores the interdisciplinary nature of the project. Such integration is a direct outcome of the significant effort dedicated to disseminating and sharing the obtained results across the project team. The continuous exchange of information between the partners ensures that knowledge is efficiently transferred, which in turn facilitates the seamless integration of diverse working groups. Furthermore, this collaborative approach fosters an environment conducive to the development of new research avenues, enabling the exploration of novel ideas and solutions.

3 Description of process development

List of process development tasks planned for partners in Sustronics project is presented in Table 35Table 35. A description of process development testing results partner by partner is presented in the following sub-sections. This section presents only the processing-related results that remained out of D1.5.

Table 35. Process development tasks in the Sustronics project.

Technology	Owners	Sustainability claims				Pilots targeted									
		Compatible with sustainable materials	Material efficient	Energy efficient	Working safety[1]	Pilot#1.1	Pilot#1.2	Pilot#1.3	Pilot#2.1	Pilot#2.2	Pilot#2.3	Pilot#3.1a	Pilot#3.1b	Pilot#3.2	Pilot#3.3
Printing	• RISE, SCR, TAU	X	X	X	X			X	X	X	X	X	X	X	X
3D printing	• GUT: dielectrics	X			X									X	X
Structural electronics	• CEA, SYM	X			X						X				
Component assembly	• WUR, FHG, CEA, SYM, VTT, RISE	X		X	X			X		X	X	X	X	X	X
Wire bonding	• WUR	X												X	X
Paper fluidics	• VTT	X	X	X	X							X	X		
Wearable systems	• EDI	X								X					

[1] e.g. no harmful solvents

3.1 Printing

3.1.1 Printing test results at RISE

The summary table of the work reported by RISE in D1.5 is presented in Table 36 below.

Table 36. Summary of the work reported by RISE in D1.5.

Developed process	Tests carried out	Linkage to pilots
Printing of temperature sensor layer	• Initial printability tests • Adhesion • Electrical characterisation	Pilot #3.2
Printing of humidity sensor layer	• Initial printability tests • Adhesion	Pilot #3.2
Printing of conductive materials	• Initial printability tests • Adhesion • Electrical characterisation	Pilot #3.2

New results from RISE after the delivery of D1.5 presented in the next section.

3.1.1.1 **Printing of temperature sensor layer**

Processes have been developed for screen printing the sensing layer in temperature sensors using inks developed in T1.2. Additional printability and adhesion tests, and electrical characterisation have been performed on the printed silver-carbon-based ink and the results are reported here. The methodology and test patterns used are the same as described in section 2.2.4. Two different substrates were used: thinstar plus 45 gsm paper from TER with dielectric coating, since this has been selected as the main substrate for Pilot #3.2, and a conventional PET substrate for reference.

Optical microscopy images of different printed line test structures with varying line width (LW) and line spacing (LS) are shown in

Figure *45*. The ink shows excellent printability on PET, allowing for printing narrow lines with relatively smooth edges. The lines printed on the paper have noticeably more uneven edges, but the results are still acceptable.

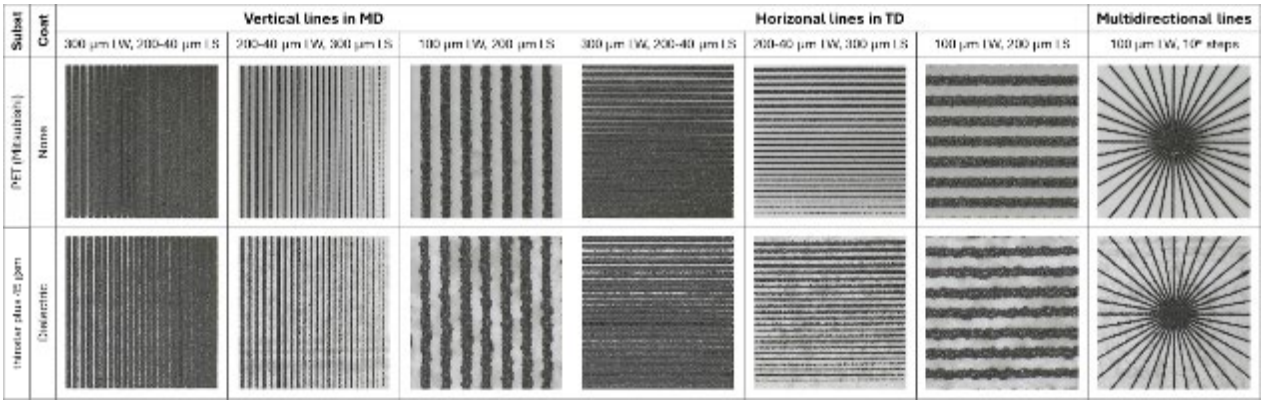

Figure 45: Optical microscopy images of different test patterns screen printed on PET and on thinstar plus 45 gsm paper from TER with screen printed dielectric layer using the temperature sensor ink. The nominal LW and LS are indicated for each pattern.

Surface topography and profiles of lines printed on the paper substrate, measured by optical profilometry, are shown in Figure 46. The height of the printed lines appears to be quite uniform. The printed lines have a relatively uneven surface, but this can be expected from this material mixture.

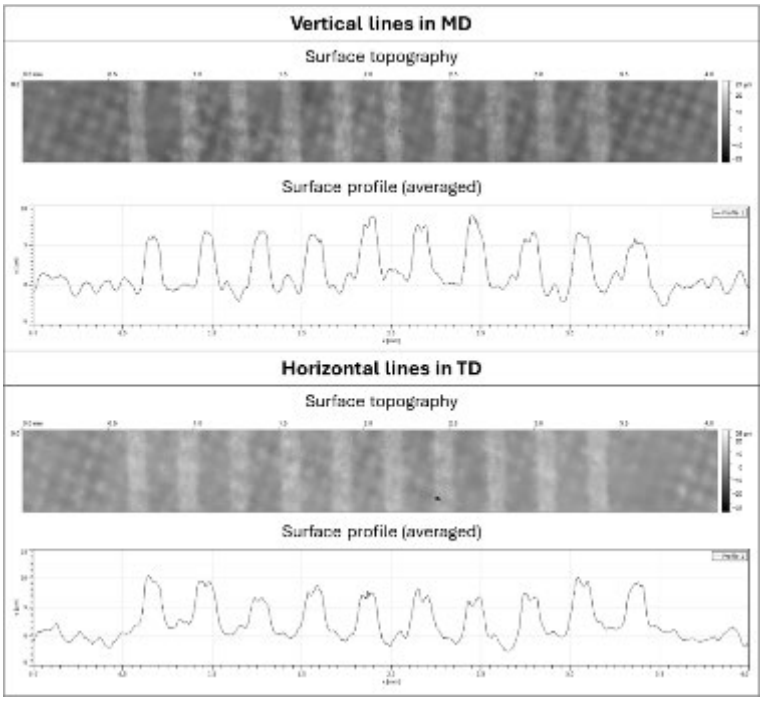

Figure 46: Results from optical profilometry of screen-printed temperature sensor lines with 100 µm LW and 200 µm LW printed on thinstar plus 45 gsm with dielectric coating.

The widths of nominally (in design) 100 µm wide printed lines were measured by optical microscopy and the resulting average values are shown in Figure 47. The lines are clearly wider than in the design, indicating that the ink is spreading on the substrates. The variation in line width is larger on paper, which also is evident from the optical images. The orientation of the printed lines has a minor influence on the line width.

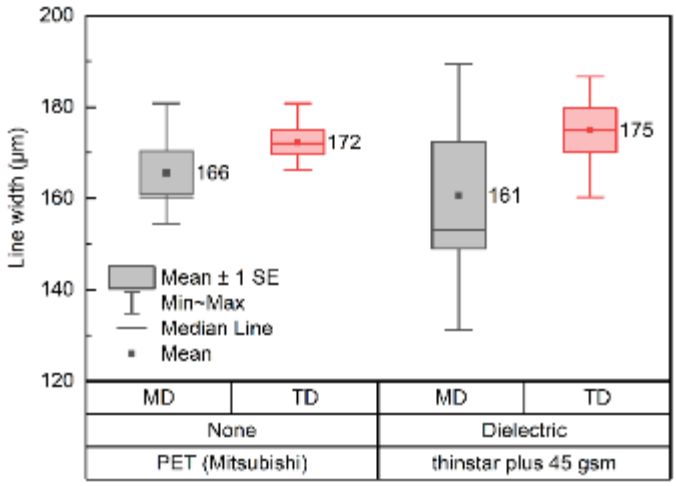

Figure 47: Results from measurements on printed temperature sensor lines with a nominal width of 100 µm.

The results from sheet resistance measurements on the printed lines are shown in Figure 48. Similar sheet resistance values are obtained for the lines printed on paper in the machine direction (MD) and the transverse direction (TD), which is of importance since the sensing layer is printed as narrow line meander structure in the temperature sensor to obtain a certain resistance.

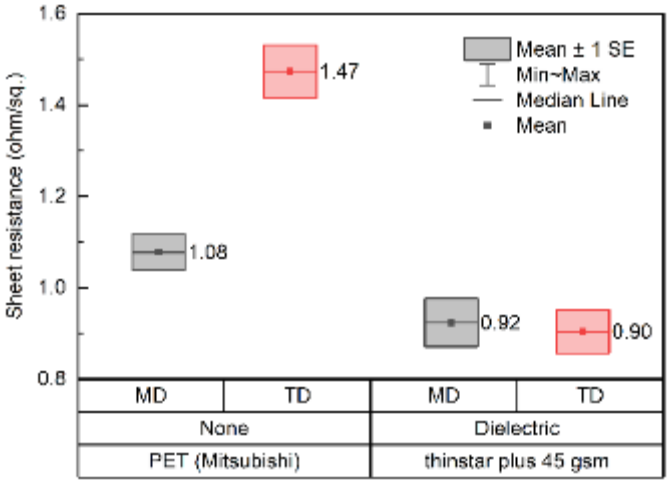

Figure 48: Results from sheet resistance measurements on printed temperature sensor lines.

The results from cross-cut adhesion tests are shown in Table 37. The temperature sensor ink shows excellent adhesion to both the paper and PET substrates.

Table 37. Results from cross-cut adhesion tests for printed temperature sensor ink. (classification: 0 = excellent adhesion, 5 = poor adhesion).

Cross-cut adhesion test results (classification 0-5)			
Substrate	**Coating**	**Classification**	
PET (Mitsubishi)	-	0	
thinstar plus 45 gsm	Dielectric	0*	* 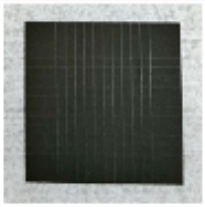

Conclusions:

The printability tests show that the temperature sensor ink can be printed with good results. Narrow lines printed on paper have evident edge roughness but the variation in resistance, which is what matters in the end, is anyhow low. Moreover, the printed ink shows great adhesion to the substrate. The ink and the developed printing process have been used in the development of temperature sensors in WP2 and will also be used in Pilot #3.2.

3.1.1.2 Printing of humidity sensor layer

Processes have been developed for screen printing the sensing layer in humidity sensors using inks developed in T1.2. Additional printability and adhesion tests have been performed on the printed lignin-based ink and the results are reported here. The methodology and test patterns used are the same as described in section 2.2.4. Three different substrates were used: thinstar plus 45 gsm paper from TER with dielectric coating, since this has been selected as the main substrate for Pilot #3.2, a commercial paper substrate and a conventional PET substrate for reference.

Optical microscopy images of different printed line test structures with varying line width (LW) and line spacing (LS) are shown in

Figure *49*. The widths of nominally (in design) 100 µm wide printed lines were measured by optical microscopy and the resulting average values are shown in Figure 50.

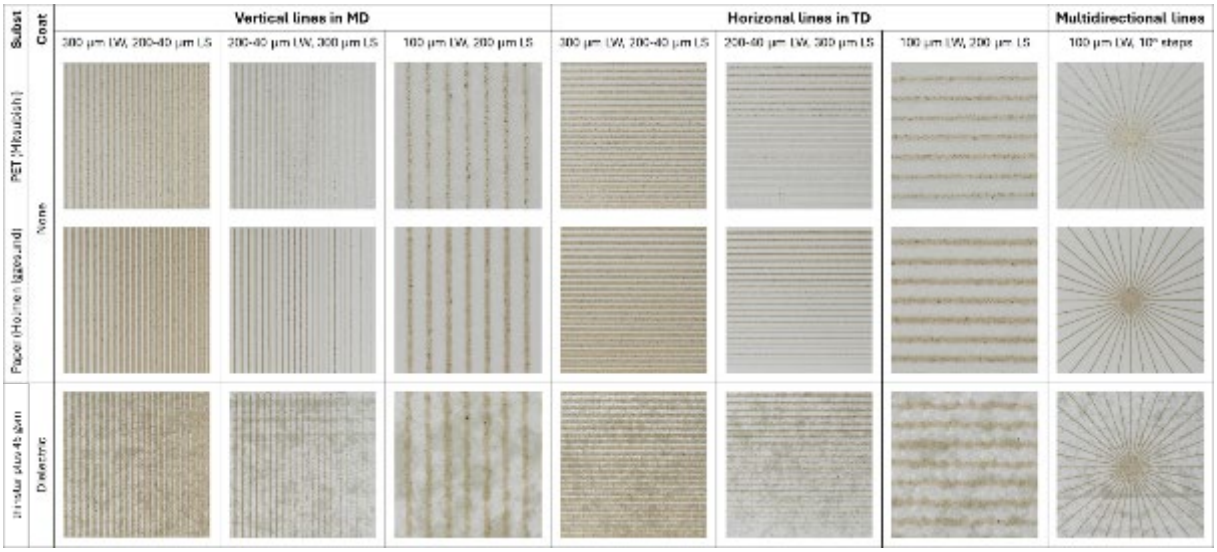

Figure 49: Optical microscopy images of different test patterns screen printed on PET and paper substrates using the humidity sensor ink developed by RISE. The nominal LW and LS are indicated for each pattern.

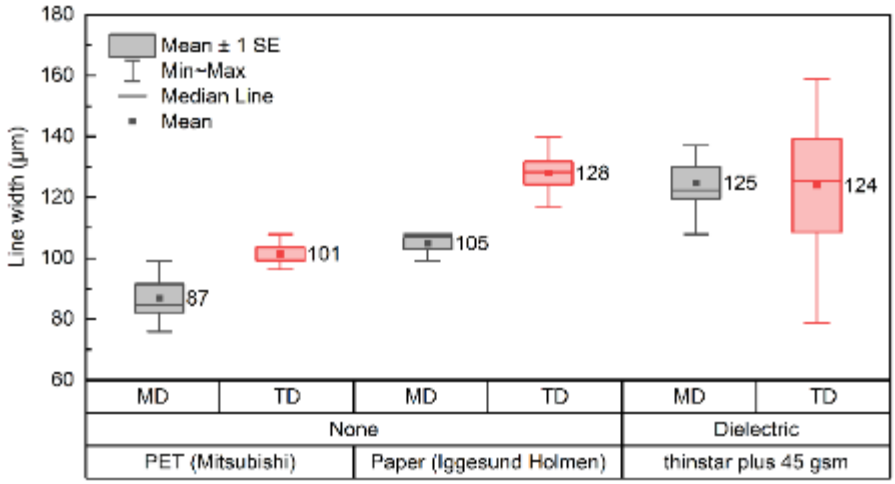

Figure 50: Results from measurements on printed humidity sensor lines with a nominal width of 100 µm.

The ink shows good printability on all three substrates. The ink shows some dewetting tendency on PET which also produces somewhat narrower lines. Excellent results are obtained when printed on the commercial paper from Iggesund Holmen, which has a very smooth surface, but also is very thick (too thick for use in Pilot #3.2). The lines printed on the thinstar plus paper are wider and have rougher edges. Since the humidity sensor ink will be printed as a mm-sized rectangle in the humidity sensor, the observed edge roughness is of no importance.

The results from cross-cut adhesion tests are shown in Table 38. The humidity sensor ink shows very poor adhesion to PET. Perhaps this can be improved by a treatment of the substrate (e.g. corona treatment or a coating of an intermediate dielectric layer) before printing. The adhesion of the ink to the paper is very good and fully acceptable.

Table 38. Results from cross-cut adhesion tests for printed humidity sensor ink. (classification: 0 = excellent adhesion, 5 = poor adhesion).

Cross-cut adhesion test results (classification 0-5)			*
Substrate	**Coating**	**Classification**	
PET (Mitsubishi)	-	5	
Paper (Iggesund Holmen)	-	0	
thinstar plus 45 gsm	Dielectric	1*	

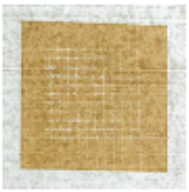

Conclusions:

The printability tests show that the humidity sensor ink can be printed with good results and that the printed ink has good adhesion to the paper substrates. The ink and the developed printing process have been used in the development of humidity sensors in WP2 and will also be used in Pilot #3.2.

3.1.1.3 **Printing of conductive materials**

RISE has tested and evaluated commercial copper inks for screen printing of conductors, potentially providing a more sustainable and cost-effective alternative to silver inks. A 2-component copper ink from PrintCB (CI-004 CopPair LT) was identified as the most promising candidate, mostly due to its relatively low curing temperature (nominally 120 °C) and its wide compatibility with substrates. The copper particles in this ink are coated with a thin layer of silver (<10%).

Additional printability and adhesion tests, and electrical characterisation have been performed on the printed copper ink and the results are reported here. The methodology and test patterns used are the same as described in section 2.2.4. Four different substrates were used:

- A conventional PET substrate from Mitsubishi Polyester Film
- A commercial paper from Iggesund Holmen
- Thinstar plus 45 gsm paper from TER
- Thinstar plus 45 gsm paper from TER with screen printed dielectric coating

Optical microscopy images of different printed line test structures with varying line width (LW) and line spacing (LS) are shown in Figure 51. The widths of nominally (in design) 100 µm wide printed lines were measured by optical microscopy and the resulting average values are shown in Figure 53. The ink generally prints well on all four substrates. Lines printed on PET have very smooth edges, but horizontal lines printed in the transverse direction (TD) are noticeably wider than vertical lines printed in the machine direction (MD). Narrower lines and less difference between MD and TD were obtained for the commercial paper substrate, which has a very smooth surface. However, the edge roughness of the lines is somewhat larger than for PET. Lines printed on uncoated thinstar plus paper are wider and have larger edge roughness. The lines in TD are clearly wider. Lastly, lines printed on dielectric-coated thinstar plus paper have relatively smooth edges, but the line widths are much larger than the design, up to twice the width.

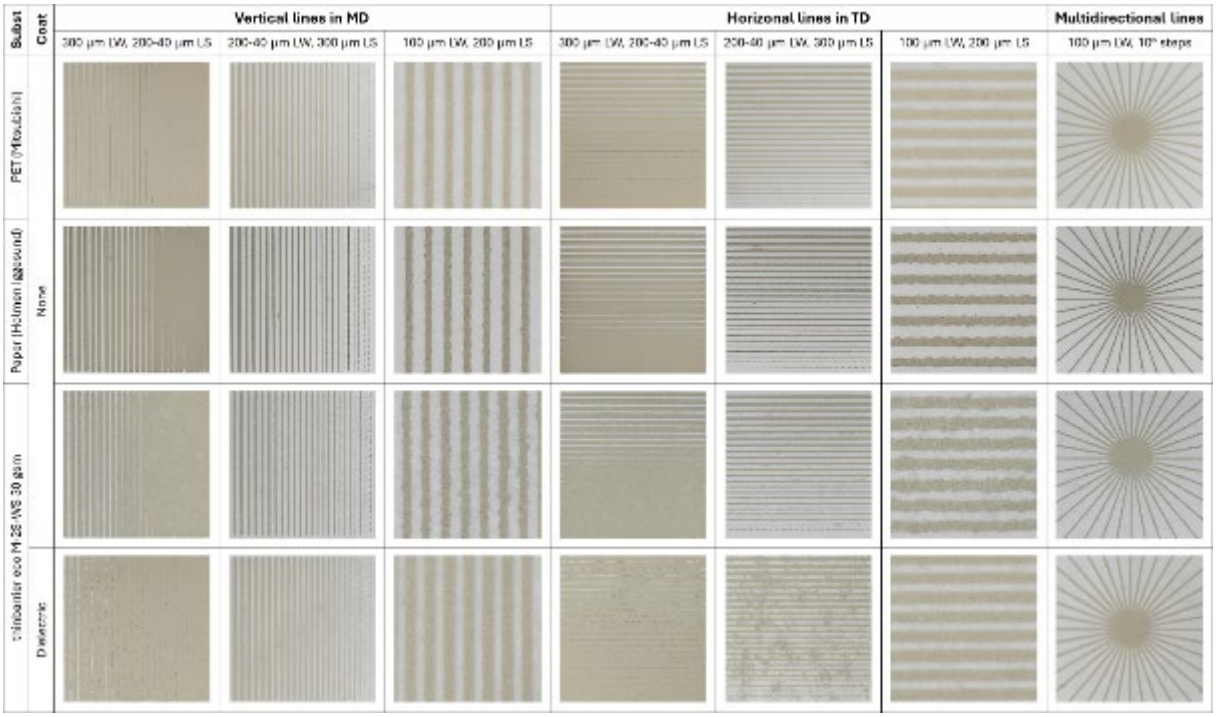

Figure 51: Optical microscopy images of different test patterns screen printed on PET and paper substrates using copper ink. The nominal LW and LS are indicated for each pattern.

Surface topography and profiles of lines printed on the paper substrate, measured by optical profilometry, are shown in Figure 52. The roughness of the substrate is clearly visible. Nevertheless, the printed lines appear to be quite uniform with smooth profiles.

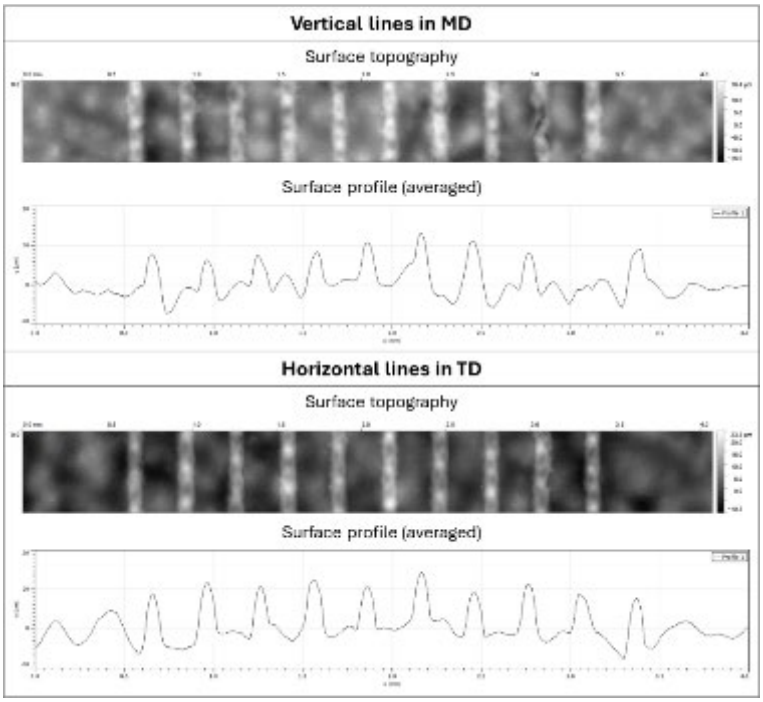

Figure 52: Results from optical profilometry of screen-printed copper lines with 100 µm LW and 200 µm LS printed on thinstar plus 45 gsm with dielectric coating.

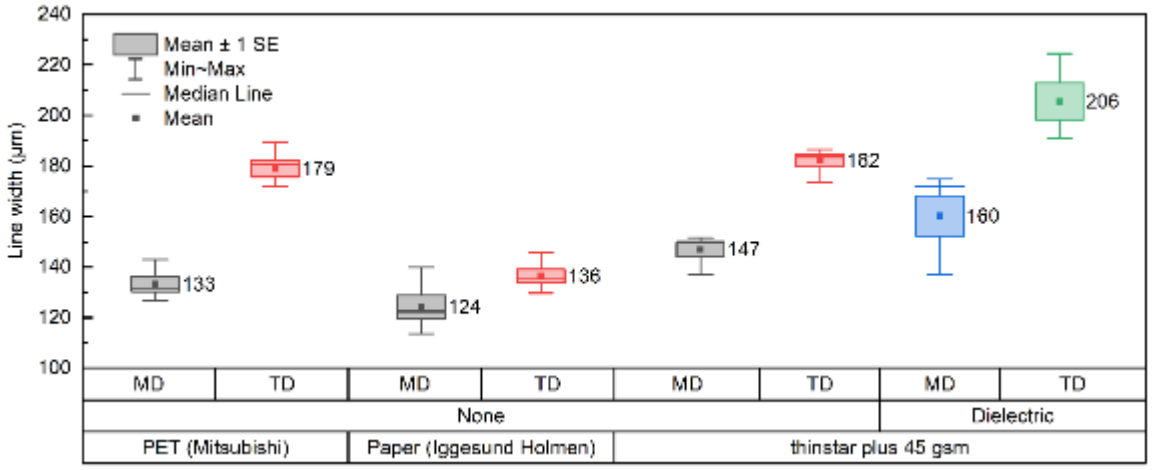

Figure 53: Results from measurements on printed copper lines with a nominal width of 100 µm.

The results from sheet resistance measurements on the printed lines are shown in Figure 54. There is a relatively large spread between the different substates. Interestingly, the PET and the dielectric-coated thinstar plus paper substrates give the lowest sheet resistance values. Tests indicate that curing at 120 °C may not be sufficient for fully curing the printed copper ink, and that higher temperatures, up to 140 °C, may have to be applied. The rightmost values in Figure 54 shows the obtained sheet resistance after post-curing at 140 °C.

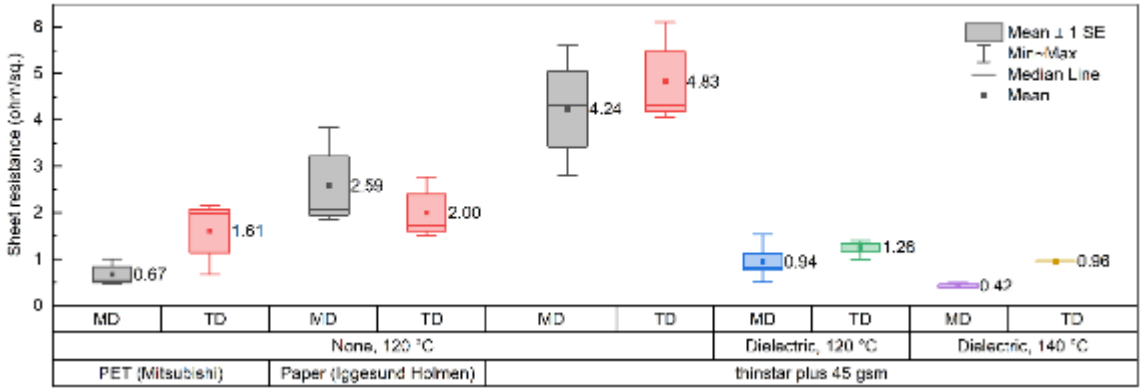

Figure 54: Results from sheet resistance measurements on screen printed copper lines.

The results from cross-cut adhesion tests are shown in Table 39. The copper ink has intermediate adhesion on PET, with some flaking in the tests, while the adhesion is better and acceptable on the paper substrates.

Table 39. Results from cross-cut adhesion tests for printed copper ink. (classification: 0 = excellent adhesion, 5 = poor adhesion).

Cross-cut adhesion test results (classification 0-5)			*
Substrate	**Coating**	**Classification**	
PET (Mitsubishi)	-	2	
Paper (Iggesund Holmen)	-	1	
thinstar plus 45 gsm	-	0	
thinstar plus 45 gsm	Dielectric	1*	

Conclusions:

The tests show that the copper ink can be printed on different substrates generally with good results and good adhesion. The resistivity of the printed copper is most likely low enough for replacing printed silver as a general conductor in various circuitry. However, the resistivity of the printed copper may be too high for use in NFC antenna coils. Moreover, it is challenging to print very narrow lines with small pitch. Thus, it may be difficult to replace printed silver contacts for assembly of microchips (see section 3.3.4). All this will be further investigated in the development of printed sensor labels in Pilot #3.2.

3.2 3D-printing

3.2.1 Testing at GUT

Advanced characterisation of 3D-printed dielectric materials and application to miniaturised reconfigurable antennas. In Table 40 the work reported by GUT in D1.5 is summarised. See also Figure 55 and Figure 56.

Table 40. Summary of the work reported by GUT in D1.5.

Developed process	Tests carried out	Linkage to pilots
Advanced characterisation of 3D-printed dielectric materials and application to miniaturised reconfigurable antennas	A comprehensive dielectric characterisation process was developed and implemented for a wide range of 3D-printing materials, including virgin PLA and ABS, PLA composites (with wood, hemp, flax, algae), recycled PLA and ABS, and commercially available high-permittivity ABS filaments.	Pilot #3.2: Development of innovative materials and components for reconfigurable antennas in low-power IoT communication scenarios. Pilot #3.3: Integration of sustainable material technologies into base station antenna design, addressing energy efficiency and recyclability in future network infrastructure.
	Measurements were conducted using SPDR (Split-Post Dielectric Resonator) and waveguide techniques. These allowed for the determination of dielectric permittivity (εr) and loss tangent (tanδ) across frequencies up to 7 GHz, including 2.4 GHz (ISM band).	
	Additional microscopic analysis (SEM imaging) and chemical composition assessments were performed on selected filaments, confirming the presence of ceramic fillers (TiO_2, $SrTiO_3$) and evaluating their distribution quality.	
	A process for recycling PLA and ABS was developed and optimised. It included shredding, drying, and re-extruding the material into filament form using the Felfil Evo Complete Kit. The process was repeated up to five times to evaluate the effect of reprocessing on dielectric homogeneity and performance.	
	Based on the characterised materials, dielectric overlays were designed and produced using 3D printing. These overlays were applied to a miniaturised ESPAR (Electronically Steerable Parasitic Array Radiator) antenna.	
	The antenna was prototyped and tested in an anechoic chamber, including full S11 measurements and 360° radiation pattern characterisation in both E- and H-planes, with overlay materials applied.	

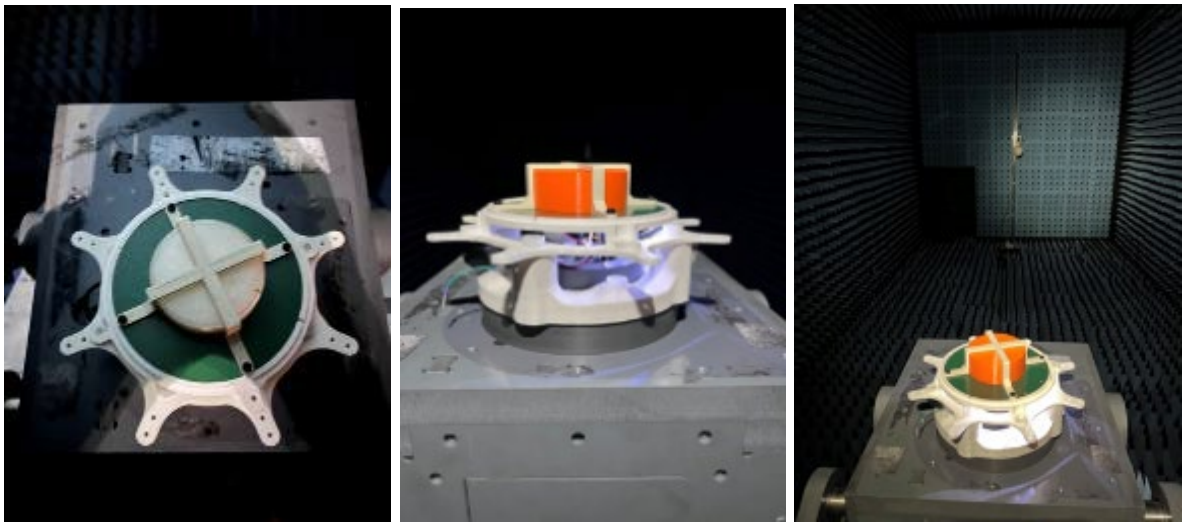

Figure 55. AUT mounting for measurement in H-plane

Figure 56. AUT mounting for measurement in E-plane.

New results from GUT after the release of D1.5 are described in the following section.

3.2.1.1 Miniaturization of ESPAR Antenna

By using high-permittivity dielectric overlays, the physical dimensions of the ESPAR antenna were significantly reduced (from Ø152.4 mm, h 27.35 mm → Ø118 mm, h 26 mm) without compromising radiation performance (see Figure 57). This was achieved using tailored 3D-printed structures based on materials with optimised εr and tanδ.

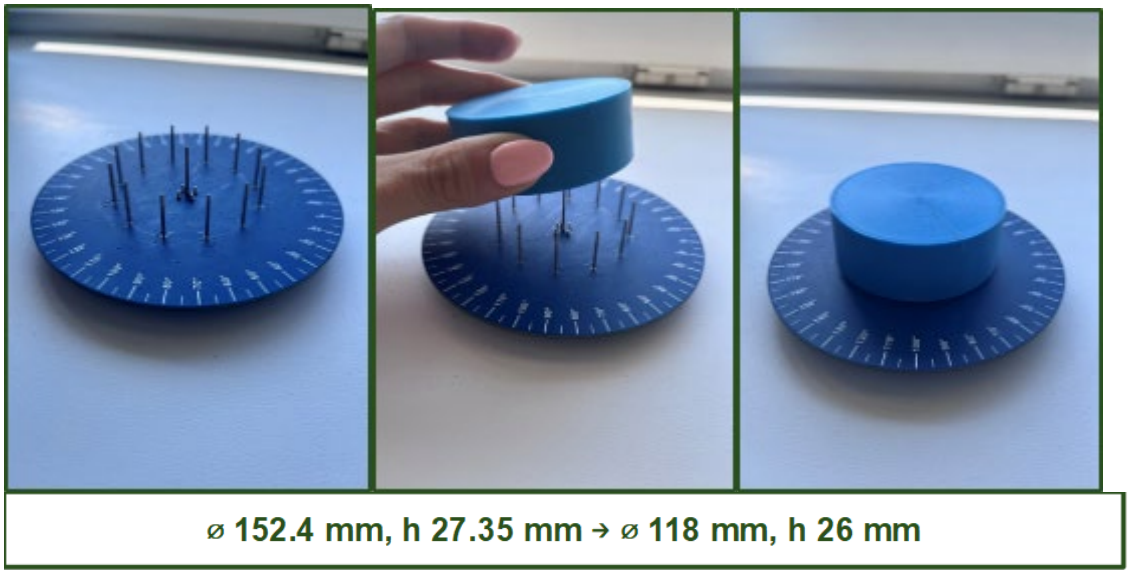

Figure 57. Miniaturisation of reconfigurable antenna

3.2.1.2 Material Performance Validation

More than 20 overlay variants were tested, such as differing in material base (PLA, ABS, Polyethylene), infill percentage, infill pattern (e.g. gyroid, circle, triangle), and wall configuration (see Figure 58).

Figure 58. ABS and PLA overlays and one Polyethylene overlay.

The measurements showed that:

- Dielectric overlays with higher εr (especially from ABS with ceramic fillers) led to noticeable shifts in radiation performance
- The infill percentage had the most significant effect on effective permittivity
- Natural additives and recycling of PLA showed minimal degradation in electromagnetic performance, proving viability of eco-friendly alternatives.

Development of Sustainable Materials

Reprocessing trials confirmed that both rPLA and rABS maintain acceptable dielectric properties after multiple cycles. A new filament made from rABS blended with TiO_2 was successfully produced and homogenised after 3+ cycles of extrusion and shredding (see Figure 59). Microscopy revealed even dispersion of ceramic particles, indicating promising material consistency.

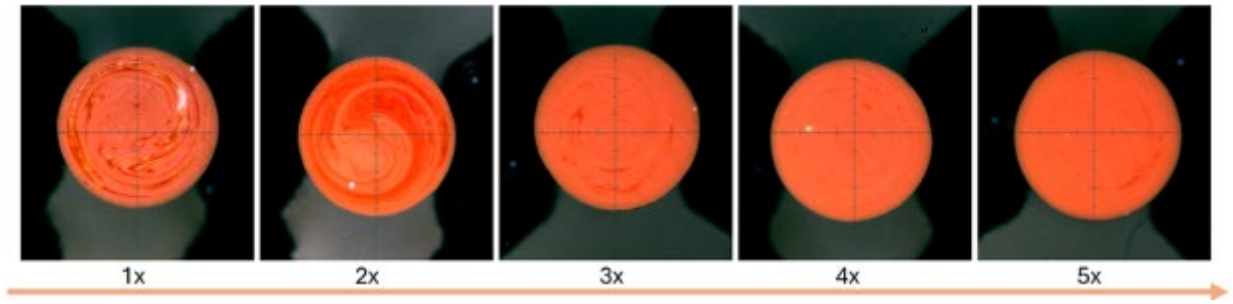

Figure 59. Filament cross-sections, after up to five extrusion cycles.

Conclusions:

As scientific insight, chemical and SEM analyses provided deeper understanding of material structures. It was confirmed that commercial high-εr filaments contain TiO_2 and $SrTiO_3$ particles, which are critical for enhancing permittivity. This informed the internal development of similar sustainable composite materials.

Some measurement method limitations were acknowledged. Some inconsistencies in tanδ values at higher frequencies (5.5–7 GHz) were documented, particularly for low-loss materials. These were attributed to limitations of the waveguide method, and proper error consideration was introduced. The results of dielectric permittivity measurements are presented in Table 41 below.

Table 41. Results of dielectric permittivity measurements.

	Material	Manufacturer	Measured Dielectric Permittivity (2,47 GHz) SPDR	Measured Loss Tangent tanδ (2,47 GHz) SPDR	Measured Dielectric Permittivity (5,5-7 GHz)	Measured Loss Tangent tanδ (5,5-7 GHz)
1	PLA	Spectrum	2,63	0,0046	2,6	0,017
2	ABS	Spectrum	2,58	0,0041	2,5	-0,0013
3	HIPS	Fiberology	2,37	0,0008	2,45	0,014
4	PETG	Rosa 3d	2,82	0,008	2,85	-0,001
5	Nylon PA6 Low Warp	Spectrum	3,09	0,013	3,08	0,039
6	ASA	Fiberology	2,67	0,011	2,68	0,011
7	PETG FX120	Spectrum	2,79	0,034	2,83	0,039
8	eTPU	eSUN	2,95	0,034	3,13	0,04
9	ABS1000 TP21315	Preperm			7,73	-0,0095
10	PVA	Orbi-Tech	3,24	0,019	3,12	0,037
11	FiberFlex 40D	Fiberology	2,73	0,05	2,63	0,07
12	Zetamix Al2O3	Zetamix			5,11	-0,0005
13	SiCeram Al2O3	SiCeram			5,32	0,0134
14	Greentec Pro	Extrudr			2,69	0,0129
15	PLA WOOD	Spectrum			2,48	0,028
16	HTPLA brass	ProtoPasta			5,99	0,039
17	HTPLA Bronze	ProtoPasta			4,41	0,021
18	HTPLA copper	ProtoPasta			4,89	0,018
19	PLA steel	ProtoPasta			3,57	-0,0018
20	PLA Iron	ProtoPasta			4,21	0,072
22	PMMA	Devil Design	2,51	0,0025	2,5	0,008
23	S-Flex Fluo	Spectrum	2,85	0,046	2,3	0,05
24	FEco 5%TiO2	Colfeed			3,19	0,081
25	FEco 10%TiO2	Colfeed			3,47	0,037
26	FEco 15%TiO2	Colfeed			3,76	0,052
28	PCTG	Spectrum	2,75	0,0069	2,71	0,0047
29	PETG+PTFE	Spectrum	2,64	0,0057	2,62	-0,0086
30	PLA Aero	Bambulab	1,88	0,0079	1,84	0,0098
31	ecoPET 9021	Spectrum	3,22	0,0079	3,11	0,0069
32	rPLA	Spectrum	2,77	0,0043	2,67	0,0041
34	HIPS-X	Spectrum	2,44	0,0007	2,37	0,001
36	Porcelite (print)	Tethon 3D			4,69	0,02
37	Porcelite (sintered)	Tethon 3D			4,65	0,039
38	Grey V4	Formlabs			2,86	0,02
39	High Temp V2	Formlabs			2,8	0,028
40	Calorite235	Tethon 3D			2,81	0,032
41	Ferrolite	Tethon 3D			6,24	0,021
42	High Alumina (print)	Tethon 3D			5,63	0,032
43	High Alumina (sintered)	Tethon 3D			8	0,012
44	rPLA	GUT Recycled	2,64	0,0058		
45	rABS	GUT Recycled	2,75	0,0057		
46	ABS Dk=6.4	Avient	6,36	0,003		
47	ABS Dk=8.0	Avient	7,68	0,0027		
48	ABS Dk=10.0	Avient	9,13	0,0025		

The missing values in the table 42 are due to measurement limitations related to the assessment of the dielectric properties of conductive materials, as well as, for some of them, the inability to produce samples suitable for SPDR measurements.

Below mainly focuses on the miniaturized ESPAR antenna measurement results. The results are presented in two subsections PLA + Polyethylene (from Figure 60 to Figure 61) and ABS (from Figure 62 to Figure 63). For each overlay, S11 and radiation pattern of the antenna were measured. In order to observe the influence of effective permittivity of the individual overlays, the radiation is presented as a received power level at the point of maximum radiation of the antenna as a function of frequency. The effective permittivity depends almost directly on the level of infill of the overlay. Moreover, it was observed that the type of used infill pattern does not have a significant influence on the effective permittivity. It has also been shown that both the use of natural admixtures and the re-processing of PLA do not significantly affect the final parameters of the antenna, which opens a potential path to the development of ecological solutions.

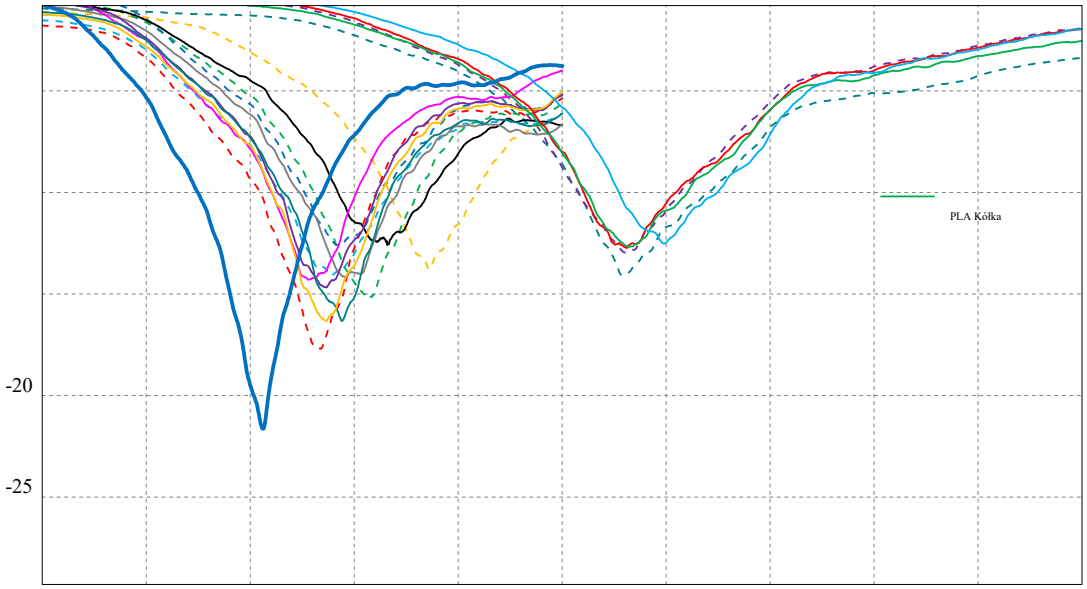

Figure 64. PLA and polyethylene overlays – S11.

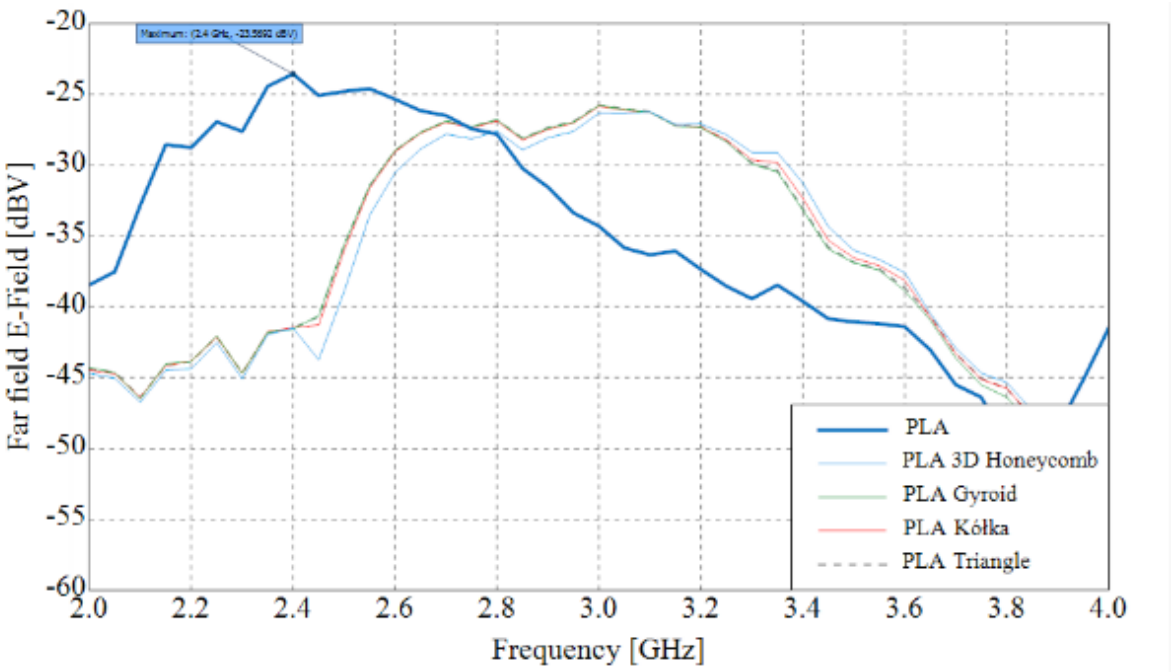

Figure 65. PLA with different infill patterns – radiation.

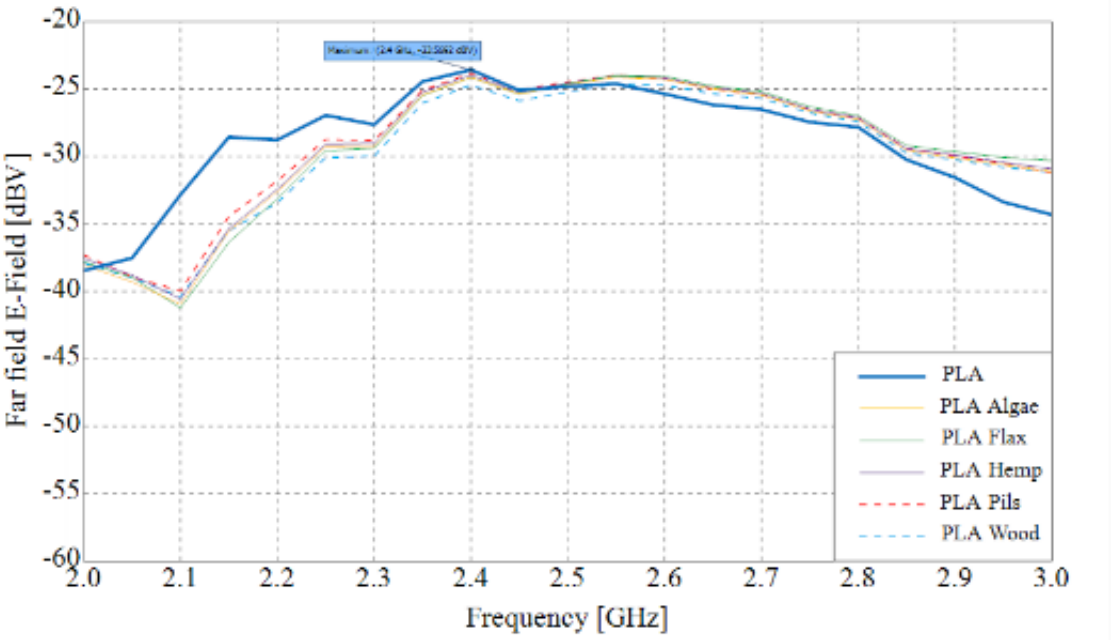

Figure 66. PLA mixed filaments – radiation.

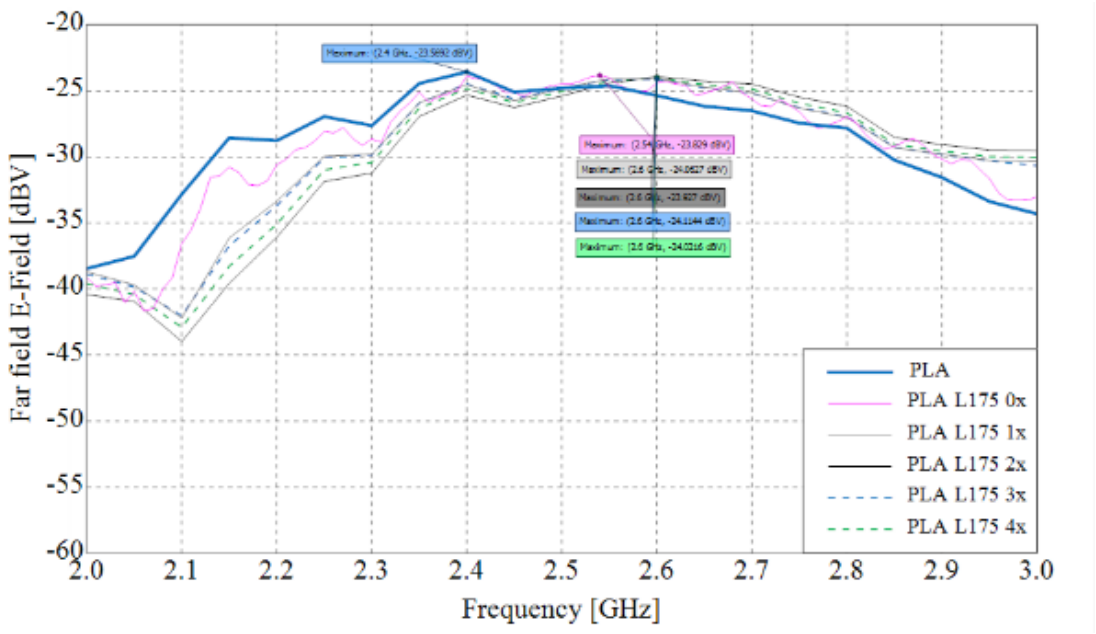

Figure 67. PLA after reprocessing – radiation.

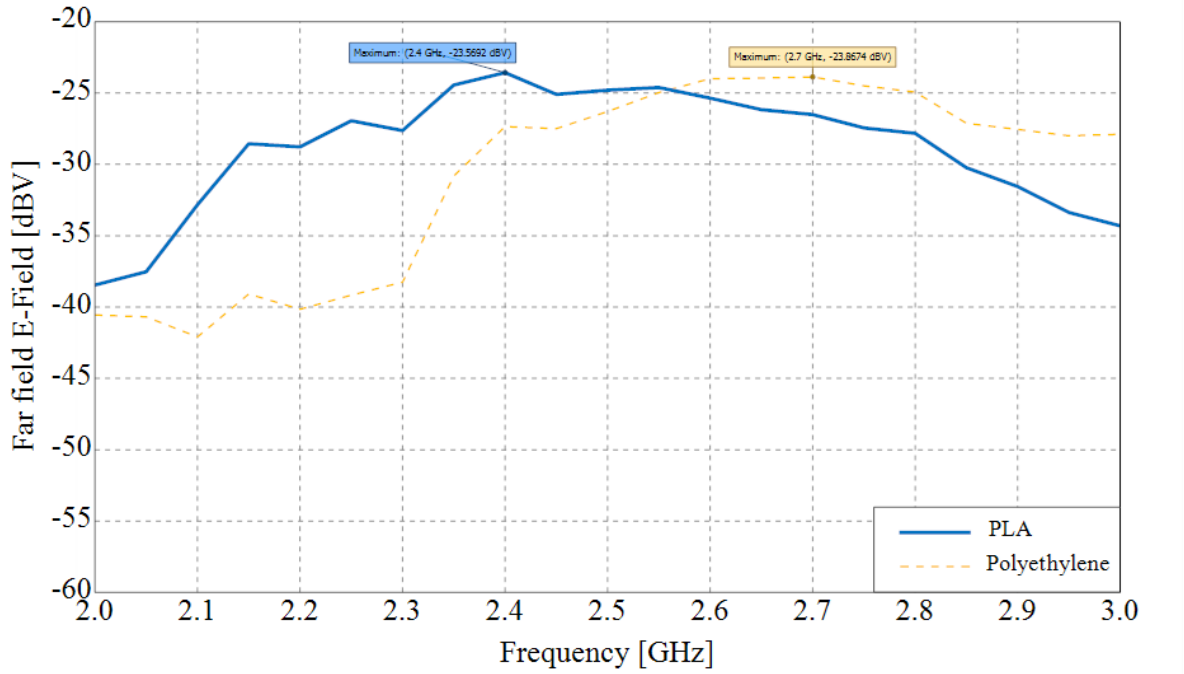

Figure 68. Polyethylene overlay – radiation.

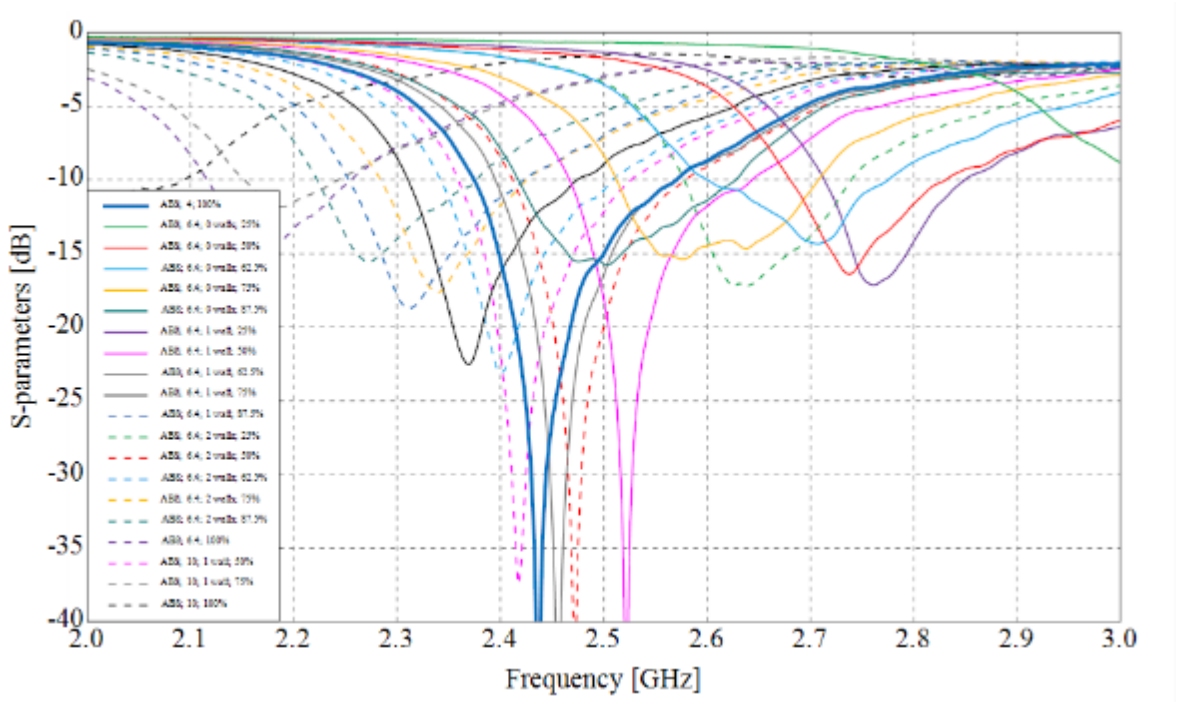

Figure 69. Overlays printed using ABS filaments – S11.

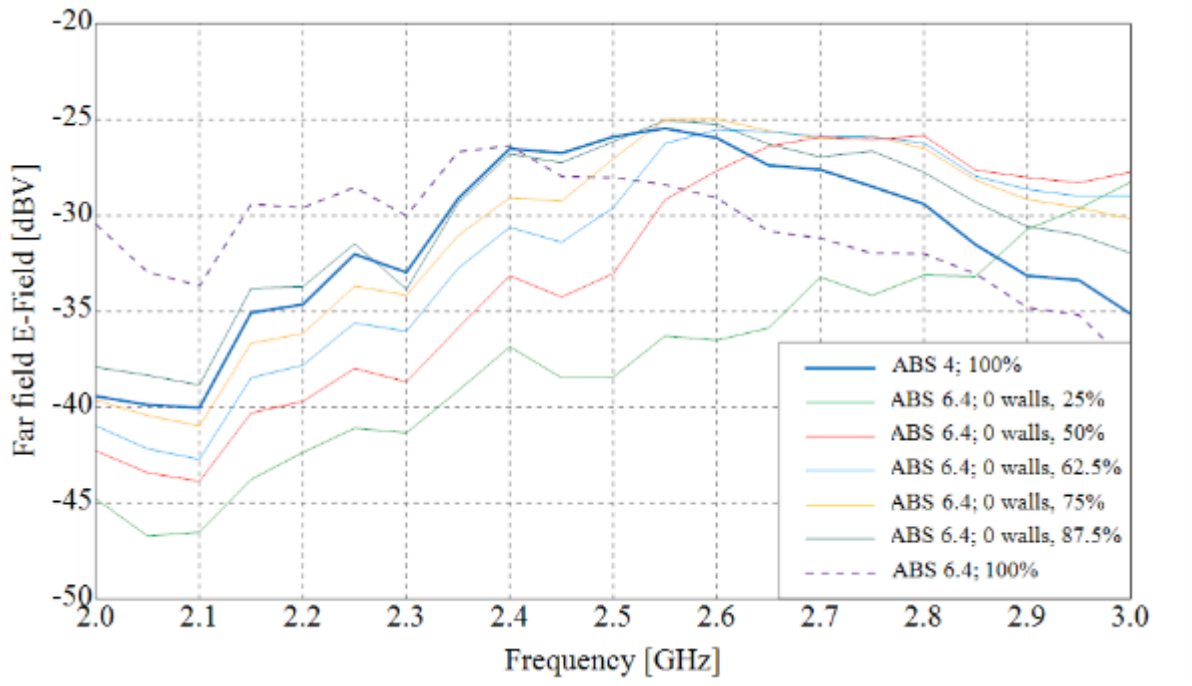

Figure 70. ABS with dielectric permittivity of 6.4 with different infill - radiation.

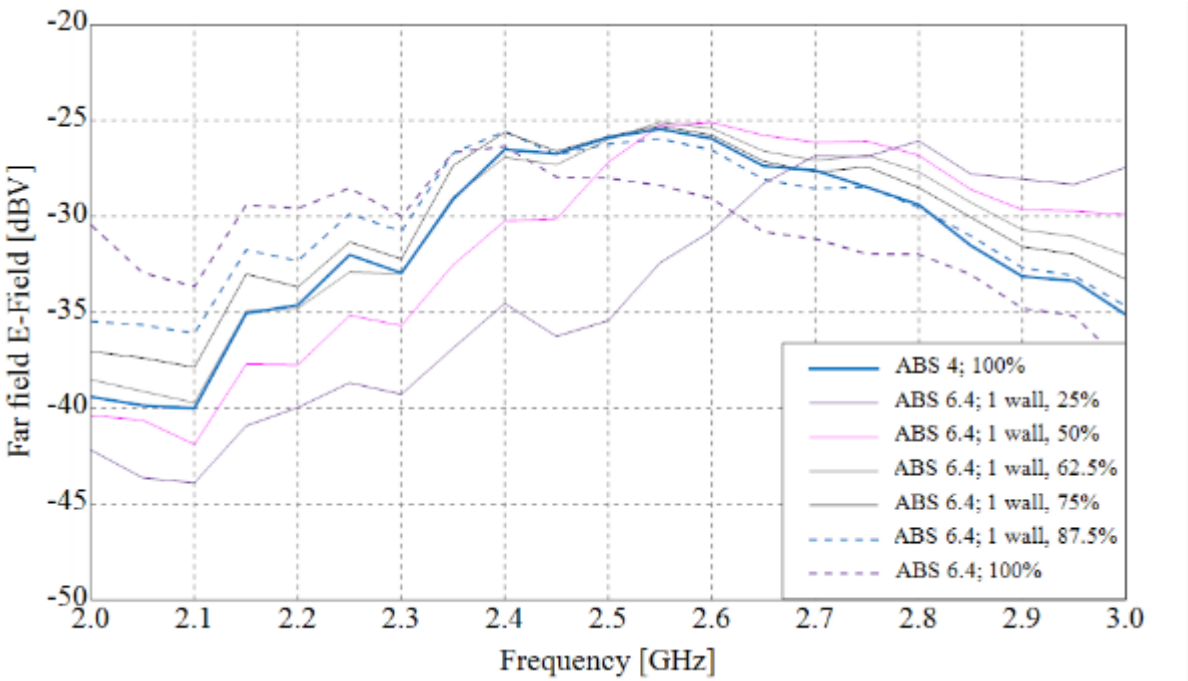

Figure 71. ABS with dielectric permittivity of 6.4 with different infill and one outer wall – radiation.

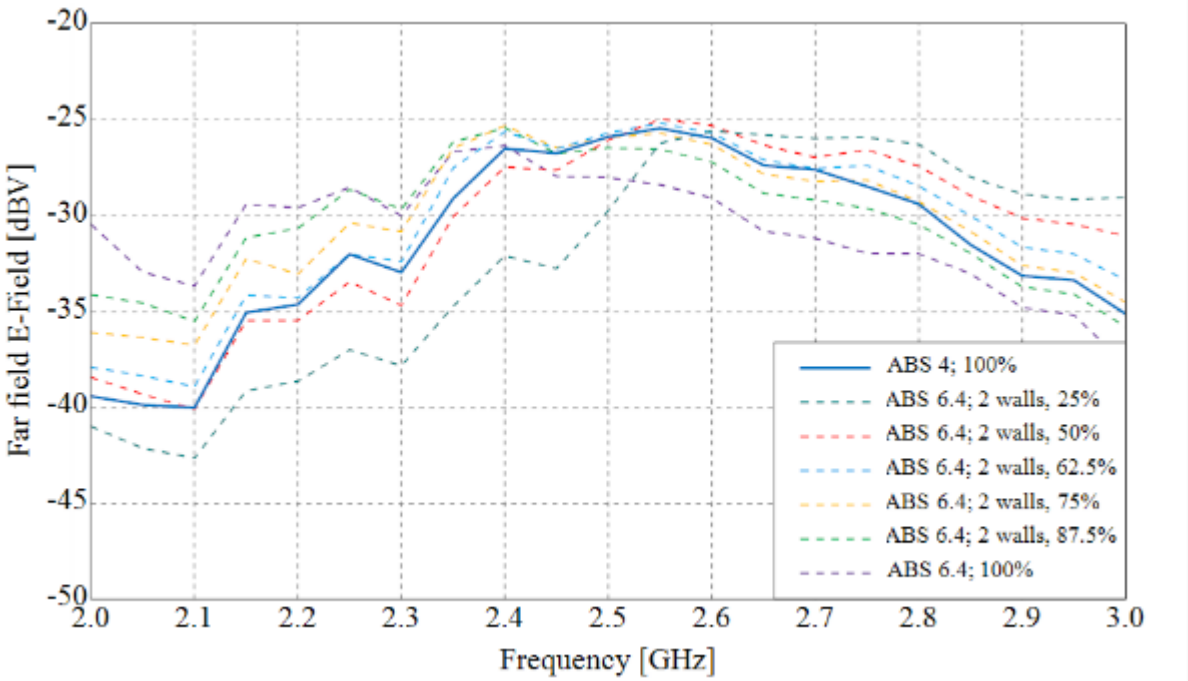

Figure 72. ABS with dielectric permittivity of 6.4 with different infill and two outer walls – radiation.

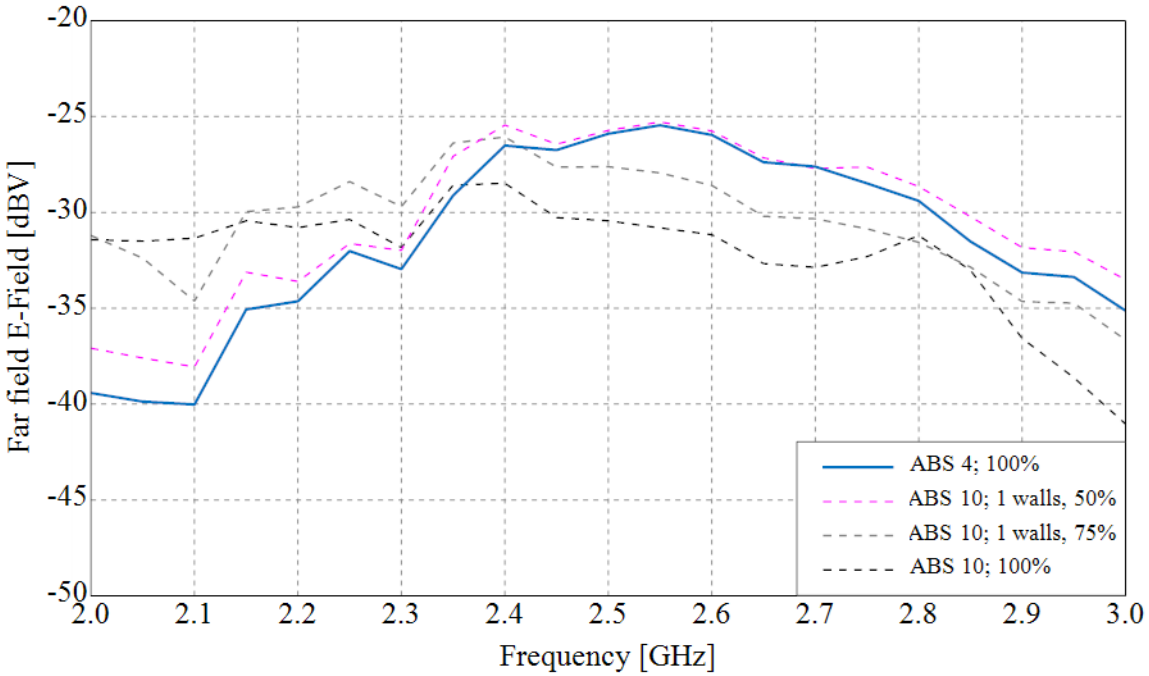

Figure 73. ABS with dielectric permittivity of 10 with different infill – radiation.

3.3 Component assembly

3.3.1 Testing at VTT

Methodology for chip and high pitch SMD component bonding by VTT. The summary of the work reported by VTT in D1.5 is presented in Table 43 below.

Table 43. Summary of the work reported by VTT in D1.5.

Developed process	Tests carried out	Linkage to pilots
SMD component ICA+NCA bonding on silver ink printed paper substrates	DVM diode testing of bonding's	Pilots #1.3, #2.2, #3.1a and #3.2
QFN56 µprocessor package ICA+NCA bonding on silver ink printed paper substrates	DVM diode testing of contacts, µX-ray imaging of bonding's	Pilots #1.3, # 2.2, #3.1a and # 3.2
SMD component bonding achieved using sustainable novel ACF manufactured by CondAlign	DVM diode testing of component contacts	Pilots #1.3, #2.2, #3.1a and #3.2
QFN56 µprocessor package bonding achieved using CondAlign ACF on PET and paper substrates	DVM diode testing of contacts, µX-ray imaging of bonding's	Pilots #1.3, #2.2, #3.1a and #3.2

New results from VTT after the release of D1.5 are reported below.

3.3.1.1 Chip bonding on copper ink patterns

Copper ink printed paper substrate samples were received from CSIC. RFID Tag (SIC4341) as bare RFID silicon chips were received from CSEM as well. RFID devices were targeted to bond on copper ink printed substrates. Copper ink printed plastic and paper substrates samples are shown in Figure 74 below.

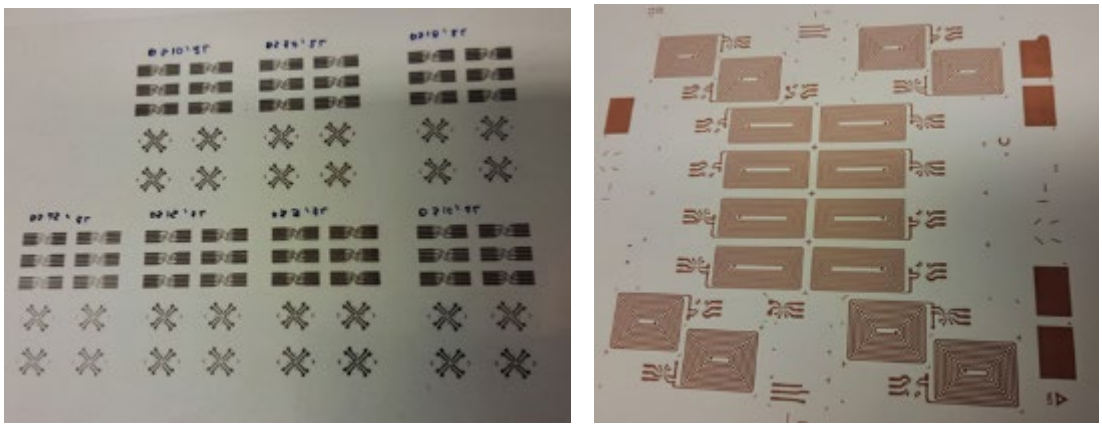

Figure 74. Copper ink printed on plastic (on the left) and on paper substrates (on the right) for SIC4341 chip bonding tests.

In bonding tests two methods were applied. First, NFC chip contacts were equipped with 17,5 µm Au studs before performing bonding tests on copper ink printed plastic and paper substrates. Bonding of chips on substrates performed by Finetech flip-chip bonder using temperature of 80°C DELO NCA type Dualbond AD345 dispensed on substrate for chip mechanical bonding. Electrical contacting achieved through Au studs. This novel adhesive tested in bonding to due to short pwere p by Figure 75 shows a SIC4341 chip bonding

performed on paper substrates. Chip bonding was characterised by µX-ray imaging, see Figure 76. Functionality of chip bonding performed by DVM diode testing with positive results.

Figure 75. SIC4341 chip bonding performed on paper substrates.

ACA bonding was applied as alternative bonding method for NFC chip. In this case DELO Monopox AC2264 adhesive applied in bonding. Monopox AC2264 adhesive was cured with thermode using 150°C temperature for 9 seconds. Functionality of chip bonding performed by DVM diode testing with positive results.

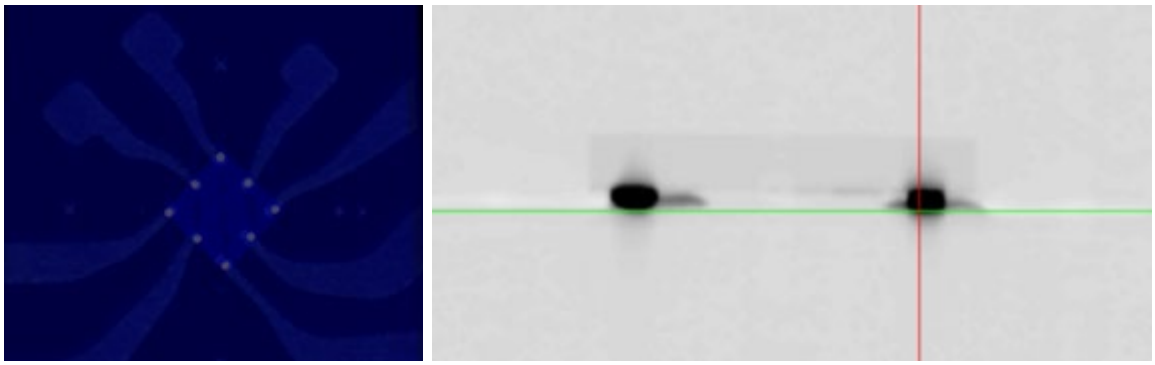

Figure 76. SIC4341 chip bonding on copper ink printed substrate characterisation by µX-ray microscope

µX-ray microscope characterisation introduces that chip bonding on copper ink printed paper substrate performed successfully. Final verification of chip bonding on copper ink printed paper substrate achieved by DVM diode testing introducing that contact from contact pin to electronics was achieved.

Conclusions:

Assembly of bare silicon devices on copper ink patterned paper substrates was developed. Two bonding methods were tested for chip bonding. First, bare silicon device equipped with gold studs and assembly of chip performed using Finetech flip-chip bonder and NCA adhesive in elevated heat and pressure. Secondly, devices bonded using ACA adhesive using elevated heat and pressure. Device bonding's were first characterised using X-ray microscope and functionality of bonding's were then tested positively using DVM diode testing.

3.3.2 Testing at WUR

3.3.2.1 Integration of components on TPU

Following the successful development of a working process, the properties of the epoxy adhesive were left to be analysed. The minimum dissolution of the adhesive and its conductivity compared to the low temperature solder has been analysed.

It is also monitored whether the adhesives attack the TPU in the long term due to the plasticisers or solvents they contain (see Table 44 and Table 45.There were also plans to test other adhesives recommended by the IZM.

Table 44. Status of the conductive adhesive tests as reported in D1.5.

Test	Status
Production test	done
Temperature compatibility with TPU	done
adhesion	done
conductivity	planned
resolution	planned
Compatibility with TPU	on-going

Table 45. Summary of the work reported by WUR in D1.5.

Developed process	Tests carried out	Linkage to pilots
Low temperature soldering on stretchable substrate	• Processability: soldering on TPU successfully applied. • Temperature compatibility: slight deformation	Pilot #3.3: assembly of components on single use part
Conductive adhesive on stretchable substrate	• Processability: applying components due adhesive on TPU successfully applied and cured. • Temperature compatibility: No deformation, no colour change. • Adhesion on TPU: stably attached.	Pilot #3.3: assembly of components on single use part

The process has been carried out at WUR on their own equipment. The parameters collected so far are being optimised for the company's own systems and another SnBi solder with a lower melting temperature is being tested. In addition, the conductivity of low-temperature solders will be compared with the tested adhesives (compare Table 5)

New results from WUR after the release of D1.5 are presented below.

3.3.2.2 Adhesive testing

New adhesive has been tested on TPU. New results relating to the planned testing of adhesive conductivity, resolution and compatibility with TPU from WUR after the release of D1.5 are described in Table 46

Table 46

Table 46 below. See also Figure 77.

Table 46. New results of adhesive conductivity, resolution and compatibility with TPU.

Test	Result
Conductivity	Adhesives and solder used are suited for the tested components
Resolution	Planned
Compatibility with TPU	Solvents in the adhesive used do not attack the TPU. Adhesive is suited for 0201 components.

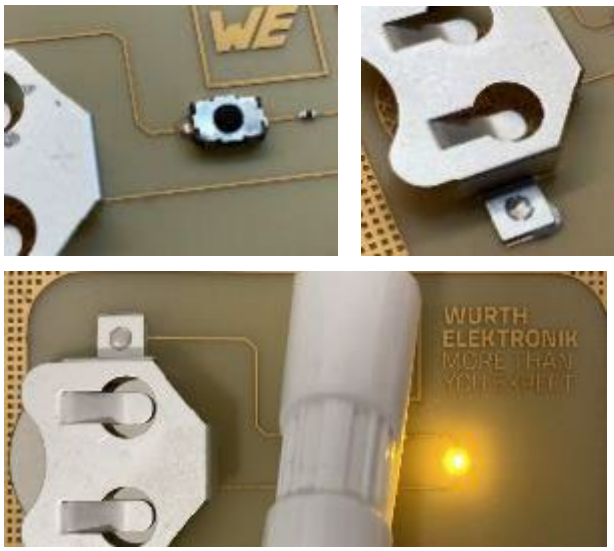

Figure 77. Examples of components assembled.

Conclusions:

After successful development and testing, the process is available for selection to assemble components to the PCB in Pilot #3.3.

3.3.3 Testing at FHG

Summary of the work reported by FHG in D1.5 is presented in Table 47 below. Next steps planned were:

- TPU-based mesh-structures (single copper-layer), that can be laminated around signal lines. Connection to the common ground by a conductive glue over a pad-to-pad contact.
- Lamination of a conductive textile around the critical paths and connection to the common ground by mechanical crimping.
- Stretchable conductive ink applied around critical paths.

Table 47. Summary of the work reported by FHG in D1.5.

Developed process	Tests carried out	Linkage to pilots
Assembly of pH sensors and ref. electrode (ACC)	Conductive glueing - sealing of assembled sensors	#UC3.3
Assembly of conventional SMD-components	Soldering of components 0402 NTC for temperature measurements	#UC3.3
Line crossings complex circuitries: Avoidance of plated through holes using jumper structures	Lamination of TPU circuitries and soldering thereon	#UC3.3
Implementation of shielding structures	Multilayer lamination of TPU and vertical contact formation	#UC3.3

New results from FHG after the delivery of D1.5 are described below.

3.3.3.1 Add-on shielding structures

Add-on shielding structures to improve signal vs. noise during data acquisition from the sensors. Different approaches to add shielding layers layouts around critical signal lines and their connection to a common ground (respectively connection to an “active shielding”) were explored. Different shielding layer (Cu-) densities are explored and shown in Figure 78 below.

The results show that:

- TUP-based mesh structures (single copper layer) were laminated around signal lines. Connection to the common ground by a conductive glue over a pad to pad contact on to the signal layer. They are visible in the pictures above as silver spots at the edge of the substrates.
- Lamination of a conductive textile around the critical paths and connection to the common ground by mechanical crimping is another option to implement shielding, but so far not tested.
- Electrical testing and check whether shielding improves the signal quality is planned to be finished by the end of April 2025.

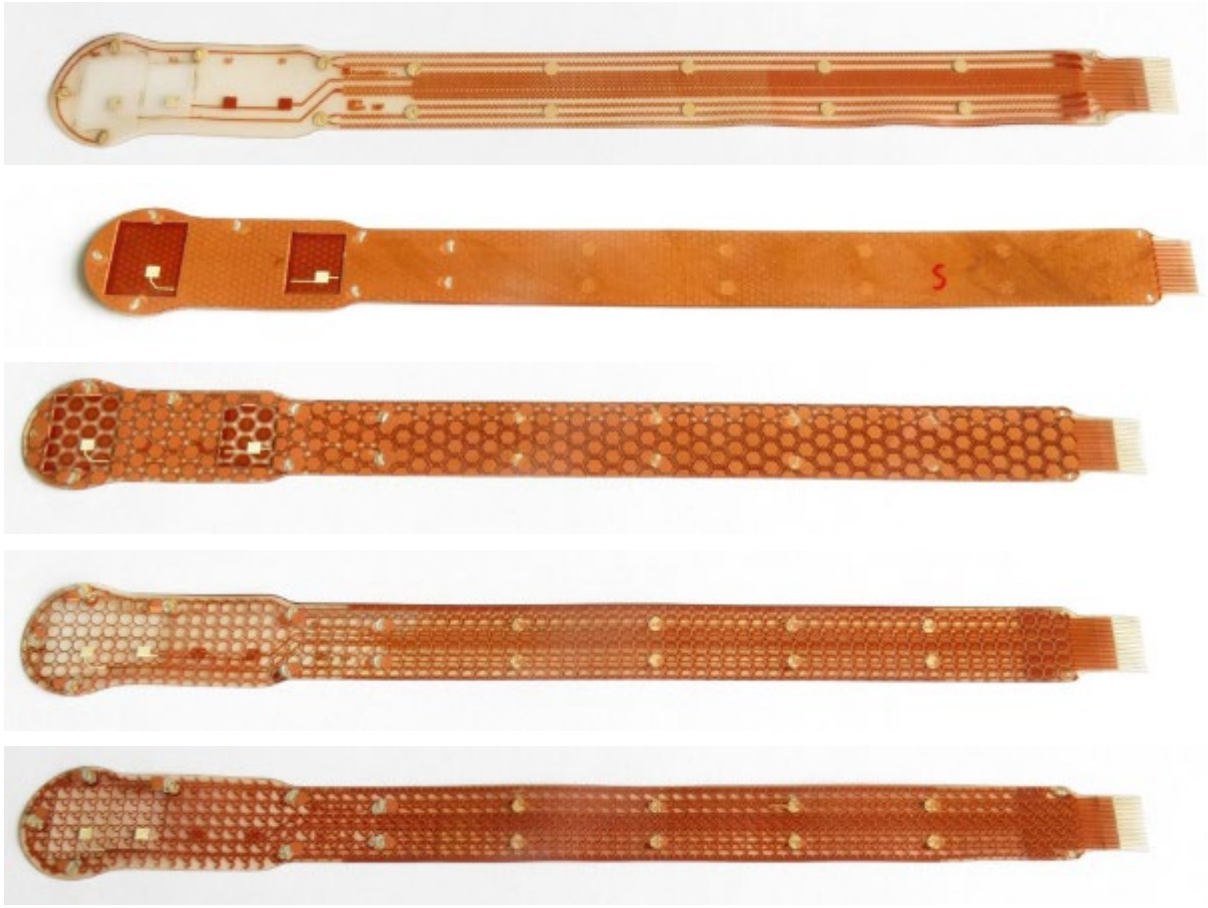

Figure 78. Different shielding layer (Cu-) densities explored.

3.3.4 Testing at RISE

The summary of the work reported by RISE in D1.5 is presented in Table 48 below.

Table 48. Summary of the work reported by RISE in D1.5.

Developed process	Tests carried out	Linkage to pilots
Methodology for assembly of components on sustainable substrates	Electrical contact yield tests using microchips with stud bumps and commercial ACAs	Pilot #3.2

New results from RISE since D1.5 are reported in the following section.

3.3.4.1 Methodology for assembly of components on sustainable substrates

Bonding of bare die microchips (ASIGxS) from IFAT have been carried out on thinstar plus 45 gsm paper substrates from TER with screen printed silver electrodes (see section 2.2.4). The printed contact pads have a nominal line width of 100 µm and a pitch of 200 µm, which corresponds to the pitch of the contact pads on the microchip. Screen printed copper electrodes, a potentially more sustainable alternative to silver, have not been tested since the resolution of the printed copper electrodes so far has not been good enough.

The bonding was performed in a BESI Datacon 2200 EVO automatic pick and place machine. The equipment has a bonding head that can provide both pressure and heat during the set bonding time. The bonding temperature, pressure and time is determined by conditions such as type and size of microchip, substrate, printed electrodes and bonding adhesive. Two different anisotropic conductive adhesives (ACA) have been used: a commercial ACA from Delo (Monopox 265) and an ACA developed by RISE within the project, in T1.2 (see ACA reported in section 0). The established process parameters for these two ACAs are shown in Table 49Table 49. The RISE ACA requires just slightly higher curing temperature, double the bonding time compared to the commercial ACA from Delo, but the same pressure applied during bonding, to establish proper electrical contact between the microchip contact pads and the printed conductive silver electrodes. Moreover, bare dies from IFAT with two different types of pads have been used: stud bumped pads (Au) and electroplated pads (Ni/Au). Both pads extend approximately 20 µm above the passivation surface of the microchip, but the stud bumps are cylindrical with a dome-shaped top that has a relatively rough surface while the electroplated pad is larger, rectangular in shape and much smoother. The topography of the stud bumped pad may make it easier to establish a contact to the printed electrode, but the electroplated pads are more commercially relevant since such a manufacturing process is scalable and more cost-effective. Thus, the target has been to establish a process for bonding of microchips with electroplated pads.

Table 49. Process parameters for bonding of bare die microchips on paper substrates with printed silver electrodes using both commercial ACA from Delo and ACA developed by RISE.

ACA	Bonding temperature (°C)	Bonding weight (g)	Bonding time (s)	Microchip pad type
Delo	180	700	10	Stud bumped
Delo	180	700	10	Electroplated
RISE	220	700	20	Stud bumped
RISE	220	700	20	Electroplated

After bonding the microchip to the paper substrate, a conformal coating of polyurethane (HumiSeal 1A33) is applied on the bonded microchip to provide moisture and environmental

protection. Curing is done at room temperature for an extended time to reduce any potential stress that could be induced at rapid curing at elevated temperature. Figure 79 shows microscopy images of a bare die microchip from IFAT bonded to a thinstar plus paper substrate with screen printed silver electrodes using the ACA developed by RISE. The polyurethane protective coating covering the entire device can also be observed.

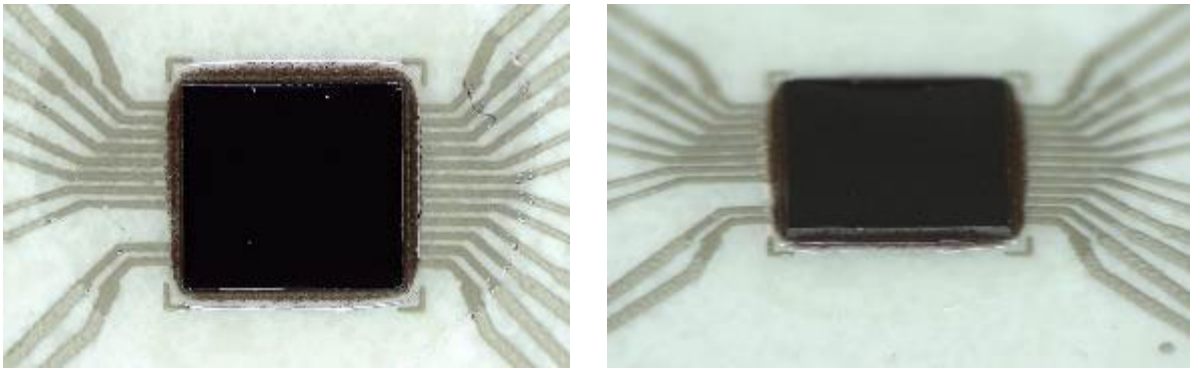

Figure 79. Microscopy images of a bare die microchip from IFAT bonded to a thinstar plus 45 gsm paper substrate from TER with screen printed silver electrodes, using ACA developed by RISE.

Electrical measurements have been performed on bonded microchips to investigate if electrical contacts between the chip pads (or pins) and the printed conductors were accomplished. The measurement setup used for these tests, which was proposed by IFAT, is illustrated in Figure 80. A voltage of 1.5 V is applied between the pin VSSA and the pin to test. The 3 kohm resistor makes the test circuit current limited. The voltage between the two pins is measured with a voltmeter. For a proper connection, the voltmeter will show the diode voltage (V_{Diode}) of the ESD protection diode against VSS. An open connection (pin not connected) will show a voltage of 1.5 V, while a short circuit between the pins (very unlikely to occur) will show a voltage of 0 V.

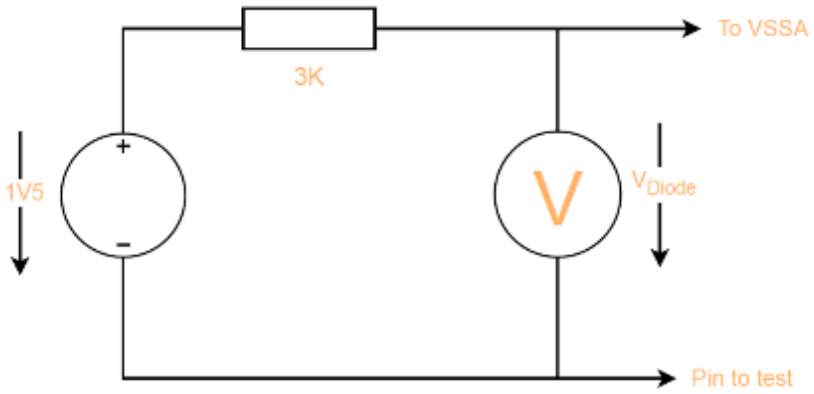

Figure 80. Electrical test setup for investigating if electrical contacts between microchip pads and printed conductors were made.

Examples of results from electrical contact tests on bonded microchips with both stud bumped and electroplated pads using both commercial ACA and ACA developed by RISE are shown in Table 50Table 50. The second column in the table lists the reference diode voltages for different pins on the microchip. The measured voltages are all very close to the reference diode voltages indicating successful contacts. It has not been possible to estimate reliable chip bonding yield values for the electroplated microchips due to their limited availability. However, the results obtained indicate that the chip bonding yields are high, and sufficiently

high for making functional prototypes in Pilot #3.2. Moreover, chip bonding yield as well as environmental stability will be further investigated as a part of the development of Pilot #3.2.

Table 50. Results from diode tests for assessing successful microchip bonding contact.

Pin name	Reference diode voltage (V)	Measured diode voltage (V)		
		Delo ACA		RISE ACA
		Stud bump	Electroplated	
RSTN	0.695	0.686	0.697	0.697
SWDIO	0.540	0.538	0.546	0.550
SWCLK	0.720	0.690	0.692	0.697
VMAIN	0.422	0.430	0.429	0.429
CE	0.529	0.535	0.524	0.525
RE	0.773	0.779	0.777	0.780
WE3	0.751	0.756	0.757	0.756
WE2	0.737	0.747	0.742	0.742
WE1	0.748	0.726	0.755	0.754
WE0	0.720	0.727	0.729	0.729
BAT1	0.729	0.735	0.739	0.737
LB	0.612	0.620	0.624	0.623
LA	0.612	0.620	0.624	0.624

Conclusions:

Processes for bonding bare die microchips from IFAT, both with stud bumped and electroplated pads, on paper substrates with printed silver electrodes, using both commercial ACA and ACA developed by RISE, have been established. Electrical testing of bonded microchips indicates high contact yields. The developed bonding processes will be utilised in the development of NFC-enabled sensor labels in Pilot #3.2. The bonding yield and environmental stability will be further investigated in this work.

3.4 Paper fluidics

3.4.1 Testing at VTT

In D1.5 *Sustainable processes and their characteristics* the development of the manufacturing process for paper fluidics using printing processes was described. The summary of that work can be found in Table 51 below.

Table 51. Summary of the work reported by VTT in D1.5.

Developed process	Tests carried out	Linkage to pilots
Printing of hydrophobic channel boundaries on paper substrates for paper fluidics	• Liquid flow test using coloured water • Mouse/anti-mouse immunoassay	Pilot #3.1a

New results from VTT after the delivery of D1.5 are reported below.

3.4.1.1 Papers Tesorb 93 and Tesorb 165

Porous Tesorb 93 and Tesorb 165 papers from Tervakoski were used as substrates and the hydrophobic channel boundaries were printed with self-formulated beeswax (BW) ink. The backside of the paper was fully covered with the BW layer via flexographic printing. The ink transfer volume of this layer was optimised by using anilox roller having cell volumes of 28.4, 39.0, and 50.1 ml/m2. The actual boundaries for the fluid guiding structures were screen printed onto the frontside of the paper using a coloured beeswax ink.

The thinner Tesorb paper (93 gsm) performed nicely. Coloured water flowed quickly along the channels without staining the background areas, as seen in Figure 81. BW ink formed hydrophobic channel boundaries reliably and repeatably. The ink transfer volume of the background printing needed to be less than 40 ml/m2 in order to prevent the channel area to turn hydrophobic, thus preventing the liquid flow along the channel. With the thicker Tesorb 165 paper, background staining was seen despite of the ink transfer volume. Thus, the paper itself was too thick, and no hydrophobic channel boundary could be formed across the substrate thickness.

Figure 81. Printed fluid guiding structures on Tesorb 93 and Tesorb 165 papers using different ink transfer volume during flexo-printing on the backside of the paper. The front side was printed with screen printing.

3.5 Wearable systems

3.5.1 Testing at EDI

EDI has proposed a new methodology for a more sustainable manufacturing process of wearable systems, which has the promise of reducing the ecological footprint of each smart clothing item produced while at the same time making the manufacturing of smart clothing more economically viable. The testing of this methodology was carried out using computer simulations to demonstrate the efficiency and sustainability of the interconnect approach (see Table 52 below).

Table 52. Testing of the EDI methodology.

Process	Tests carried out	Linkage to pilots
Methodology for manufacturing process of wearable systems	The testing of this methodology was carried out using computer simulations to demonstrate the efficiency and sustainability of the interconnect approach. Specific tests included: • Reachability of any randomly placed[3] wearable node on the interconnect • The percentage of useful vs. redundant interconnect lanes • The average length and number of jumps in the interconnect • Efficiency of use of the interconnect material	Methodology will be applied as part of Pilot #2.2 of the smart wearables interconnect. Specifically, the interconnect specification (shape and size of wiring patterns, interconnection of sensor nodes) to prove the plausibility of the methodology.

New results from EDI after the release of D1.5 are presented below.

3.5.1.1 Sustainable manufacturing process of wearable systems

Since D1.5 we have used simulated tests to prove the overall plausibility of the Methodology for manufacturing process of wearable systems. The testing/validation process itself is described in D1.5. The testing results will be described briefly here, but an interested reader can find the full testing and validation report of this process in the Sustronics web site, titled “Sustainable and green electronics for circular economy.[4]

The simulations were run on 170 clothing schematics of different cuts and sizes. Several key measures for the process sustainability are directly related to the interconnect wiring configuration/pattern. Of these 13 most promising patterns were chosen for these tests, as shown in Figure 82 below:

[3] The Montecarlo (random placement) analysis is to prove that the interconnect will work for generalized case. The Pilot is to validate this approach with a specific placement. The important part being, that the Pilot placement is not something to be optimized for, otherwise the sustainability benefits would not extend to other future wearables implementing this interconnect approach.

[4] https://www.edi.lv/en/projects/european-electronics-industry-towards-a-circular-economy-paradigm-sustronics/

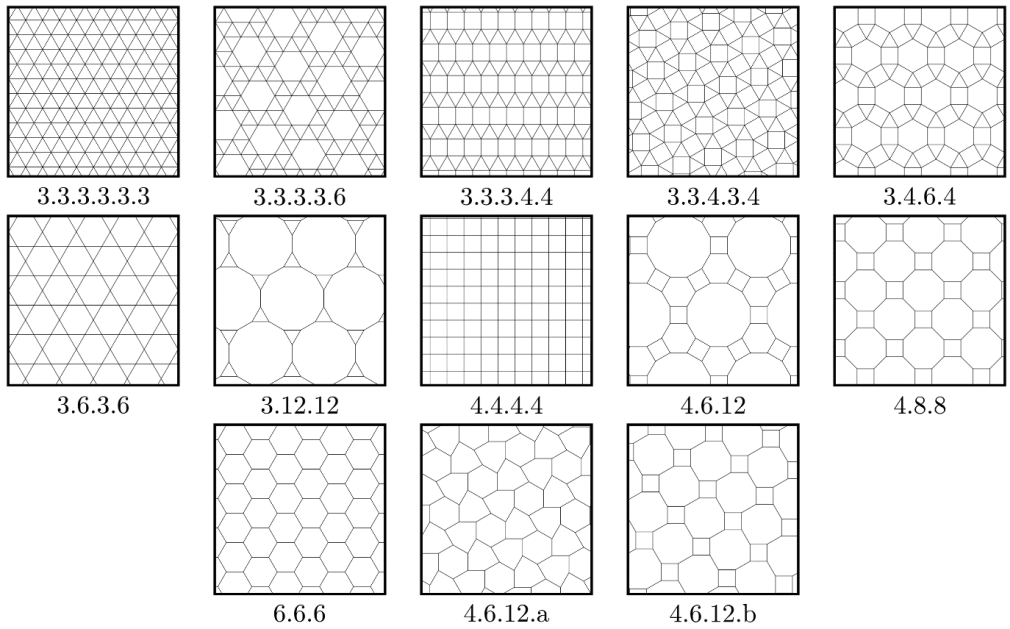

Figure 82. The 13 most promising interconnect configuration patterns that were used in the tests.

The simulations were also run on a wide range of different potential interconnect parameters, such as length of wiring sections and maximum allowed length of jumper connections.

In total 8840 simulated experiments were executed, with multiple parameter configurations resulting in total in 44200 different executed tests for the process validation.

The total predicted runtime of these simulations on a single processing core was calculated to amount to 4.61 years, or around 52.7 days on a 32-core computer in ideal load balancing scenario. Each separate simulation test run could vary in time, with the longest taking 15.12 hours. To reduce the wait time these tests were run in parallel on 6 compute units each equipped with 32 cores, thus reducing the theoretical execution time to 8.78 days. In practice due to balancing inefficiencies, the practical execution time varied between the compute units with shortest taking just 5 days, 11 hours and 25 minutes, while the longest took 9 days, 15 hours and 51 minutes to run all assigned tests. The final completion time of all simulations from start to end, thus took a bit longer than planned and was completed in 10 days, 17 minutes and 44 seconds.

The methodology of simulations was based on Monte Carlo simulation with multiple sensor and actuator placement configurations, which led to probability distributions for each tested value and enough measurements to reach statistical significance exceeding 95 %.

The initial tests allowed us to identify the overall interconnect configurations, that would yield the most sustainable results for the process. The test data clearly shows a trade-off between reachability of sensor nodes placed on the resulting smart wearables versus the average total wire length required to manufacture the interconnect fabric, as shown in Figure 83 below.

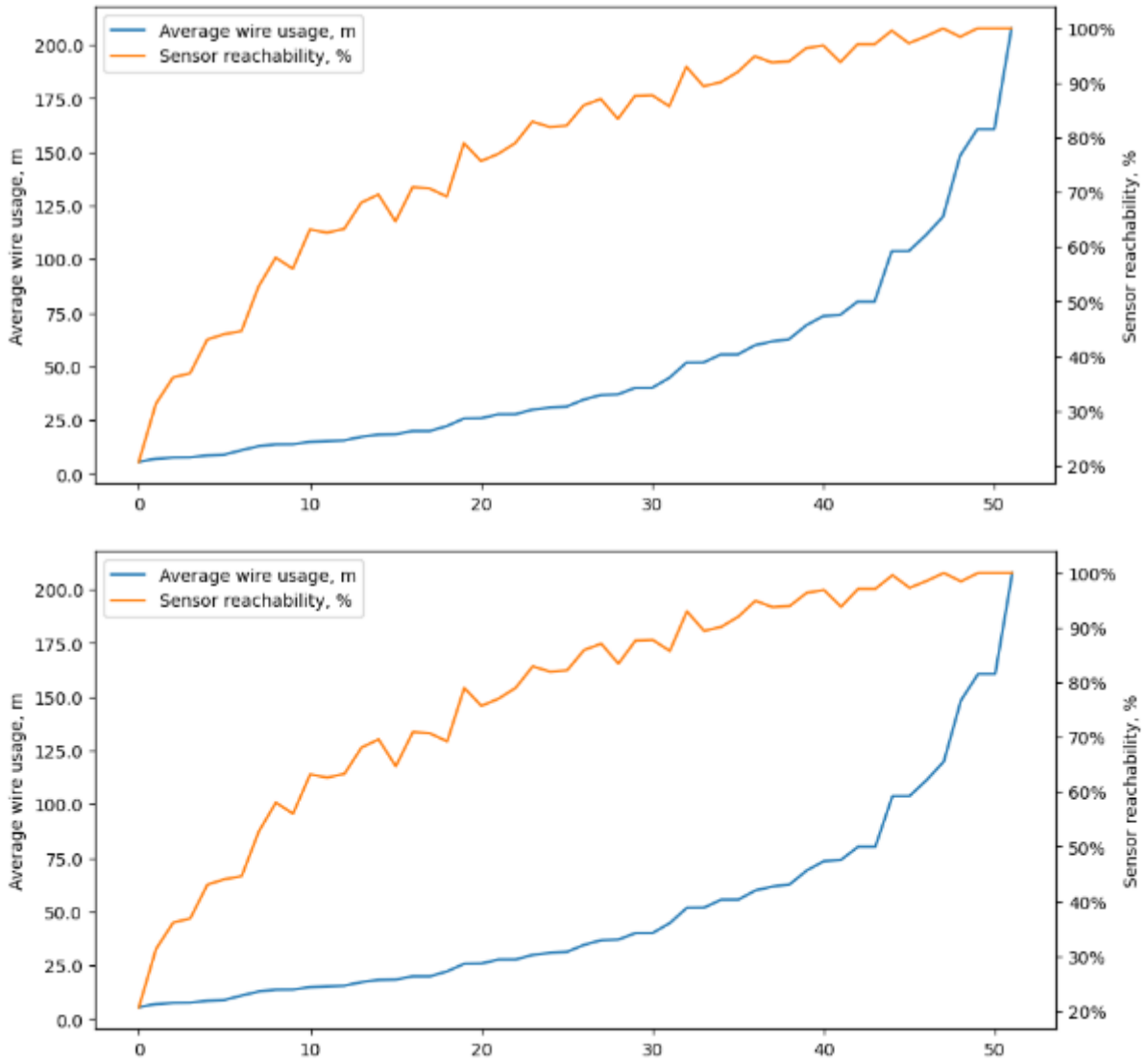

Figure 83. Trade-off between the total simulated average wire length of all configurations vs the reachability percentage of the simulated sensor placement. The X-axis represents the number of selected configurations.

Depending on the needs of smart clothing manufacturing and specific scale of sensor placement error allowed, we identified three interconnect patterns that both maximise the reachability of the sensors (>95% reachable) while minimising the total wire material expenditure:

Pattern 3.3.3.3.3.3 with 3 configurations:

10 mm jumper length limit and 40 mm wire sections yielding **97.7% reachability** and using **103.8 m** of wire on average;

20 mm jumper length limit and 80 mm wire sections yielding **97.6% reachability** and using **51.8 m** of wire on average;

40 mm jumper length limit and 160 mm wire sections yielding **96.1% reachability** and using **25.8 m** of wire on average.

Pattern 4.4.4.4 with 1 configuration:

80 mm jumper length limit and 160 mm wire sections yielding **98.6% reachability** and using **14.9 m** of wire on average.

Pattern 3.6.3.6 with 1 configuration:

160 mm jumper length limit and 160 mm wire sections yielding **96.4%** reachability and using **12.9 m** of wire on average.

There are some other potential parameter configurations for these three patterns, that tests showed would provide at least 95% reachability of the sensors, while at the same time minimising the total wire usage and maximising sustainability. These are shown in Figure 84 below (Zone A=pattern 3.6.3.6 is most sustainable, zone B=pattern 4.4.4.4 is most sustainable, zone C=pattern 3.3.3.3.3.3 is most sustainable and zone D=no pattern can provide 95% sensor reachability in this configuration, so it is not sustainable with any pattern):

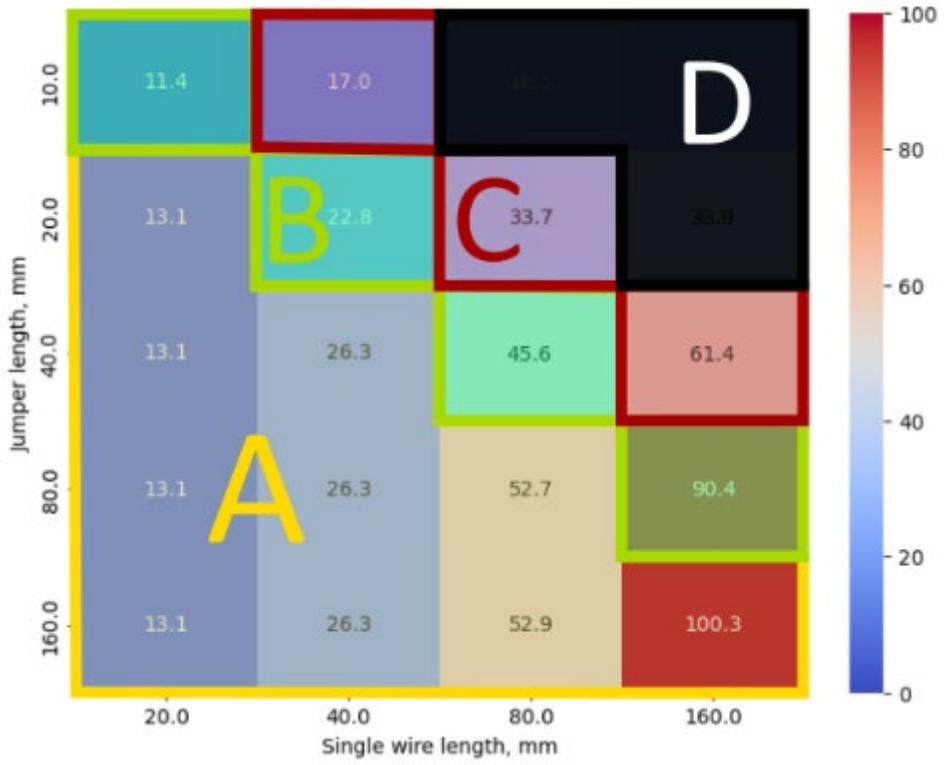

Figure 84. Efficiency of most sustainable configurations providing 95%+ sensor reachability based on maximum jumper length and single wire segment length.

Thus, the tests show that in situations, where maximum jumper length of 160 mm can be supported, **the most sustainable interconnect pattern is 3.6.3.6**, which will also be selected for validation by implementing a part of the Pilot 2.2. Additionally, from the sustainability perspective, if the interconnect wiring requires cables with multiple wires inside, the connectors between these cables are simpler to manufacture in pattern 3.6.3.6 or 4.4.4.4 requiring only **n clamps** (where n is the number of wires per cable), while the 3.3.3.3.3.3 configuration **requires 3*n** clamps instead as shown in the example images (see Figure 85, Figure 86 and Figure 87) below illustrating n=4 case:

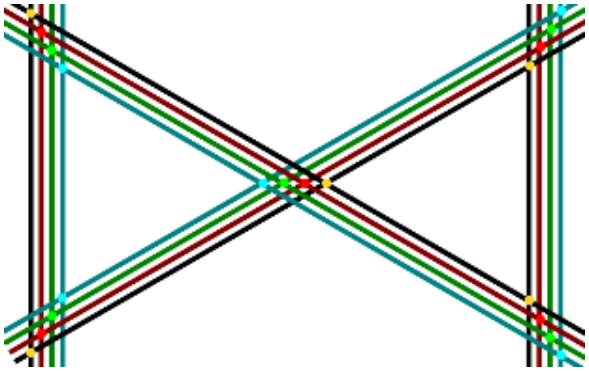

Figure 85 - Cable connector with 4 wires and clamps (3.6.3.6).

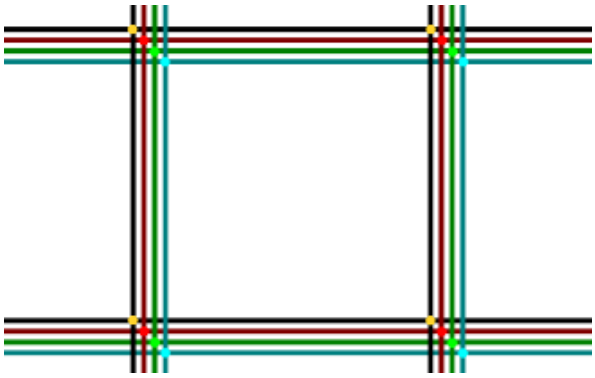

Figure 86 - Cable connector with 4 wires and clamps (4.4.4.4).

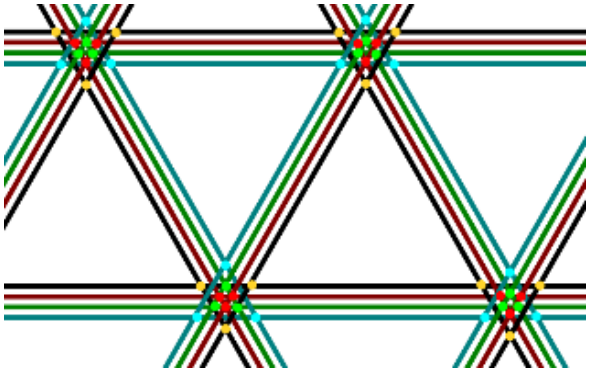

Figure 87 - Cable connector with 4 wires and 12 clamps (3.3.3.3.3.3).

The most sustainable configuration was selected for validation tests (3.6.3.6 with 160 mm jumper length maximum and 160 mm wire section length). The execution of the validation tests yielded the following results to the originally posed testing and validation questions:

What is the reachability of any randomly placed wearable node on the interconnect?

The overall reachability of randomly placed wearable nodes on this interconnect configuration is **96.37%** (mean) with standard deviation of **10.4%.** The percentiles of this statistic are:

25^{th} = 99.39%

50^{th} (median) = 99.82%

75^{th} = 99.99%

What is the percentage of useful vs redundant interconnect lanes in any random wearable configuration?

The overall percentage of useful vs redundant interconnect lanes in any random wearable configuration **58.86%** (mean) with standard deviation of **5.89%.** The percentiles of this statistic are:

25th = 57.06%

50th (median) = 59.15%

75th = 62.47%

What is the average length and number of jumps in the interconnect between any two random wearable nodes?

The average length of wire in the interconnect between two random wearable nodes is **769 mm** (mean) with standard deviation of **171 mm.** The percentiles of this statistic are:

25th = 632 mm

50th (median) = 762 mm

75th = 868 mm

The average number of jumps in the interconnect between two random wearable nodes is **6.1** (mean) with standard deviation of **1.3.** The percentiles of this statistic are:

25th = 5.0

50th (median) = 6.0

75th = 6.9

What is the efficiency of use of the interconnect material (e.g. copper)?

The overall efficiency of the interconnect material measured as reachability percent of sensor nodes per 1000 m of interconnect total material used is **100%** (mean) with standard deviation of **56%**. The percentiles of this statistic are:

25th = 57%,

50th (median) = 87%,

75th = 100%

Conclusions:

The overall simulation-based tests have validated the concept of the interconnect-based methodology. This demonstrated that high efficiency and reachability can be achieved with relatively minimal use of material, thus proving that the selected interconnect configuration is more sustainable than other dismissed configurations. Regardless of the minimal use of materials, it is practical enough to be used in most smart clothing manufacturing scenarios, thus leading to sustainability of implementation of this methodology by minimal replacement of equipment and training that is currently used in the standard modern clothing manufacturing methodology.

4 Conclusions

The Table 53 summarises the envisaged technologies (materials, processes) from D1.3 that were developed and tested in T1.2-T1.4, and thus reported in D1.4-D1.6. The table indicates in which deliverable each technology and its properties (characterisation, performance) were reported.

Table 53. Summary of the technologies developed in WP1, and where they are reported.

Technology from D1.3	Owner	Development reported in	Characterisation reported in	Characterisation carried out by	Performance testing reported in	Testing carried out by
Materials						
Bio-plastic substrates	VTT, ARNP, UPM	D1.4: film processing	D1.4: material properties	VTT, TNO, ARNP, UPM	D1.6: printability	VTT, TNO, CEA, SIG
Cellulose-based substrates	TER	D1.4: material development	D1.4: material properties	TER, TNO	D1.6: printability	VTT, TNO, RISE
Nano-cellulose	VTT	D1.4: material development	D1.4: material properties	VTT	D1.6: printability	VTT
Plastics (medical grade)	Commercial material	-	D1.4: material properties	TAU, TNO, SCR	D1.6: printability	TAU, TNO
Pressure sensitive adhesives	UPM	D1.6: material development	D1.6: material properties	UPM	D1.6: skin irritation	UPM
Non-conductive and conductive adhesives	RISE	D1.4: material development	D1.4: material properties	RISE	D1.6	RISE
Sensor inks	RISE, UGOT	D1.4: material development	D1.4: material properties	RISE, UGOT	D1.6: performance	RISE, UGOT
Electrode ink	TAU	D1.4: material development	D1.4: material properties	TAU	D1.4: printing	TAU
Conductive ink	CAN	D1.4: material development	D1.4: material properties	CAN	D1.4: performance	CAN
LDS metallisation	PIEP	D1.4: material development	D1.4: material properties	PIEP	D1.6: printability	PIEP
CNT	CAN	D1.4: material development	D1.4: material properties	CAN, URV, MEDUG, CBmed, CSEM	D1.6: performance	CAN
Processes						
Printing	RISE, SCR, TAU	D1.5: process development	D1.5: process properties	RISE, SCR, TAU	D1.5 & D1.6: process performance	RISE, SCR
3D printing	GUT	D1.5: process development	D1.5: process properties	GUT	D1.6: process performance	GUT
Structural electronics	CEA, SYM	D1.5: process development	D1.5: process properties	CEA, SYM	D1.5: process performance	CEA, SYM
Component assembly	WUR, FHG, CEA, SYM, VTT, RISE	D1.5: process development	D1.5: process properties	WUR, FHG, CEA, SYM, VTT, RISE	D1.6: process performance	WUR, FHG, VTT

Technology from D1.3	Owner	Development reported in	Characterisation reported in	Characterisa-tion carried out by	Performance testing reported in	Testing carried out by
Wire bonding	WUR, VTT	D1.5: process development	D1.5: process properties	WUR	D1.6: process performance	WUR, VTT
Paper fluidics	VTT	D1.5: process development	D1.5: process properties	VTT	D1.6: process performance	VTT
Wearable systems	EDI	D1.5: process development	D1.5: process properties	EDI	D1.6: process performance	EDI
Thermal laminator	MOV	D3.2: process development	D3.2: process development	MOV	D3.2: process development	MOV

5 References

Ham Y.R., Kim S.H., Shin Y.J., Lee D.H., Yang M., Min, J.H., Shin J.S. *"A comparison of some imidazoles in the curing of epoxy resin".* Journal of Industrial and Engineering Chemistry 16 (2010) 556–559. https://doi.org/10.1016/j.jiec.2010.03.022